A study of mass reconstruction in $Z^0 \rightarrow \tau^-\tau^+$

Master Degree Thesis in Experimental Particle Physics

Alette Aasvold

Department of Physics and Technology
University of Bergen
Norway

June 1, 2010

Dedicated to God the Almighty. Thank you, Lord, for creating such a wonderful and exciting universe. And thank you for permission and opportunity to study it. By the way, where did you hide the Higgs?

Acknowledgements

I would like to thank my supervisor Bjarne Stugu for great help in forming the ideas of this thesis, holding the work in progress, and sharing your knowledge of physics. Thank you, Post Doc Thomas Burgess, for invaluable help with programming and hands-on ideas and solutions. Thanks to PhD Peter Rosendahl for creating the data files used in this thesis. Thanks to the particle physics group in Bergen, and especially the tau group, for good discussions, corrections and ideas. And thanks to the rest of the tau group for good discussions, corrections and ideas. Thanks to my office mates: Ørjan Svandal, Kristine Helle, Jørn H. Mæland and Anita Olausen, for funny discussions and motivational pep talks during the last two years. Thank you, Henrik Vaula Rasmussen, and Randi Vaula Rasmussen, for reading trough this thesis and helping me to write better and precisely language. And last, but not least, thanks to all my friends and family for prayers, encouragement and support.

Alette Aasvold

Abstract

Neutrinos escaping detection is one of the main problems in mass reconstruction with tau leptons. They must be neglected or corrected for in some way. This thesis discusses two methods of handling the neutrinos in different ways. *The Collinear Approximation* (CA) builds upon the assumption that the neutrinos travel in the same direction as the visible tau decay products. *The boost method* neglects the neutrino energy contribution in the leading visible tau, as seen from the mother particle's reference system. The methods have been studied with simulated $Z^0 \rightarrow \tau^-\tau^+$, $H^0 \rightarrow \tau^-\tau^+$, and QCD samples, and with early data from ATLAS. This work shows that the weaknesses of CA is that the transverse angle of the E_T^{miss} has to lie between the transverse angle of the two visible taus, and that it collapses with back-to-back taus in the transverse plane. A strength of the CA is that it uses the missing energy, which is all information available about the neutrinos. The CA works better for boosted taus, i.e. taus decaying from heavy particles, like H^0 and Z^0. The weaknesses of the boost method are that it does not use the E_T^{miss} information, and that the distribution is not easily fitted, but the method is still under development on these points. The strength of the boost method is that it works for all tau pairs, making it a good complimentary method to the CA. Both methods work in $Z^0 \rightarrow \tau^-\tau^+$ and $H^0 \rightarrow \tau^-\tau^+$ events, and can be potentially applied to other decay chains as well. In the future, many studies will include mass reconstruction from tau leptons, where both the CA and the boost method will be important methods.

Contents

List of Figures

List of Tables

Introduction

Some people look at the world thinking: "How does all this stuff work?" and use their lives to work out and test explanations. We can thank generations of such people for all the theories and natural laws we have today. But the work is not finished. Could it be possible to obtain a complete explanation of nature? I don't know, but together with thousands of other scientists all over the world, I'm working towards it.

The most successful theory at subatomic level is the Standard Model (SM). But despite its success, there are phenomena which are not explained by this model. Extended version of the SM or a totally new theory is therefore required. Examples of these phenomena are

- **Dark matter.** Measurements in outer space tell us that there exists a lot of invisible energy and matter. Dark matter consists of particles not described by the standard model.
- The most common force, **gravitation**, is not accounted for.
- SM does not explain why there is much more matter than antimatter in the universe.
- The Higgs mechanism is not experimentally verified.

Predictions of a Higgs field is fundamental in today's explanation of subatomic physics, and searching for and finding the Higgs boson is the main motivation for building the largest particle accelerator in the world, the Large Hadron Collider (LHC) at CERN [1], started up September 10th 2008. If we fail to find the Higgs with this machine, we can say with relative certainty that it does not exist or has properties that are inconsistent with SM predictions. This would imply that there is either something wrong with the Higgs mechanism or some other theoretical concepts. [6].

[1] European Organization for Nuclear Research

Searching for new phenomena and their explanations requires a thorough knowledge of the already existing standard model. That is the main motivation for studying $Z^0 \rightarrow \tau^-\tau^+$ decays. Only when this decay is well observed, one can be able to separate out and study new phenomena like $H^0 \rightarrow \tau^-\tau^+$.

Other motivations for studying $Z^0 \rightarrow \tau^-\tau^+$ are to

- Check the detector for defects
- Calibrate the detector
- Measure the production cross section
- Check lepton universality

An overview of this thesis

Starting with the basic theory of particle physics, **chapter 1** gives an introduction to the *Standard Model* of particle physics. Here the classification system of the particles and forces between them will be briefly described. Since the main decay channel studied in this thesis is the $Z^0 \rightarrow \tau^-\tau^+$, the τ-lepton and Z^0 boson will be taken a deeper look into before the chapter is ended by mentioning the missing parts as well as possible extensions of the Standard Model. **Chapter 2** describes the experimental setup, which is the ATLAS and the LHC at CERN. After a summary of history of CERN, the main lines of the LHC will be drawn, followed by the layers of ATLAS briefly described. The complicated process of reconstructing tau candidates and selecting well-reconstructed candidates is described in a simplified way in **chapter 3**. In **chapter 4**, the taus are used to show how to reconstruct the Z^0 mass. This could be transferred into any two-body decay. The main chapter of this thesis is **chapter 5** where the Collinear Approximation is described; this method corrects for the missing energy lost by neutrinos. Finally, the strengths and weaknesses of the method are discussed, concluding with a need for complementary methods. The boost method is one such promising method, which is described and discussed in **chapter 6**. The C++ source code to implement these methods is given in **Appendix B**. One of the main purposes of studying $Z^0 \rightarrow \tau^-\tau^+$ is to get a grip on the main background for the similar process of $H^0 \rightarrow \tau^-\tau^+$. Hence, **chapter 7** concentrates on the Higgs decaying process $H^0 \rightarrow \tau^-\tau^+$. By April 2010, at the finishing of this study, the LHC has started to collide protons and ATLAS has given some real data output. In **chapter 8** some main concepts from the thesis will be compared with the latest ATLAS data. The conclusion is found in **chapter 9**.

This thesis aims to be a good introduction to particle physics to new master students. All calculations and logical lines of thought should be easy to follow. Common acronyms and expressions are listed in **Appendix A**; some of them are not used in this thesis, but is included since they are commonly used among particle physicists.

Chapter 1

The standard model

The standard model describes the fundamental pieces of our material world, and the forces between them. The chemical elements are built up of atoms, which in turn consist of nucleons - protons and neutrons. The nucleons also have a substructure; they are built up of quarks and gluons. The common name of both quarks and gluons is **partons**.

1.1 Forces - bosons

In order to keep track of all the particles, they are grouped together with other particles having the same properties. One of the most fundamental properties is the spin. Spin is known from classical mechanics, where it describes the angular momentum of an orbiting particle — both describing an object rotating around another, e.g. the Earth around the Sun, or an object spinning around itself. At subatomic [1] level, spin is no longer classical, but quantum mechanical and can not be understood classically. The unit is $\hbar$, which is an extremely small quantity. The spin of a particle is always an integer or a half integer unit of $\hbar$. One groups particles into these two categories, — the particles with integer spin (i.e. $0, \pm 1, \pm 2, \dots$) are called bosons, and the particles with half-integer spin (i.e. $\pm 1/2, \pm 3/2, \dots$) are called fermions. On the fundamental level, the bosons act like force carriers, and the fermions like building bricks.

In the SM there are three different forces, here listed from the weakest to the strongest:

1. Gravitational force

   The gravitational force acts on every particle that has mass. This force makes water fall down a waterfall as well as the earth move around the sun.

[1] Everything smaller than an atom.

Despite that gravity is the most common force in everyday life, a way to include it in the SM is not yet found. There is theoretically assumed to exist a mediating particle, called graviton, but this is not experimentally verified. On subatomic level, however, gravity is many orders of magnitude smaller than the other forces and can be neglected.

2. Electroweak force

   Electroweak force is the common name of the electric, magnetic and weak nuclear forces. The two first are also called the electromagnetic force. One commonly distinguishes between the electromagnetic force and the weak force, since they first unify and become indistinguishable at high energies. The electric and magnetic forces, on the other hand, are always unified and can never be observed alone. [2]

   The electromagnetic force acts on electrically charged particles. This force explains molecular structure and determines the properties of the elements. In quantum electrodynamics, the electromagnetic force is mediated by the massless photon.

   The weak nuclear force, or, put simply, the weak force, acts on all particles except photons and gluons. See table 1.2. This force allows leptons and quarks to decay. The comparatively heavy bosons $W^{\pm}$ and Z^0 carry the weak force.

3. Strong nuclear force

   The strong nuclear force works between quarks, binding them together to form strongly interacting particles, hadrons. The force carriers themselves are called gluons. These also interact between themselves. A "leak-out" of the gluons holds the nucleons together in the nuclei. This leak-out is small compared to the forces inside the nucleon, but strong enough to cause nuclear binding. Although smaller than inside the nucleon, the nuclear binding is strong enough to release the energy of an atomic bomb.

1.2 Quarks and leptons - fermions

All the existing quarks and leptons can be arranged into three generations as seen in table 1.1.

Leptons are characterised as fermions not participating in the strong force. They only react with the weak force and, if charged, also the electromagnetic

[2] That is not always true; a charged particle at rest produces static electricity without any magnetic field.

Leptons				Quarks		
gen		Charge (e)	Mass $\mathrm{MeV/c^2}$	Flavour	Charge (e)	Mass $\mathrm{MeV/c^2}$
1	ν_e(e neutrino)	0	$< 2 \times 10^{-6}$	*u* up	2/3	3
	e	-1	0.511	*d* down	-1/3	5
2	ν_μ(μ neutrino)	0	$< 2 \times 10^{-6}$	*c* charmed	2/3	1.3×10^3
	μ	-1	106	*s* strange	-1/3	104
3	ν_τ (τ neutrino)	0	$< 2 \times 10^{-6}$	*t* top	2/3	171×10^3
	τ	-1	1777	*b* bottom	-1/3	4.2×10^3

Table 1.1: Charge and mass of the quarks and leptons [5].

force. They are fermions, i.e. having spin 1/2 or integer + 1/2. In addition, they have a quantum number called lepton flavour number, which is conserved within each generation.

Each particle has its own antiparticle, organised in the same way. The physical nature on Earth, i.e. all the elements, is built up of particles from the first generation. Could there be more generations? A quote from the CERN web-pages tells us that that is not the case:

> Measurements performed at LEP also proved that there are three — and only three — generations of particles of matter. [3]

But why there exist these two "extra" generations that almost never occur in nature, and furthermore why there are only three generations, are still unanswered questions.

A the neutrino escapes detection in ATLAS, we call it invisible. The neutrinos are the only invisible particles detected by other experiments [4]. However, models beyond the standard model predict other invisible particles as well, e.g. the supersymmetric neutralino.

As seen in table 1.2, different subatomic particles interact through one or more of the three forces. Leptons are particles that do not interact through the strong force, and hadrons are particles which do. Hadrons are built up of quarks. It is therefore just halfway correct to put quarks into the hadron group, since they *are* quarks, not built up from such. Hadrons are grouped into mesons; built up of one quark and one antiquark, and baryons; built up of three quarks. Quarks cannot be isolated, but form baryons and mesons. Baryons are built up of three quarks, while mesons are formed by a quark and an antiquark. When summing up the spin of the quarks, a baryon turns out to be fermion and a meson turns out to be a boson.

[3] This statement assumes that a possible fourth neutrino is lighter than $\frac{m_Z}{2}$

[4] Detected by, among others, Icecube. http://icecube.wisc.edu/

Particle	Type	Weak	Electromagnetic	Hadronic
Photon	Gauge boson	No	Yes	No
$W^{\pm}$, Z^0	Gauge bosons	Yes	Yes	No
(Gluon)	Gauge boson	No	No	Yes
Leptons				
Neutrino	Fermion	Yes	No	No
Electron	Fermion	Yes	Yes	No
Muon	Fermion	Yes	Yes	No
Tau	Fermion	Yes	Yes	No
Hadrons				
Mesons	Bosons	Yes	Yes	Yes
Baryons	Fermions	Yes	Yes	Yes
(Quarks	Fermions	Yes	Yes	Yes)

Table 1.2: Subatomic particles and their interactions [4].

1.3 The Z^0 boson

The Nobel Prize in Physics 1984 went to Carlo Rubbia and Simon van der Meer *for their decisive contributions to the large project, which led to the discovery of the field particles W and Z, communicators of weak interaction* [7]. The Z^0 has spin 1 and hence is a boson.

Z^0 is a quite heavy particle (91 GeV) compared to most other ones in the "particle zoo". The lifetime is too short for Z^0 to be detected directly in ATLAS. It must hence be reconstructed from its decay products.

In figure 1.1 one can see that the Z momentum is generally higher in the longitudinal direction, which means that the Z^0 is boosted. This will become important in the discussion of Collinear Approximation in chapter 5, and of the boost method in chapter 6.

1.3.1 Z^0 production at the LHC

W and Z bosons are abundantly produced in the Large Hadron Collider (LHC), mainly produced by valence-sea quark interaction [8]. The valence quarks are the three quarks we normally talk about as building up a nucleon. In addition there is a "sea" of quark-antiquark pairs continuously being created/annihilated from/to gluons, called sea quarks. In LEP, a former electron positron accelerator at CERN, the electrons collided with the positrons with a centre of mass energy of

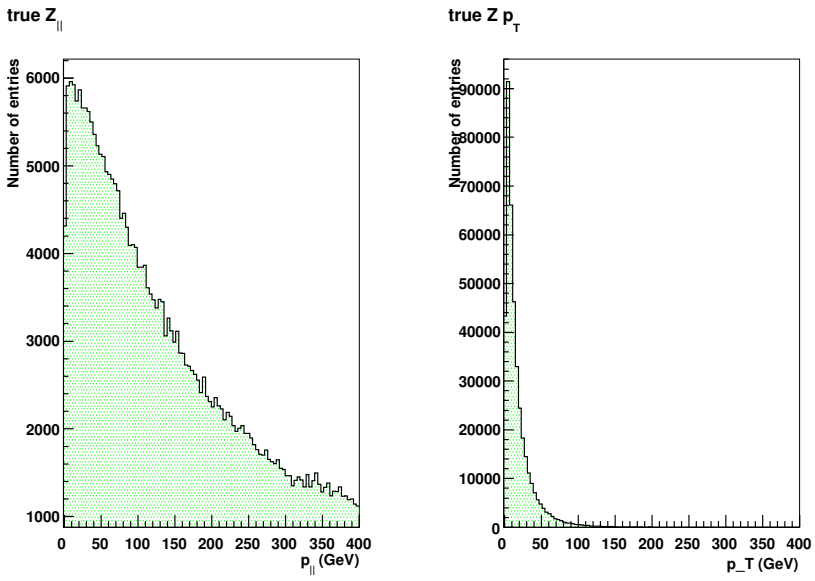

Figure 1.1: MC truth Z^0 momenta, $\sqrt{s} = 7$ TeV

91 GeV. Since electrons and positrons do not have an interior structure [5], a head-on collision would provide 91 GeV of available energy. In the LHC, by colliding protons with an interior structure, the energy available depends on exactly how much energy the quarks or gluons had. One can produce particles with mass up to about one sixth of the total energy.

Cross section, σ, is an area proportional to the probability of a process to happen. The unit of σ is barn $= 10^{-28}m^2$. σ is related to the luminosity, $\mathcal{L}$, like this:

$$\mathcal{L} \cdot \sigma = \dot{N}, \tag{1.1}$$

where $\dot{N}$ is the number of events with the chosen process per second. More about luminosity at the LHC in 2.2.5.

The cross section for a Z^0 to be produced in the LHC is energy dependent. At 7 TeV $\sigma(\mathrm{pp} \rightarrow \mathrm{Z}^0 + \mathrm{X}) = 25.2$ nb [5][9].

1.3.2 Z^0 decay

Z^0 can decay leptonically, $Z^0 \rightarrow l\bar{l}$, or hadronically, $Z^0 \rightarrow$ h.

[5] At least not at these energies

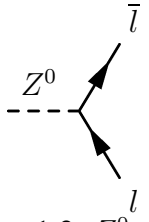

Figure 1.2: $Z^0 \rightarrow \mathrm{l\bar{l}}$

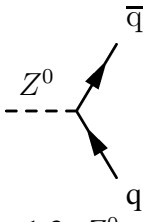

Figure 1.3: $Z^0 \rightarrow \mathrm{q\overline{q}}$

In fig. 1.2 there are six possibilities, $l = e^-, \nu_e, \mu^-, \nu_\mu, \tau^-, \nu_\tau$ and their corresponding antiparticles. In fig. 1.3 there are $5 \cdot 3 = 15$ possibilities, $q = u, d, c, s, b$ (Z^0 is lighter than the top quark, and can hence not decay to top). The factor 3 come from the three different colours each quark can carry. Assuming that each possibility has an equal chance of happening, one would expect:

$$\frac{\Gamma(Z^0 \rightarrow hadrons)}{\Gamma_{tot}} = \frac{15}{15+3+3} = 71,4\% \tag{1.2}$$

$$\frac{\Gamma(Z^0 \rightarrow l\bar{l})}{\Gamma_{tot}} = \frac{\Gamma(Z^0 \rightarrow \nu_l\overline{\nu_l})}{\Gamma_{tot}} = \frac{1}{21} = 4,76\% \tag{1.3}$$

And hence the sum of the three neutrinos: $4,76\% \cdot 3 = 14,29\%$. Comparing with the experimental values from table 1.3, one observes that they do not fit. The main reason is that the weak interaction is treated alone. The electroweak unification explains the experimental results, modifying the vertex factors by putting the leptons in weak isospin doublets.

Mass: (91.1876$\pm$ 0.0021) GeV
Lifetime: 2.64 $\cdot 10^{-25}$ s
Decay products:
- e^+e^- (3.363 $\pm$ 0.004) %
- $\mu^+\mu^-$ (3.366 $\pm$ 0.007) %
- $\tau^+\tau^-$(3.370 $\pm$ 0.008) %
- invisible (20.00 $\pm$ 0.06) %
- hadrons (69.91 $\pm$ 0.06) %

Table 1.3: Z^0 characteristics [5]. Invisible is to be interpreted as neutrinos

$\sigma(Z^0 \rightarrow \tau^-\tau^+)$ = $\sigma(\mathrm{pp} \rightarrow \mathrm{Z^0 + X}) \cdot \mathrm{Br}(Z^0 \rightarrow \tau^-\tau^+)$
$= 25.2 \cdot 0.0337 = 0.8486$ nb [5][9].

1.4 The τ-lepton

As seen in the section 1.3.2 the Z^0 can decay into two taus who further decay into leptons and hadrons as illustrated with the Feynman diagram in figure 1.4.

J (spin) =$\frac{1}{2}$
Mass m = (1776.84 ± 0.17) MeV
Mean life $\tau = (290.6 \pm 1.0) \cdot 10^{-15}$ s
c$\tau = 87.11\mu$ m

Table 1.4: Some properties of tau: [5]

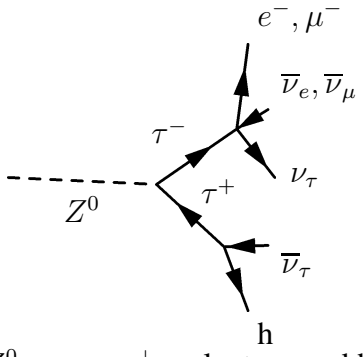

Figure 1.4: $Z^0 \rightarrow \tau^-\tau^+ \rightarrow$ leptons and hadrons

Table 1.3 shows that the Z^0 decays to all charged leptons with the same probability. This property is called the **lepton universality**. When the masses are accounted for, or the amount of energy is so large that the mass can be neglected, the probability to create an electron-antielectron pair is the same as for creating a muon-antimuon pair and for tau-antitau. Except from the mass and the properties connected to it, the electron, muon and the tau are all the same. I call muon and tau the big brothers of the electron. They're similar, only heavier.

The τ-lepton was discovered at SLAC [6] in 1975 by Martin L. Perl. In 1995 he received a shared Nobel Prize in Physics *"for pioneering experimental contributions to lepton physics"* and *"for the discovery of the tau lepton"*. Tau received its name from the Greek word triton meaning third - the third charged lepton. The observation of the tau was the first evidence of a third generation.

> (...) there was no other evidence for a third particle generation. Two sets of particles - u, d, $\mathrm{e}^-, \nu_\mathrm{e}$, and c, s, μ^-, ν_μ - seemed acceptable, a kind of doubling of particles. But why three sets?
>
> *Martin L. Perl* [10]

With a mass of nearly 1.8 GeV, tau is the heaviest lepton. It can decay to μ (17.36%), e^- (17.84%), and to hadrons (64.8%), as shown in table 1.5.

[6] Stanford Linear Accelerator Center in California

Some processes end up with electrons or muons as their decay products. Electrons or muons coming from taus are therefore difficult to distinguish from the ones coming from other processes. Except from some information gained from the impact parameter, electrons and muons are non-reducible components of the background.

By choosing hadronic tau decay one must fight backgrounds that are reducible. Hadrons are decay products in many other processes as well, but the hadrons coming from a tau decay are often collected in a narrow cone, and can hence be distinguished from other hadron decays, i.e. QCD-background. A hadronically decaying tau decays mostly to pions (mesons built up from up and down quarks), but also to kaons (mesons containing a strange quark) and rarely to other particles. In order to conserve lepton number, there is always a tau-neutrino among the decay products. This neutrino will get much attention in the rest of the thesis while we try to compensate for the energy it carries away. Because of the charge conservation, an odd number of charged pions (or kaons) have to occur, while the number of neutral pions can be arbitrary as long as there is enough energy to produce them. Examples of the hadronic tau decay, and their branching fraction:

Decay mode	Γ_i/Γ
$\tau^- \rightarrow e^-\overline{\nu}_e\nu_\tau$	$(17.36 \pm 0.05)\%$
$\tau^- \rightarrow \mu^-\overline{\nu}_\mu\nu_\tau$	$(17.85 \pm 0.05)\%$
$\tau^- \rightarrow \mathrm{h}^-\mathrm{X}$	$(48.68 \pm 0.11)\%$
$\tau^- \rightarrow \mathrm{h}^-\ \mathrm{h}^-\ \mathrm{h}^+\mathrm{X}$	$(14.56 \pm 0.08)\%$

Table 1.5: Main decay modes of the tau — the first two leptonically and the latter two 1-prong and 3-prong respectively [5].

1.5 The Higgs boson

The Higgs theory describes an omnipresent field which all massless particles pass through without reacting with it. The massive particles, on the other hand, react with the Higgs field, which is what gives them mass. This means that the massive particles are not originally massive, but some kind of potentially massive. One can draw a (weak) analogy to colours: unless you put it in light, a blue ball isn't blue, but potentially blue.

The predictions of the Higgs field require also that the field itself should be seen as a massive particle — the Higgs particle, just like W and Z^0. Searching for this particle gives thus an opportunity to search for the whole theory. The problem is where to look, because the mass is poorly determined by theory. Experiments

at CERN and Fermilab, however, have shown — with 95% certainity — that the Higgs mass must be less than 114 GeV/c^2.

Theoretical boundaries indicate that the Higgs particle should be light enough to be detected by the LHC with 14 TeV collision energy. There should therefore be a high probability of finding the Higgs particle in the next few years, or — at a high confidence level — exclude it.

A significant background to the H^0 is from Z^0 because of their similar decay modes. If they have very different masses, they can be discriminated with a good method of calculating the invariant mass. If not, one might use polarisation to distinguish them. The Z^0 have J=0 and H^0 have J=1, and the conservation of the spin affects the kinematics of the decay products [11].

1.6 Beyond the Standard Model

1.6.1 Dark Matter

Measurements from outer space, latest with WMAP [7], tell us that there is a lot more energy and matter in the universe than can be observed [12]. In fact, the visible universe is only 4% of the whole universe [4]. Dark matter (DM) does not interact electromagnetically, nor weakly, nor strongly, only gravitationally [8]. That means that it will escape all layers in ATLAS, and the only chance of finding it there, is by looking for missing energy. These kinds of particles are not explained in the SM, and hence an extension is needed. One extension candidate is Super Symmetry (SUSY).

1.6.2 SUSY

Super symmetry is the most studied extension of the SM. It predicts every boson to have a fermionic supersymmetric partner (names with -ino endings), and vice versa (names starting with s). E.g. the tau has a partner with spin 1 called stau, and the Z has a partner with spin 1/2 called zino. If the super symmetry were a conserved symmetry, the supersymmetric partners (sparticles) would have just the same mass as their partners (particles). But judging from the fact that they are all undiscovered, they have to be heavy, and SUSY must be broken. There is a great hope that the LHC will provide enough energy to make sparticles, and that ATLAS or CMS can detect them as missing energy.

[7] Wilkinson Microwave Anisotropy Probe (WMAP) has produced a wealth of precise and accurate cosmological information

[8] This assertion is model dependent

SUSY-Higgs

Although the Higgs is predicted as a part of the SM, it is also predicted beyond it. SUSY predicts 5 Higgs-particles, some even not neutral as the SM Higgs, but charged.

1.6.3 Other

There are also other theories lying beyond the SM, like Technicolour, and String theory, just to mention a few.

Chapter 2

the LHC accelerator and ATLAS detector

A study of $Z^0 \rightarrow \tau^-\tau^+$ requires proton collisions with centre-of-mass energy higher than the Z mass, 91 GeV. Such experimental setup is too expensive to build by the University of Bergen. No single European country alone can not afford to build such a large machine. That's one of the reasons a European Center for Nuclear Research have been built: to cooperate with many countries so that together they can afford to build and operate huge particle accelerators. The centre i located on the Swiss-French border, near Geneva and is called CERN. CERN is the french acronym "Conseil Européen pour la Recherche Nucléaire".

The pilot project in CERN nowadays is the LHC with its six detectors. The particle physics group in Bergen works on the experiment called ATLAS. This chapter is mostly dedicated to the history of CERN, the particle accelerator LHC and one of LHC's experiments ATLAS.

2.1 The history of CERN

Before taking a deeper look at this huge experiment, let's go back in time and look at the development of CERN [13].

2.1.1 The 50's

After some years with ideas and pioneers dreaming of a European collaboration on nuclear physics, CERN officially came into being in 1954, with the following 12 member states: Belgium, Denmark, France, the Federal Republic of Germany, Greece, Italy, the Netherlands, Norway, Sweden, Switzerland, the United Kingdom, and Yugoslavia. As you can see, Norway was a member from the beginning.

Three years later the first accelerator started operating. It was a 600 MeV Synchrocyclotron (SC). In comparison, the LHC is designed to accelerate up to 7 000 000 MeV — in each direction. SC was only used for nuclear research, i.e. accelerating nucleons, and served that purpose well enough for 33 years.

For the purpose of particle physics, accelerating protons, the Proton Synchrotron (PS) started operating in 1959. The beam energy was 28 GeV. At this time there were only fixed target experiments, meaning that an accelerator accelerates particles up to a certain energy and shoots them on a fixed target — like a car crashing in a wall.

2.1.2 The 60's

Most of the sixties went to collecting data in a very slow way, namely by detectors called bubble chambers. The particles are going through a chamber of fluid near the boiling point. By going through, the particle make the fluid boil just along its path. A picture is taken and hence the particle path is detected. See picture 2.1. All these pictures had to be analysed, and the bubble chamber had to be reinitialised to be used again. This took time, and a study of rare phenomena was nearly impossible. In 1968 Georges Charpak revolutionised the detection. By developing

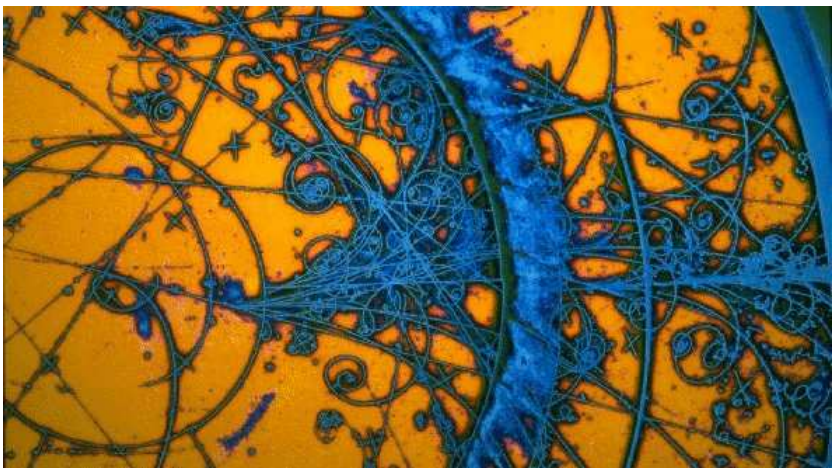

Figure 2.1: Particles making paths in a bubble chamber [1]

the multiwire proportional chamber, the detection went from analogue to digital, which meant that very much faster counting rates were possible.

2.1.3 The 70's

January 27th 1971 the world's first proton-proton collider came into operation, the ISR, Intersecting Storage Rings, at CERN. In the analogy with the car, proton-proton collisions are like two cars crashing head-on with equal velocity. Compared to fixed target experiments, the proton-proton collisions do not waste a lot of energy in recoil, and is therefore much more energy efficient. The PS was used to inject accelerated proton beams into the ISR. As the name says, the ISR stores the beams, and does not accelerate them further.

The ISR was the first of CERN's facilities on the French side of the border, and with this CERN became international ground, as it is today.

In 1973, the neutral current, theoretically predicted by Sheldon Glashow, Abdus Salam and Steven Weinberg as they combined electromagnetic and weak force into one, was found. This was an indirect evidence for the Z^0 particle.

The first accelerator crossing the Swiss-French border was the SPS, Super Proton Synchrotron. It was CERN's first giant ring, originally constructed to operate with a beam energy of 300 GeV, but later upgraded to 450 MeV. In 1979 SPS was transformed into a proton-antiproton collider. Both the PS and the SPS is still in use feeding larger colliders with protons. Today it is the last link of the protons being put into the Large Hadron Collider.

2.1.4 The 80's

A great exploration of the world of particles were done with SPS, as it collided protons which made researchers find the inner structure of protons as well as discovering the W and Z bosons in 1983. The latter gave Carlo Rubbia and Simon van der Meer the Nobel prize only a year later!

In 1986 the SPS started colliding ions as well. The reason was to search for Quark Gluon Plasma, QGP, the matter of which the universe — according to the big bang theory — consisted of in its early beginning. This search continued until year 2000 with heavier and heavier nuclei, from oxygen and sulphur to lead ions. At the end there was considerable evidence that a new type of matter was being produced. The search for QGP continues with the LHC, particularly in ALICE.

2.1.5 The 90's

The 90's was the LEP-decade. The Large Electron-Positron collider (LEP) was the largest electron-positron accelerator ever built to date. It was 27 km in circumference and started in 1989, operating at 100 GeV. After seven years it had produced 17 million Z particles, providing a detailed study of the electroweak

interacting. The next four years its energy was doubled in order to produce W bosons as well, making the study of the electroweak force reliable.

But the LEP was not the only great thing CERN did in the 90's. An other, quite different revolution, not only for scientists, was that CERN scientist Tim Berners-Lee in 1990 invented the World Wide Web. At the very beginning Tim Berners-Lee had defined the Web's basic concepts, the URL, http and html, and he had written the first browser and server software. Slowly the world wide web extended in number of servers and users, and became public, i.e. open for all, in 1994.

In 1995 CERN's Low Energy Antiproton Ring (LEAR) produced nine anti-hydrogen atoms over a three-week period. They lived for forty billionths of a second, travelled ten metres and annihilated in contact with ordinary matter. This was an important step in studying the asymmetry between matter and anti-matter.

2.1.6 2000-2010

In November 2000 the LEP ended its service, and was removed from the tunnel to make space for the next generation of proton-proton-collider: the LHC.

A new milestone in the anti-matter world was reached in 2002 as two CERN experiments, ATHENA and ATRAP, stored millions of anti-hydrogen particles that were slowed down enough to be studied.

2.1.7 2010 - · · ·

And today the LHC has finally started up. The next years will, undoubtedly, be very exciting. New phenomena will occur, and a jungle of theories will be cleaned up — most of them falsified, but hopefully also some verified.

2.2 The LHC

LHC stands for Large Hadron Collider and, as the name tells us, it collides hadrons, and it is large. With a circumference of 27 km and a designed energy collision at 14 TeV it is the largest particle accelerator in the world, both in size and in accelerated energy. It is situated under the Swiss-French border with headquarters in Geneva. The LHC accelerates mostly protons, but also lead ions. On points around the circle of the LHC, experiments like ATLAS are placed. All of them detect particles, but as described in section 2.2.7, in slightly different ways, and with different purposes.

2.2.1 The construction

The LHC is a very complex machine. On November 30th 2009 it took the world record in being the installation with the highest man-made energy acceleration ever made. 2.36 TeV were achieved, against the previous world record, held by Tevatron in Stanford, USA, at 1.96 TeV [14]. The following section will give you an overview of the main tasks of the LHC.

- **Reception and storage**

  Some of the older accelerators at CERN will be used to "feed" the LHC with particles. It all starts with hydrogen gas, which is ionised, i.e. the electrons are filtered away. The remaining protons are first accelerated in the linear accelerator LINAC2, via the PS Booster fed into the Proton Synchrotron (PS) which accelerates the protons to 25 GeV, and further sped up in Super Proton Synchrotron (SPS) to 450 GeV. SPS provides the LHC with 450 GeV protons in both directions. See figure 2.2.

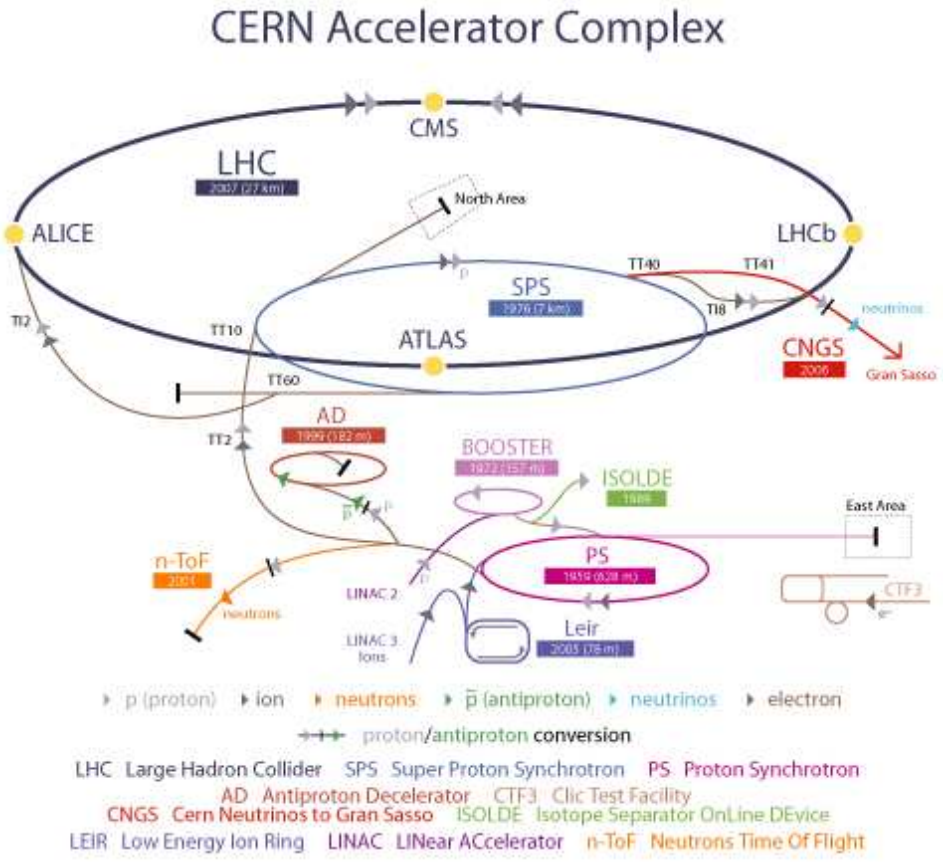

Figure 2.2: Accelerator complex [1]

- **Acceleration**

  The LHC then accelerates the beams up to (ideally) 7 TeV, trough an accelerator cavity. The LHC has one such cavity, where the protons are "kicked" once per round, getting a higher and higher speed and hence more energy. The collision energy in 2010 will be 7 TeV until the experiments have collected an integrated luminosity of 1 fb^{-1} of data. That will take 18-24 months [15].

- **Collision**

  The LHC is constructed to collide the beams inside the four detectors ATLAS, CMS, ALICE and LHCb.

2.2.2 Magnets

1232 **dipole magnets** are placed around the LHC. Their task is to bend the beam around the tunnel. They are the largest magnets in the LHC, each 15 metres long. The energy up to which the protons can be accelerated is dependent upon the strength of the magnetic field in the dipoles. Magnets are also used to focus the beam, which is very important. Two main reasons for that is that the protons are so small that to collide them in this experiment, is comparable of shooting two needles from 10 km apart, hoping to get them to collide head-on. To increase the hitting probability, the LHC accelerates 1.1×10^{11} protons in 2808 bunches around the ring. The other reason for focusing the beam is that the tube in which the protons are accelerated, are some centimetres in diameter, and if a proton hits the wall, it is lost and even worse: these extremely large and highly energetic proton bunches may destroy the experiments or the LHC if they are not controlled well enough. To focus the beam, the LHC is equipped with 392 **quadrupole magnets**, each 5-7 metres long. Approaching each detector, the beam is even more concentrated with **octopole**, **sextupole** and **decapole magnets** in order to increase the collision probability.

The magnets are superconducting electromagnets. To produce the superconducting properties, the cables need to be cooled down to 1.9K. That is colder than outer space, which is 2.7K.

The dipoles of the LHC represented the most important technological challenge for the LHC design. In a proton accelerator like the LHC, the maximum energy that can be achieved is directly proportional to the strength of the dipole field, given a specific acceleration circumference. At the LHC the dipole magnets are superconducting electromagnets and able to provide the very high field of 8.3 T. No practical solution could have been designed using "warm" magnets instead of superconducting ones [16].

2.2.3 Vacuum

To avoid collisions with other particles, an ultra-high vacuum is provided in the beam pipe. This equals a hydrogen gas density below 10^{15} H_2 m^{-3} to ensure the required 100 hours beam lifetime. The hydrogen gas density is the gas densities normalised to hydrogen taking into account the ionisation cross sections for each gas species.

In the interaction regions around the experiments the densities will be below 10^{13} H_2 m^{-3}, in order to minimise the background to the experiments.

In addition to beam vacuum, the LHC has two other vacuum systems: insulation vacuum for cryomagnets and insulation vacuum for helium distribution line (QRL).

Driven by the requirements for the cryogenic system, the room temperature pressure of the insulation vacuum before cool-down does not have to be better than 10 Pa (10^{-1} mbar). At cryogenic temperatures, in the absence of any significant leak, the pressure will stabilise itself around 10^{-4} Pa (10^{-6} mbar) [17].

2.2.4 Coordinates

In order to have a common understanding of directions in the LHC and related experiments, there is a convention of having a coordinate system like this:

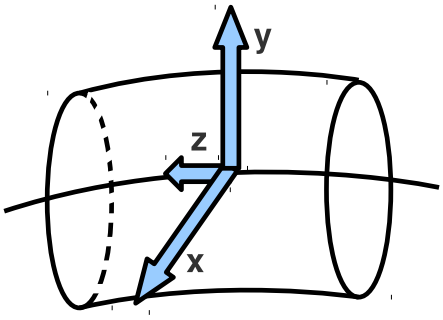

Figure 2.3: LHC coordinates

The z-direction is along the beam axis, the y is pointing upward to the Swiss-French surface, and the x-direction points towards the centre of the ring.

ATLAS uses the same set of coordinates, but in addition it is found convenient to use η (eta [1]) and ϕ (phi) as well. They are defined as follows.

$$\eta = -\ln(\tan\left(\frac{\theta}{2}\right)), \tag{2.1}$$

[1] pseudo rapidity

where θ is the angle between the particle track and the z-axis. η is convenient because it has small steps in the region near the beam pipe, where much interesting physics occurs. ϕ is the transverse angle, i.e. the angle between the particle track projected into the xy-plane and the x-axis. From the definition of the scalar product, one gets

$$\phi = \cos^{-1} \frac{p_{x1} \cdot p_{x2} + p_{y1} \cdot p_{y2}}{(p_{x1}^2 + p_{y1}^2)(p_{x2}^2 + p_{y2}^2)} \tag{2.2}$$

From figure 2.4, one can see the distribution in η when having a homogeneous θ-distribution.

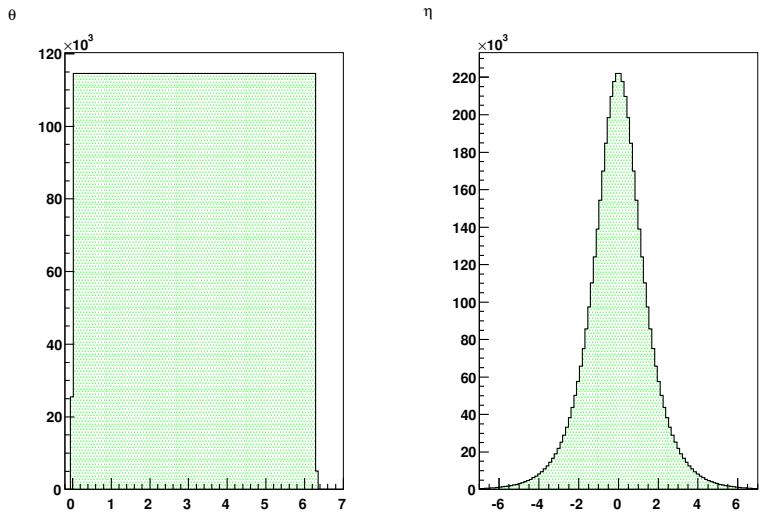

Figure 2.4: Homogeneous θ-distribution with its corresponding η-distribution.

The surface element for spherical coordinates is $\mathrm{d}r\mathrm{d}\cos\theta$, and a homogeneous sphere will hence have the η distribution shown in figure 2.5 where $\cos(\theta)$ is uniform. In proton-proton collisions at the LHC, the particle density is higher in the forward direction, but expected to be roughly uniform in η. This is why η is used instead of $\cos\theta$.

2.2.5 Luminosity

Luminosity, $\mathcal{L}$, is defined as a relation between the production rate and the cross section:

$$\mathcal{L} = \frac{\dot{N}}{\sigma_{tot}} \tag{2.3}$$

where $\dot{N}$ is the number of particles produced per second and σ_{tot} is the total cross section. From this definition one can see that luminosity has dimension $s^{-1}m^{-2}$.

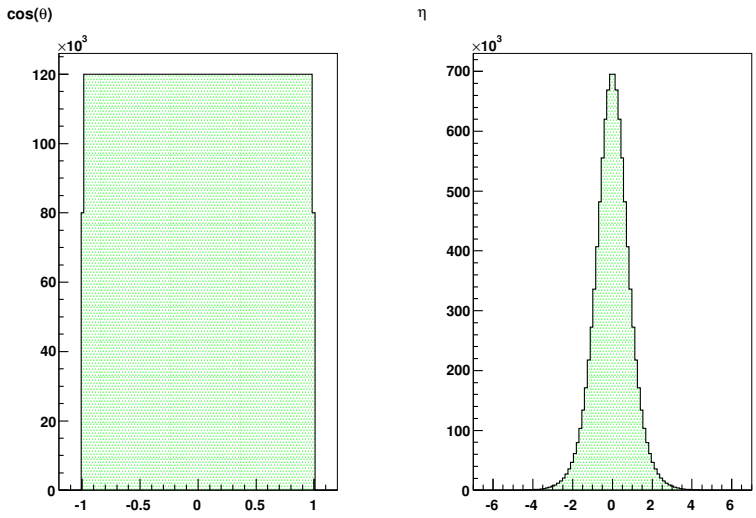

Figure 2.5: Homogeneous $\cos(\theta)$-distribution with its corresponding η-distribution.

The luminosity is the number of scattered particles per cross section. One of the special advantages to the LHC is the high luminosity, obtained through a high flux of particles. During normal operation, the LHC will have 2808 bunches in each beam, with each bunch containing about 10^{11} protons. This is the reason why the LHC is operating with protons only, and not proton-antiproton, which had been easier both in hitting each other — because of their opposite charge — and circulating — one can use same magnet system to accelerate in both directions. But since antiprotons are harder to produce in large quanta, it has been decided to use only protons.

Integrated luminosity is a certain amount of collected data. With the LHC running with a certain luminosity, the time needed to collect a certain amount of a certain particle can be calculated as follows: [6]

$$\int \mathcal{L}\,\mathrm{d}t = \frac{N - B}{\sigma_{th} \cdot a \cdot \epsilon} \tag{2.4}$$

where N is the number of observed particles, B is number of background particles, σ_{th} is the theoretical cross section, a is the acceptance and ϵ is the efficiency.

The cross section is determined from the physics as explained in 1.3.1, while the luminosity is determined by the accelerator:

$$\mathcal{L} = \frac{b}{4\pi}\frac{N_1 N_2}{\sigma_x \sigma_y} f_{rev}, \tag{2.5}$$

Quantity	Number
Circumference	26 659 m
Dipole operating temperature	1.9 K (-271.3°C)
Number of magnets	9593
Number of main dipoles	1232
Number of main quadrupoles	392
Number of RF cavities	8 per beam
Nominal energy, protons	7 TeV
Nominal energy, ions	2.76 TeV/u [Energy per nucleon]
Peak magnetic dipole field	8.33 T
Min. distance between bunches	$\sim$7 m
Design luminosity	1034 cm^{-2} s^{-1}
No. of bunches per proton beam	2808
No. of protons per bunch (at start)	1.1×10^{11}
Number of turns per second	11 245
Number of collisions per second	600 million

where b bunches circulates with a frequency f_{rev}, $N_{1,2}$ is the number of particles in each bunch and $\sigma_{x,y}$ is the area of the bunch projected unto the xy-plane.

2.2.6 Energy

The LHC is built to gain protons colliding head-on with an energy of 7 TeV each, hence 14 TeV in the collision point. This makes the LHC the particle accelerator with the highest colliding energy ever made. In outer space, however, there are particles colliding with extremely large energies, e.g. when accelerating towards a black hole. In the atmosphere of the earth, there are also collisions with higher energy than in the LHC. The proton consists of quarks and gluons, which means that it is not really protons as such, but the sub-particles inside them, that collide with each other. When two energy-rich quarks hit each other they can in reality get up to 1 TeV, and of course all energies below. With this much energy a lot of particles can be made, mainly well-known particles in the standard model. One of the biggest challenges with analyses is to separate interesting phenomena from the large amount of quarks made, called QCD-background — a jungle of all the already discovered particles. But, since more energy is available in the LHC than ever before, there is a large possibility for new phenomena to be discovered. That is one of the main motivations for building such a large accelerator as the LHC.

2.2.7 The experiments

There are six experiments along the LHC ring. Two large: ATLAS and CMS, two medium-size: LHCb and Alice, and two much smaller: TOTEM and LHCf[18]

ATLAS and CMS

ATLAS, **A** **T**oroidal **L**HC **A**pparatu**S**, and CMS, **C**ompact **M**uon **S**olenoid, are multi-purpose experiments studying a range of physical phenomena, like searching for the Higgs boson, extra dimensions and dark matter particles. The reason of having two detectors searching for the same thing is that when CMS claims a discovery, ATLAS can verify it as well as the other way around. They are constructed in different ways of different teams, and can be considered as independent of each other.

> It is always a good plan for a speculative experimenter to have two experiments going, or at least one going and one being built. *Martin L. Perl* [10].

ALICE

ALICE, **A** **L**arge **I**on **C**ollider **E**xperiment, will study the conditions closely after the Big Bang by colliding lead ions. The goal is to make a quark-gluon plasma where quarks and gluons no longer are bounded to each other in the way know today, and study this condition. The LHC will accelerate lead one month a year and protons the remainder of the year.

LHCb

LHCb, **L**arge **H**adron **C**ollider **b**eauty, will use b-quarks to find out why the universe is made up of matter, and not anti-matter. In other words, they are looking for symmetry breaking when matter is produced.

TOTEM

TOTEM, **TOT**al **E**lastic and diffractive cross section **M**easurement, will with its construction made for studying forward boosted particles, not colliding particles, study physical phenomena which other detectors are unable to study. Examples are measuring the size of the proton and measuring the LHC luminosity very accurately. TOTEM is located near the CMS detector.

LHCf

LHCf, **L**arge **H**adron **C**ollider **f**orward, will study forward particles to simulate cosmic rays, to calibrate other experiments, as well as trying to understand what is going on some hundred kilometres over our heads. LHCf is located near the ATLAS detector.

2.3 ATLAS

ATLAS is built in several cylindrical layers with end-caps around one of the LHC's collision points. The innermost layers, the inner detector, will as precisely as possible measure the tracks of every trackable particle. The next layers, the calorimeters, is measuring the energy of electrical particles like electrons and photons, and of hadrons. Outermost the muon detector tracks the only detectable particle going through all the other layers: the muon. In the following there is an in-depth description of every layer.

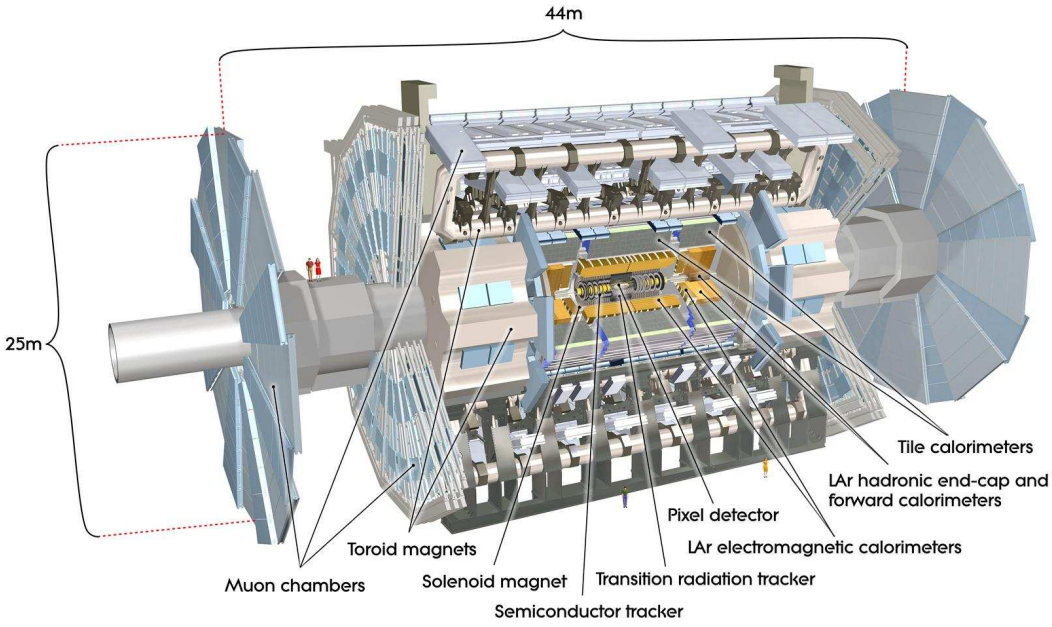

Figure 2.6: ATLAS Experiment [1]

2.3.1 Inner detector

The ATLAS inner detector (ID) is made to track the charged particles. The ATLAS ID consists of three layers. The innermost is the **Pixel** detector. It is built

up of three barrel layers and three end-cap disks on each side. The pixel detector consists of 1 744 modules with 46 080 silicon pixels in each module, adding up to 80 million channels to read out. There are two sizes of the pixels, short and long, with the respective resolutions: 12 μm in rϕ and 69 μm (short)/77 μm(long) in z. Being the innermost detector layer in ATLAS, it is extremely important to have a good resolution in order to get a good reconstruction of the impact parameter and vertex. The next layer is the **Semi Conductor Tracker (SCT)**. It uses silicon micro-strip detectors for detection. About 2000 of these detectors were tested in Bergen. The SCT is built up of four barrels and nine end-cap disks at each side. The resolution is a bit lower than in the pixel detector: 16 μm in rϕ and 580 μm in z, both for barrel and end-caps. The outermost layer in the inner detector is the **Transition Radiation Tracker (TRT)**. It uses straw detector elements to detect the particles. It consists of a barrel part with 52 544 straws aligned along the z-axis. And an end-cap part with 319 488 straws. Whilst the pixel and the SCT have a high resolution and with a small number of precision measurements, the TRT have a higher number of measurements with a lower resolution. The main task of the TRT is to identify the particles.

2.3.2 Solenoid

The ATLAS magnet system consists of one solenoid and eight barrel toroids.

The **solenoid** is between the inner detector and the calorimeters, providing a very uniform magnetic field for measuring the momentum of the charged particles. It is a 2T superconducting magnet [19].

2.3.3 Calorimeters

Calorimeters measure the energy of neutral and charged particles by absorbing them with metal plates. By absorption the particles makes "showers" which then are detected by sensing elements. Two main types of calorimeters absorb different types of particles. The **electromagnetic (EM) calorimeter** absorbs photons and electrons, whilst the **hadronic calorimeter** absorbs hadrons (like protons, neutrons and pions).

The EM calorimeter is the innermost and uses liquid argon (LAr) as sensing elements. The showers in the argon liberate electrons which are detected. The hadronic calorimeter uses plastic scintillators in addition to LAr as sensing elements and is built up of alternating layers of iron (14 mm) and scintillating tiles (3 mm). When hadrons with $E \geq 5$ GeV go through the iron, they can interact with it and make a hadronic shower. The tiles then scintillate, and the signal is read out by a photomultiplier of the end of each tile.

The calorimeters stop most of the known particles except from muons and neutrinos. Hadrons not absorbed in the calorimeters are called punch-throughs.

2.3.4 Toroids

Outside the calorimeters you'll find a huge construction of eight toroidal magnets surrounding the ID and the calorimeters like a barrel. It provides an average field of 0.5 T outside the barrel in a toroidal region outside the inner parts of ATLAS, not as uniform as inside the solenoid.

2.3.5 Muon detector

The outermost layers of ATLAS make up the muon spectrometer. The two main tasks of the muon spectrometer is to measure the tracks of the muons precisely, and to make a good trigger and pattern recognition.

2.3.6 Coverage

In the search for new physics, and especially for particles not visible in the detector, good coverage is needed in order to reconstruct missing energy. ATLAS has a good transverse (ϕ) coverage and forward/backward coverage near the beam pipe, measured with the pseudo-rapidity η [2]. ATLAS has a full 360° ϕ-coverage, while the coverage in η depends on the layer. The precision measurements for photons, electrons, muons, t-leptons and b-quark jets are performed over $|\eta| < 2.5$ (muon spectroscopy extends to $|\eta| < 2.7$), while the complete hadronic energy measurement extends over $|\eta| < 4.9$).[20]

2.3.7 Trigger

The ATLAS detector records raw data at a rate of 40 MHz. The following numbers about the trigger are estimated numbers on the nominal operation at $\mathcal{L} = 10^{34}\text{cm}^{-2}\text{s}^{-1}$ with startup number in parentheses ($\mathcal{L} = 10^{31}\text{cm}^{-2}\text{s}^{-1}$). The rate is too high to record on disk to be evaluated afterwards, therefore triggers is necessary. The triggers in ATLAS have to reduce the data rate from 40MHz to 200Hz, which is the storage capacity and what the offline computing power can handle. The trigger selects potentially interesting events and throws away the rest, following a pre-programmed selection tool. Since it is pre-programmed, a good understanding of what is searched for is required, which again requires good models of new physics.

[2] $\eta = -\ln(\tan\left(\frac{\theta}{2}\right))$

The triggers in ATLAS can be divided into three groups:

Level 1 trigger – L1

The L1 trigger has to make its decision within 2,5 μs to reduce the rate from 40MHz to 75kHz (40kHz at startup). The decision is made from multiplicities and energy thresholds from the calorimeter and muon detectors.

Level 2 trigger – L2

The L2 trigger is software-based and uses fine granularity and information not available to the L1 trigger. L2 uses L1 candidates and RoI, regions-of-interest, identified at L1, different for each type of events. L2 can initiate the processing of a new event every 10μs and have in average 40 ms available to process the algorithm. The L2 have to reduce the output data from $\sim$75 (40) kHz to $\sim$2(1) kHz.

Event Filter – EF

The EF is, as L1, performed by online software algorithms, but typically uses similar algorithms as used for the offline reconstruction. The EF has 4s available to reduce the rate from 2000 (1000) Hz to 200 Hz, corresponding to $\sim$300 MB/s. As L2, the EF works in a seeded mode, but EF now has access to the complete data for an event, since EF is performed after the event building step.

2.3.8 Tau trigger

As mentioned the trigger works in seed mode, meaning different trigger choices are made for different types of events. In the following the special trigger choices for taus will be presented. Again starting with L1.

L1 tau trigger

The algorithm considers a rectangular RoI, 4×4 towers (0.4×0.4 in $\Delta\eta \times \Delta\phi$), in both the EM and hadronic calorimeters. Among a maximum of eight trigger thresholds one requirement for passing the trigger is that the core 2×2 towers is a local E_T maximum. A candidate passing the L1 tau trigger requirements is passed to L2 for further consideration.

L2 tau trigger

The L2 tau trigger uses the full calorimeter granularity as well as track information to do a further selection on the L1 candidates. In order to reject more of the QCD

background, hadronic tau decay characteristics are exploited. In general, hadrons originating from a tau decay are more collimated and have lower track multiplicity than an ordinary hadronic shower.

Tau EF

The EF algorithm follows the offline reconstruction algorithm as closely as possible. In section 3.2 the offline tau reconstruction will be further described.

Information about the trigger section is collected from "Expected performance of the ATLAS Experiment", volume I [21] where there is more detailed information.

Chapter 3

Event reconstruction and selection of the τ-lepton

As mentioned among the τ-properties in table 1.4, the mean life of a τ-lepton is $\approx 290 \times 10^{-15} s$. Travelling with about the speed of light, it reaches in average 87.11μm. The beam pipe is in the order of cm, and the taus made at the collision point will never reach out to where the detector starts. Since there are no interaction point nor tracks for the tau directly, one needs to look at its decay products. The tau decays into electrons, muons or hadrons. Muons and electrons are coming from other sources as well, therefore mainly the hadrons-channel for τ-reconstruction is used to reconstruct the tau. All decay modes includes a ν_τ, and the lepton channel in addition a ν_e or ν_μ. These will escape detection, and carry away momentum. When reconstructing the tau, the missing energy from these neutrinos has to be taken into account. In this analysis, only the hadron channel will be studied, and E_T^{miss} from only one neutrino per tau decay needs to be taken care of.

Samples used for this study are (table 3.1):

Name	Data set
$Z^0 \rightarrow \tau^-\tau^+$	`mc09_7TeV.106052.PythiaZtautau.evgen.EVNT.e468`
J3	`mc09_7TeV.105012.J3_pythia_jetjet.evgen.EVNT.e468`
J4	`mc09_7TeV.105013.J4_pythia_jetjet.evgen.EVNT.e468`
$H^0 \rightarrow \tau^-\tau^+$	`mc08.105338.HerwigVBFH120tautauhh.evgen.EVNT.e515`
Real data	`data10_7TeV.00152409.physics_MinBias.merge.RAW`

Table 3.1: Data sets used in the analysis

In the first part of this chapter the chain from simulated and real data to

analysable output data will be described. In the second half τ-reconstruction is explained.

3.1 Simulation

To simulate colliding protons as similar to real data as possible the data need to go through three steps. The common ATLAS framework is called Athena.

Event generation

This is where the events are made. The mostly used tool for this in ATLAS is Pythia. Pythia uses a Monte Carlo (MC) generator to get randomised output within the processes and laws of the SM. The special package TAUOLA takes care of the tau decay. MC simulation is a mathematical method using random numbers to model a process [22]. One can of course also use MC simulations to look at the theoretical signals of e.g. SUSY. The event generation follows the rules of the underlying theory exactly and one get the exact MC truth variables which are good to use to check if analyses are done correctly.

Detector simulation

In the Detector Simulation, the simulated particles virtually go through ATLAS creating the same hits as real particles does. An exact knowledge about the different parts of ATLAS is then needed, and holes in the detector due to e.g. electronics or broken modules can be taken into account. Furthermore the amount and location of material in ATLAS must be known. Studies using cosmic runs have been very useful to study the response of the detector and verify the simulation.

Digitisation

The final step in the simulation is to digitise the tracks in the virtual detector as if they came from real data taking. The output of digitisation should therefore be directly comparable to real data.

3.2 Offline reconstruction

The data amount of 300 MB/s, or 2 MB/event[23], coming out of ATLAS after several triggers and filters is still for most physics purposes too large to handle in an efficient way. In offline reconstruction different output formats with smaller and more user friendly files are produced. Depending on type of study, one can choose a file format in the reconstruction chain with enough information, but not too large.

RDO Raw Data Object

As seen in figure 3.1, RDO is the file format coming out of ATLAS (or simulation of ATLAS in simulation studies). This is only used for specialised detector studies, like alignment. Contains all the information, including all detector information e.g. which channels were out.

ESD Event Summary Data

Reconstructed RDO file, used to make AOD and for detector performance studies.

AOD Analysis Object Data

Summary of an ESD file. Can be used for analyses.

DPD Derived Physics Data

Analysis specific processed AOD.

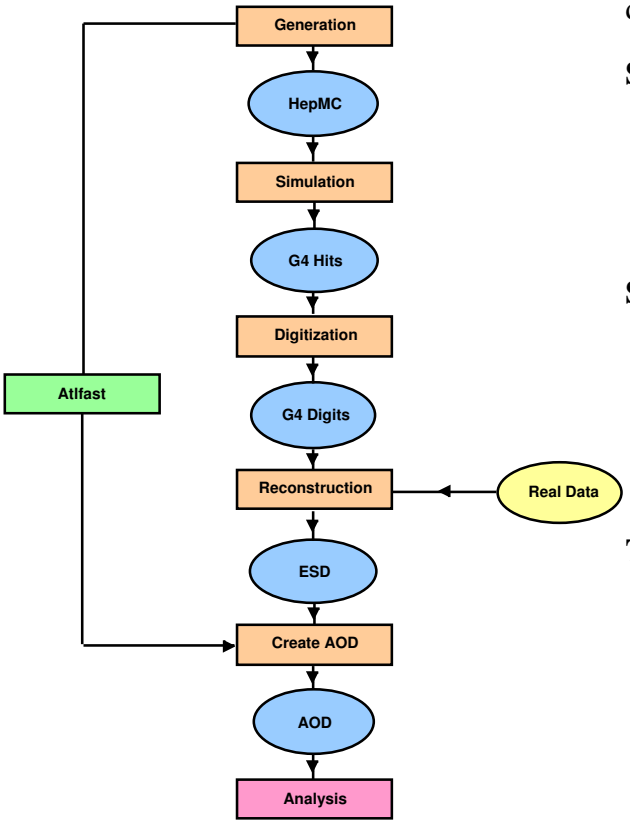

Figure 3.1: ATLAS data-flow, [2]

There are three ways of reducing the amount of data.

Skimming:

The extraction of events of interest from the data store; only the interesting events are kept.

Slimming:

Storing a subset of the data classes rather than a full copy of the event; only interesting objects are kept.

Thinning:

Limiting the objects based on usefulness for their physics [23]; only interesting information in objects, i.e. kinematics, is kept.

The sample of data used in this analysis is D3PDs made from AOD with TauD3PDMaker

by Peter Rosendahl. The AODs are made by the Tau Working Group. The $Z^0 \rightarrow \tau^-\tau^+$ -files contain one Z^0 decaying into two taus in each event. The centre-of-mass energy of this simulation is 7 TeV, the same as for the first fb^{-1} of data token. Root version 5.26b is used to analyse the D3PDs.

To reconstruct a tau, both tracking and calorimeter information is used. The algorithm starts either from a calorimeter seed or tracking seed (or both).

The D3PDs contains both MC generated data, and simulated data. The MC data contains the true momentum and direction of each tau. These are used to control the correctness of the code, as well as getting a clue of how good it possibly can get.

3.2.1 Truth matching

In truth matching, MC simulated information is used to find reconstructed tau candidates that match the MC true taus. The truth matching method used, is based on the direction only. ΔR is defined by the difference in η and ϕ of the MC simulated and reconstructed tau.

$$\Delta R = \sqrt{(\Delta\eta)^2 + (\Delta\phi)^2}. \tag{3.1}$$

See figure 3.2.

Lower ΔR means more similar directions and hence more likely to be the correct match, and we have chosen to consider reconstructed taus within $\Delta R < 0.1$ of a MC truth tau as approved taus [24]. By this method one obtains really good taus, but the disadvantage is that in real data there are no truth taus to match with.

3.2.2 Observables

After reconstruction a large number of variables are available. The momentum in z-direction differ from x- and y-direction because of boost in z-direction. (See figure 3.3). p_T is the transverse momentum, i.e. the momentum in the xy-plane and is defined as $p_T = \sqrt{p_x^2 + p_y^2}$.

The energy deposited in the detector is from the visible tau decay products, i.e. all particles except from neutrinos.

The angular distribution of the reconstructed tau is given by η and ϕ. See section 2.2.4 for definitions. One can see that the tau candidates are uniformly distributed in phi, i.e. no preferred direction in the xy-plane. This is as expected, as the protons collide along the z-axis. The η-case is intuitively more complicated, but in the scale of η, the distribution is near to uniform, as was the purpose with η.

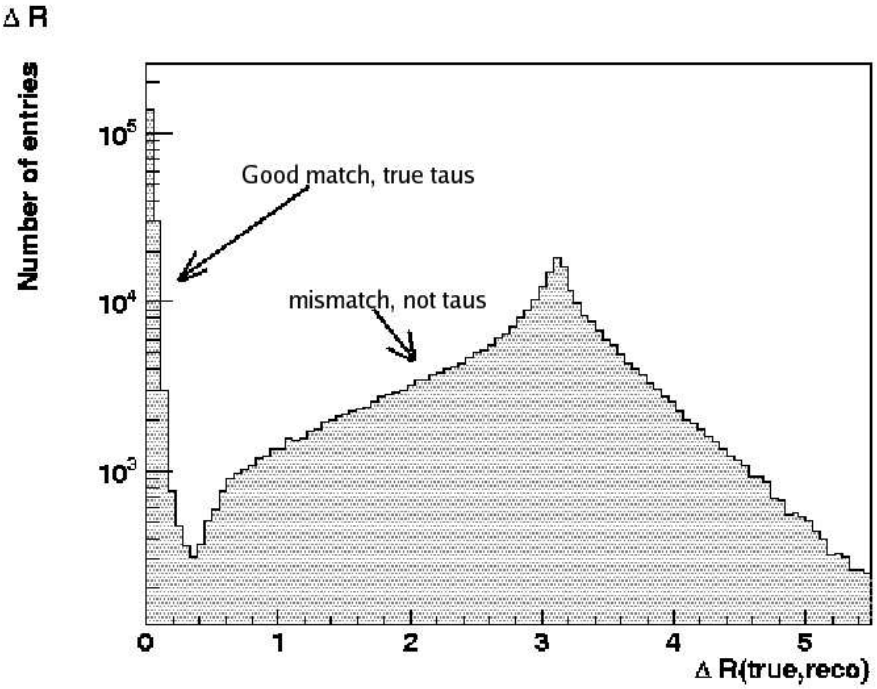

Figure 3.2: ΔR between truth and reconstructed tau. $\sqrt{s} = 7$ TeV

The charge of a particle is an important feature. The tau can only have charge ± 1, and a cut based on the whole tau pair having opposite signs is discussed in section 3.2.4.

In a single event there can occur many taus. In this sample there is one Z^0 decaying into two taus in each event. It is therefore mostly two taus in an event. In order to reconstruct the invariant mass, at least two taus are required. With events with more than two taus, the two leading (most energetic) taus are chosen.

With two tau candidates, the leading and the next-to-leading tau get different η distributions for them. The next-to-leading tau seems to be homogeneously distributed in θ, whereas the leading tau seems to have a preferred direction along the z-axis. This is explained by the leading tau to be more boosted than the next-to-leading tau. I.e. the leading tau gets its high energy from the Z^0-boost.

3.2.3 Background

There are several backgrounds which need to be addressed. The main task is to separate the taus in $Z^0 \rightarrow \tau^-\tau^+$ from products from other decay chains. These backgrounds are taus decaying from other processes than $Z^0 \rightarrow \tau^-\tau^+$, e.g. W $\rightarrow \tau\nu$, and QCD jets (showers of hadrons), that look like taus. The latter are

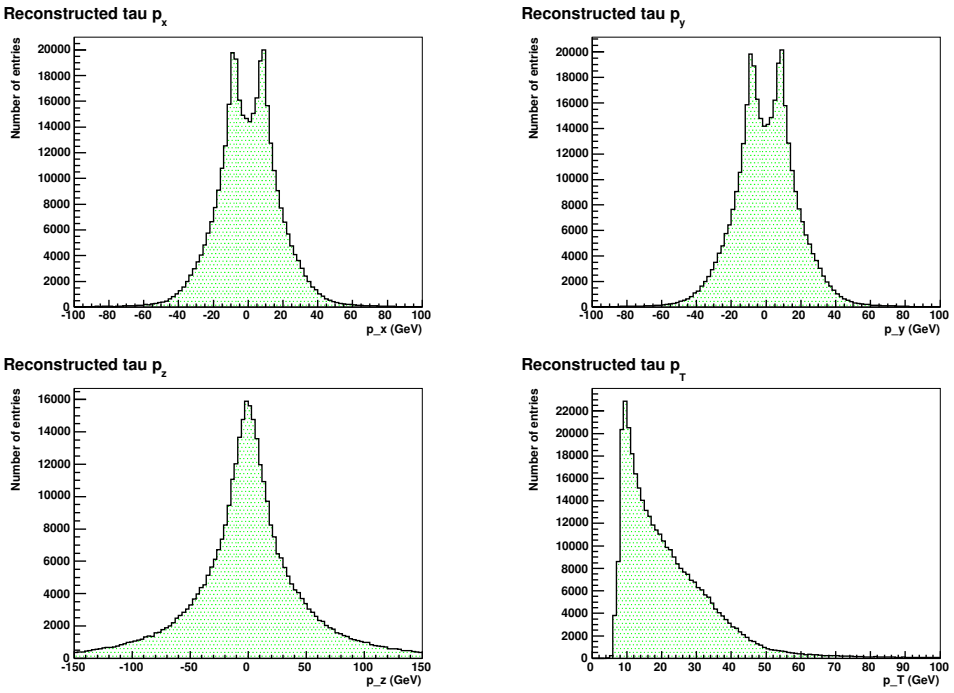

Figure 3.3: Momenta of reconstructed tau candidates, $\sqrt{s} = 7$ TeV

called fake taus. QCD jets is for convenience divided into energy ranges as shown in table 3.2, where the leading track in the jet determines the placing.

Name	Energy range	σ in used sample	# of entries in used sample
J0	8-17 GeV		
J1	17-35 GeV		
J2	35-70 GeV		
J3	70-140 GeV	$2.1960 \cdot 10^3$ nb	1317432
J4	140-280 GeV	87.8487 nb	355066
J5	280-560 GeV		
J6	560-1120 GeV		
J7	1120-2240 GeV		
J8	2240- GeV		

Table 3.2: Energy ranges for QCD

Since $m_Z^0 = 91$ GeV, the main QCD background of $Z^0 \rightarrow \tau^-\tau^+$ is J3 and J4. QCD with only two jets in an event is called dijet, and is the type of jets most similar to two tau decays. This analysis will hence consider J3 and J4 dijets as

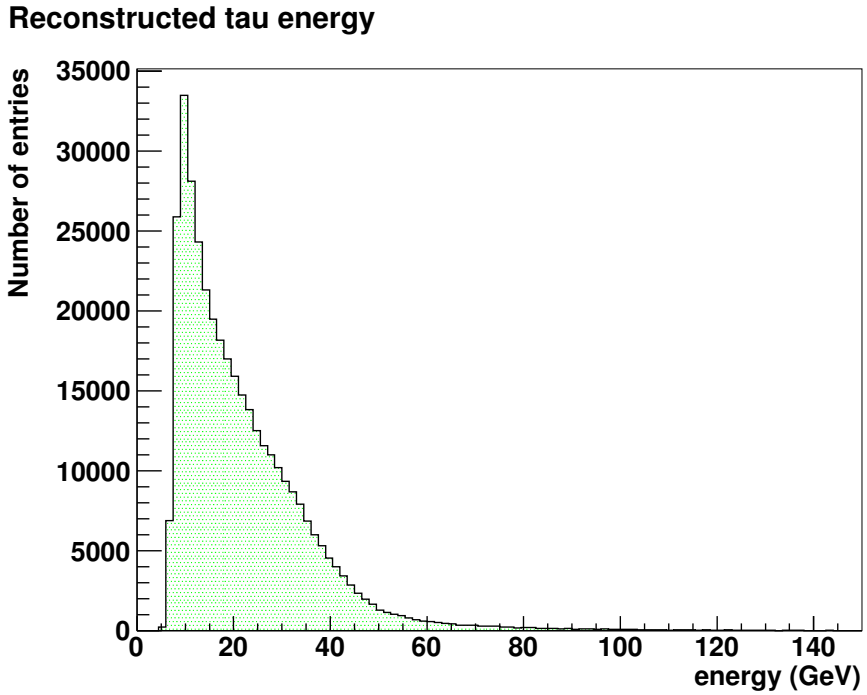

Figure 3.4: Energy of reconstructed tau candidate. $\sqrt{s} = 7$ TeV

background.

- W+Jet, W $\rightarrow$ l+ν
- Z+Jet, Z $\rightarrow$ ll
- $t\overline{t} \Longrightarrow t \rightarrow W^{+}$+$b$ and $\overline{t} \rightarrow W^{-} + \overline{b}$
- QCD jets

In the first one, one tau is coming from the W, and one taus can be faked from a jet. In the next two taus are coming from Z^0, but a jet can fake a third tau. A jet from quarks will normally be more spread and have more tracks than a tau jet, and hence have lower momentum, see figure 3.9. Therefore, when more than two taus occur in an event, the two leading (most energetic) taus are chosen. The third example is a top-antitop pair decaying to a W^+ and W^-. The $W^{\pm}$s can decay into taus as in the first example and two real taus need to be dealt with. In the last both taus are faked from jets [25].

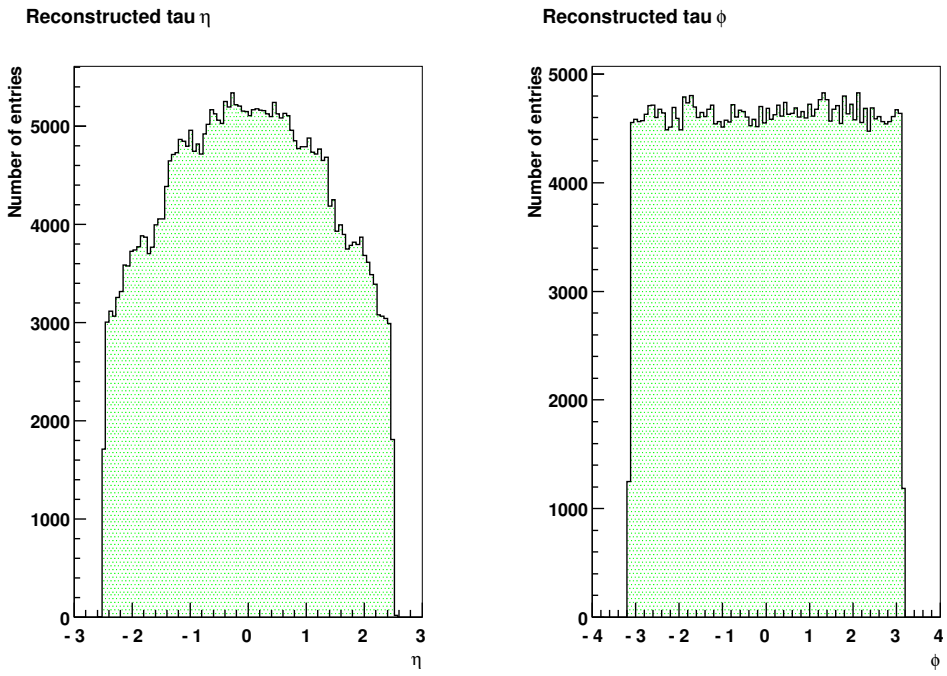

Figure 3.5: Eta and phi of reconstructed tau candidate. $\sqrt{s} = 7$ TeV

3.2.4 Requirements on single taus and tau pairs

Without any cuts, the tau signal drowns in QCD background. A main task for a good $Z^0 \rightarrow \tau^-\tau^+$ study is to make wise cuts on the variables to keep as much signal as possible and reduce as much background as possible.

The taus are selected by these cuts:

Pseudo rapidity

Cut away $1.3 < |\eta| < 1.7$ and $|\eta| > 2.4$ to suppress fake MET and fake taus from electrons. In the region of $|\eta|$ between 1.3 and 1.7 is the passage between barrel and end-cap and the detection coverage is not as good as elsewhere. A particle is therefore more probable not to be detected and make fake E_T^{miss} contribution. In the region of $|\eta| > 2.4$, electrons and pions are harder to discriminate, which can lead to fake taus from electrons.

Seed

In order to have a chance to separate taus decaying from Z^0 and the ones decaying from H^0, good taus are needed. Taus that are both tracking and calorimeter seeded are more alike to be a tau. A cut requiring both seeded taus is done in the following.

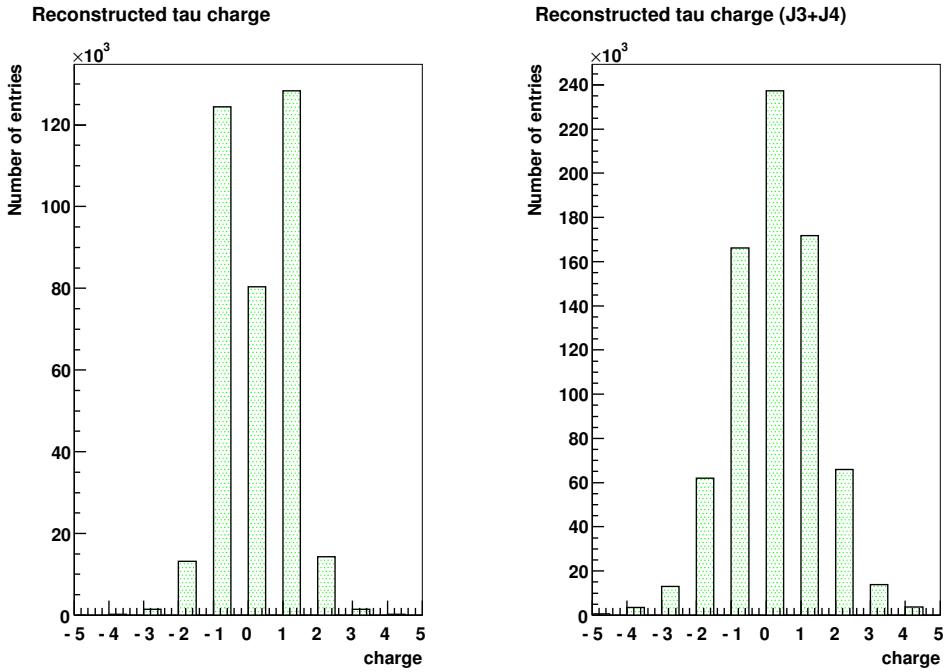

Figure 3.6: Charge of reconstructed tau candidates, with QCD (J3) background. $\sqrt{s} = 7$ TeV

Charge

A tau always have charge ± 1. All other tau candidates are cut away.

Number of prongs

A cut on prongs is not necessary, this is already taken care of when choosing the right charge. See figure 3.11.

When two tau candidates meeting all these criteria is found in an event, they are selected to be further investigated as a pair. Any event with no tau or only one tau candidate with these requirements fulfilled is rejected. If more than two tau candidates pass the cuts, the two leading (most energetic) of them are chosen. When later a safe cut is made, this is also done before the two leading tau candidates are selected. The tau candidate pair must further pass the following requirements:

OS-SS

Because of charge conservation the two taus decaying from Z^0 always have opposite charge sign. Using this fact, and that QCD will not have any preferences of same sign (SS) or opposite sign (OS), one can subtract the first from

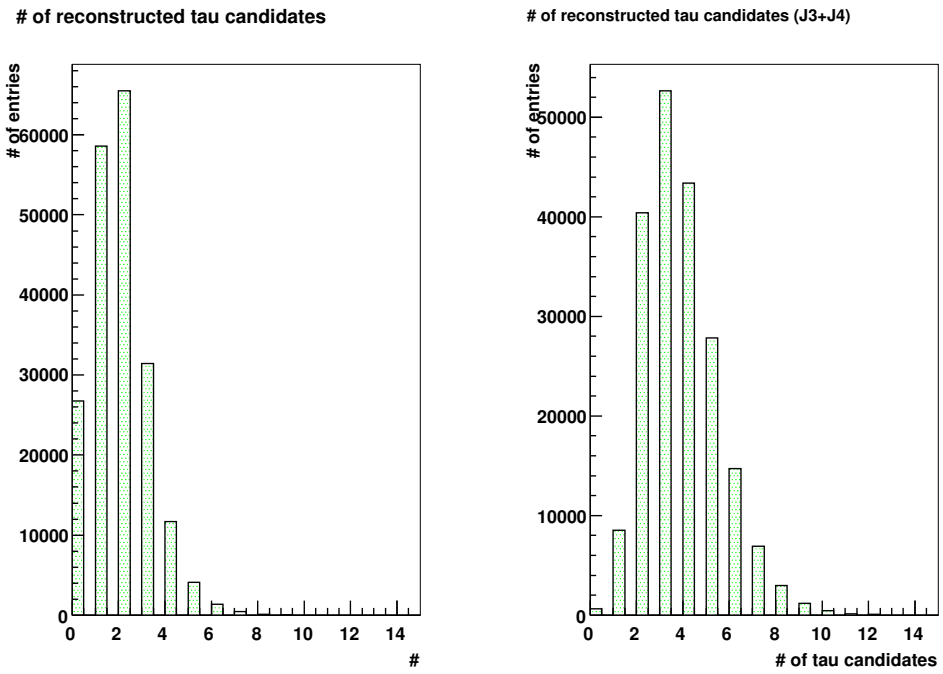

Figure 3.7: Number of reconstructed tau candidates in an event. $\sqrt{s} = 7$ TeV

the last (OS-SS) and theoretically remove no signal and all background. This is a smarter cut than only removing the SS events, which will give a clear signal sample, but remove only half of the background. According to table 3.3, this is the strongest cut in this analysis.

Tau Safe Cuts

The tau reconstruction algorithm has a selection tool with three different efficiencies and rejection factors. Tau Safe Loose cut keeps 70% of the signal, Tau Safe Medium keeps 50% and Tau Safe Tight keeps 30%. In figure 3.10, the combinations of charge sign and safe cuts are shown for signal and the J3 background (J4 behaves in the same way). These are not weighted to cross sections and should not be directly compared with each other, only indirectly by looking at the internal distributions of each. One can see that the dijet sample have about the same number of OS as SS, independent of safe cut, while the signal have an increasing ratio between OS and SS with stronger safe cuts. Background also reject more events than the signal with stronger safe cuts, which will be the reason of choosing a strong safe cut in the following. The lower right plot shows no background. The reason is that on the run over 100000 events, there are only 6 OS and 7 SS tau candidates from J3 that pass the tight criteria, not enough to be

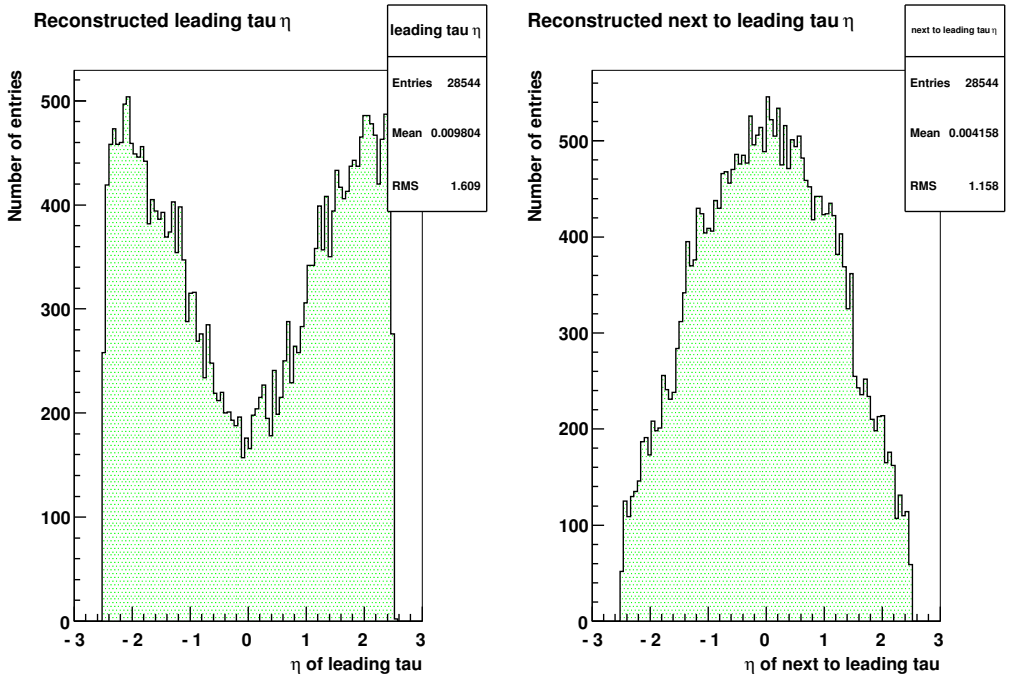

Figure 3.8: η of leading and next-to-leading tau candidate. $\sqrt{s} = 7$ TeV

visible on the picture.

Table 3.3 shows how much signal and background one gets after certain cuts and the significance of signal over background. Above the double line are cuts done on single taus, whereas below the double line the cuts are required on (at least) two taus in the event. In the case of OS-SS, numbers of tau pairs above zero after subtracting SS from OS were counted. To choose a safe cut, three scenarios are chosen: Both tau candidates are loose, both are medium and both are tight. One can see that 2 tight taus give the clearest signal from background. From now on, 2 tight taus will be selected, both in the CA and boost method as well as by looking at $H^0 \rightarrow \tau^-\tau^+$ and real data (when possible). By doing this, one can compare the results directly.

The cross section tells us that in real data, there are about 2500 times more J3 and 100 times more J4 than $Z^0 \rightarrow \tau^-\tau^+$. In the samples used in this analysis, there are 2-3 times more signal than background events. The w is correcting for this, but with much less background compared to signal than in real data, the scaling will cause high single background peaks instead of a spread.

As an illustration, figure 3.12 and 3.13 shows how the different safe cuts affect signal and background in the Collinear Approximation and the boost method respectively.

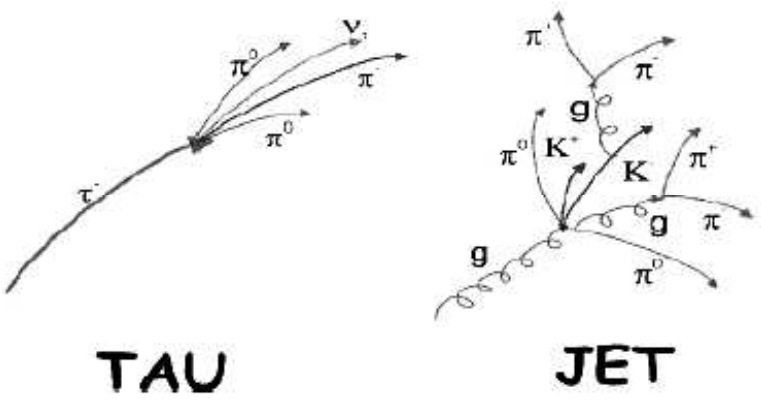

Figure 3.9: Tau signature vs jet signature

E_T^{miss} and $cos(\Delta\phi)$
The cut of E_T^{miss} and $cos(\Delta\phi)$ will be discussed more closely when handling each of the methods. As one can see in figure 3.14, $\cos(\Delta\phi)$ and E_T^{miss} are independent of safe cuts and can be treated separately.

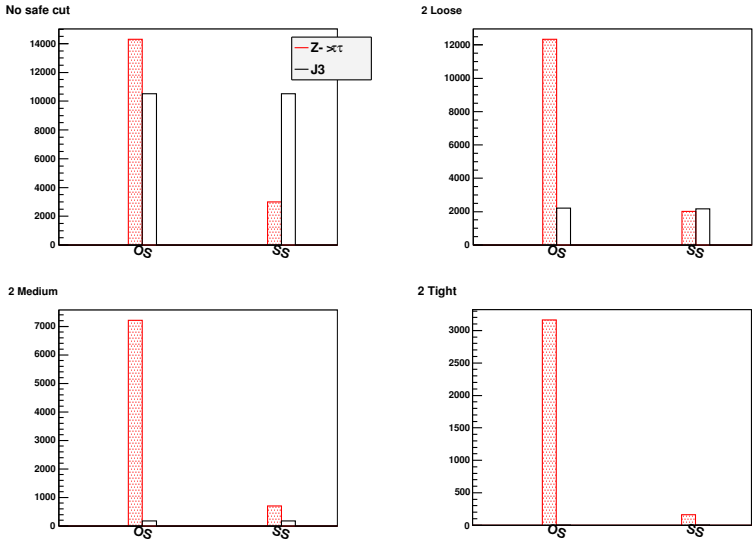

Figure 3.10: Number of events with tau pair with opposite sign (OS), and with same sign (SS).$\sqrt{s} = 7$ TeV.

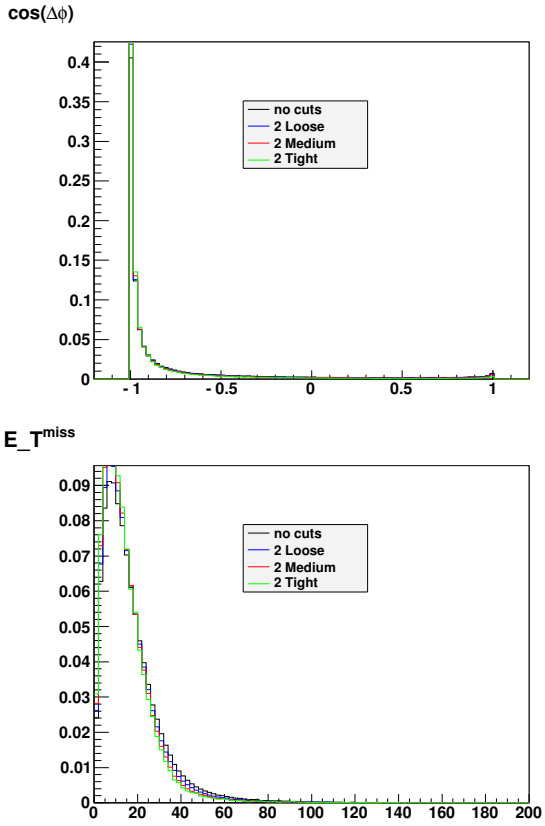

Figure 3.14: $\cos(\Delta\phi)$ *(upper)* and E_T^{miss} *(lower)* with different safe cuts, normalised to 1. $\sqrt{s} = 7$ TeV.

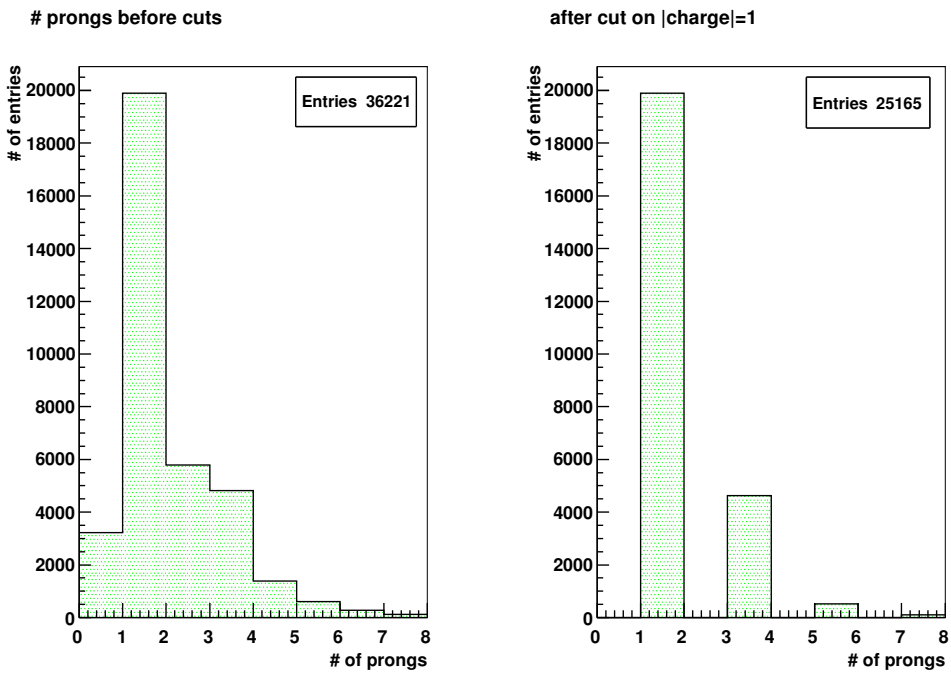

Figure 3.11: Number of prongs before and after cut on tau charge. $\sqrt{s} = 7$ TeV.

$Z^0 \rightarrow \tau^-\tau^+$

Requirement	σ [fb]	% of prev.	% of all
all	$1.55{\cdot}10^6$		100
both seeded	$1.27{\cdot}10^6$	82.18	82.18
|charge|=1	$6.73{\cdot}10^5$	52.99	43.54
$\eta < 1.3$, $1.7 < \eta < 2.4$	$5.33{\cdot}10^5$	79.2	34.48
2 tau candidates	$1.06{\cdot}10^5$	19.83	6.84
OS-SS	$6.64{\cdot}10^4$	62.79	4.29
2 loose	$5.96{\cdot}10^4$	89.77	3.85
2 medium	$3.73{\cdot}10^4$	62.59	2.41
2 tight	$1.78{\cdot}10^4$	47.78	1.15

J3

Requirement	σ [fb]	% of prev.	% of all
all	$1.27{\cdot}10^9$		100
both seeded	$1.05{\cdot}10^9$	83.22	83.22
|charge|=1	$5.52{\cdot}10^8$	52.35	43.56
$\eta < 1.3$, $1.7 < \eta < 2.4$	$2.64{\cdot}10^8$	46.07	20.09
2 tau candidates	$5.51{\cdot}10^7$	21.7	4.35
OS-SS	$3.34{\cdot}10^5$	0.61	$2.64 \cdot 10^{-2}$
2 loose	$2.01{\cdot}10^5$	60.03	$1.58{\cdot}10^{-2}$
2 medium	$5.25{\cdot}10^4$	26.14	$4.14{\cdot}10^{-3}$
2 tight	$5.25 \cdot 10^4$	26.14	$4.14 \cdot 10^{-3}$

J4

Requirement	σ [fb]	% of prev.	% of all
all	$2.67{\cdot}10^9$		100
both seeded	$2.67{\cdot}10^9$	84.25	84.25
|charge|=1	$1.14{\cdot}10^9$	50.85	42.85
$\eta < 1.3$, $1.7 < \eta < 2.4$	$4.96{\cdot}10^8$	43.36	18.58
2 tau candidates	$1.16{\cdot}10^8$	23.3	4.33
OS-SS	$2.15{\cdot}10^5$	0.19	$8.05{\cdot}10^{-3}$
2 loose	$1.47{\cdot}10^5$	68.22	$5.49{\cdot}10^{-3}$
2 medium	$5.17{\cdot}10^4$	35.23	$1.93{\cdot}10^{-3}$
2 tight	$6.67{\cdot}10^3$	12.9	$2.50{\cdot}10^{-4}$

Table 3.3: Table over who much different cuts affect signal and background, all numbers are weighted by cross section. $\sqrt{s} = 7$ TeV.

Requirement	$\frac{Z^0 \to \tau^+\tau^-}{Z^0 \to \tau^+\tau^- + \text{J3+J4}}$
all	$3.92 \cdot 10^{-4}$
both seeded	$3.84 \cdot 10^{-4}$
|charge|=1	$3.97 \cdot 10^{-4}$
$\eta < 1.3$, $1.7 < \eta < 2.4$	$7.10 \cdot 10^{-4}$
2 tau candidates	$6.19 \cdot 10^{-4}$
OS-SS	0.11
2 loose	0.15
2 medium	0.26
2 tight	0.62

Table 3.4: The fraction of signal remaining after different cuts.

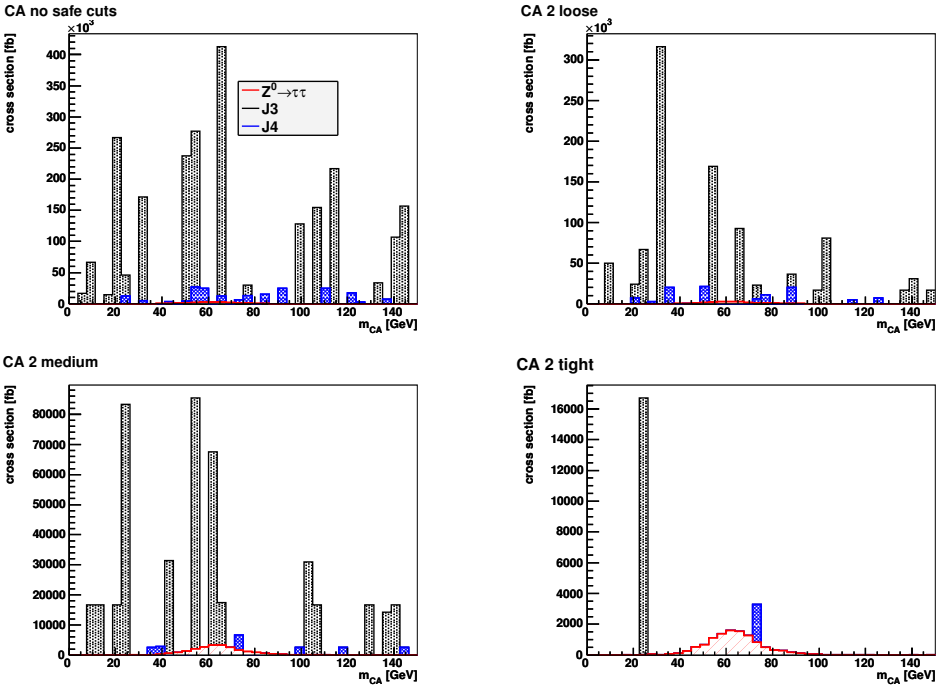

Figure 3.12: CA's mass distribution with different safe cuts. *(Upper left:)* CA with no safe cut, *(upper right:)* CA with two loose taus, *(lower left:)* CA with two medium taus, *(lower right:)* CA with two tight taus. $\sqrt{s} = 7$ TeV.

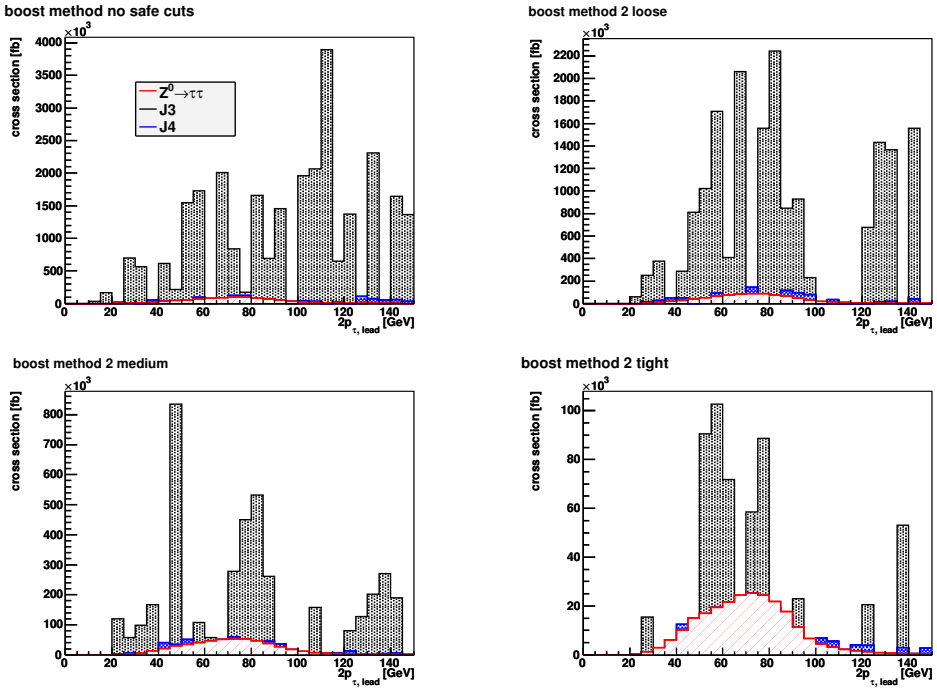

Figure 3.13: Boost method's mass distribution with different safe cuts. *(Upper left:)* boost method with no safe cut, *(upper right:)* boost method with two loose taus, *(lower left:)* boost method with two medium taus, *(lower right:)* boost method with two tight taus. $\sqrt{s} = 7$ TeV.

Chapter 4

Reconstruction of $\tau^+\tau^-$ invariant mass in $Z^0 \rightarrow \tau^-\tau^+$

Mass Reconstruction from $Z^0 \rightarrow \tau^-\tau^+$ is studied for both MC true taus and reconstructed ones. For MC truth, no cuts are required.

In the MC truth information, the Z^0-mass is not given by an exact value, but a distribution as shown in figure 4.1. This means that irrespective of how good the tau selection and the Z^0 reconstruction are, a narrower peak than this can never be expected. In the first part of the chapter, reconstruction is done from MC truth taus. In the second part reconstruction from the visible tau decay products is explained.

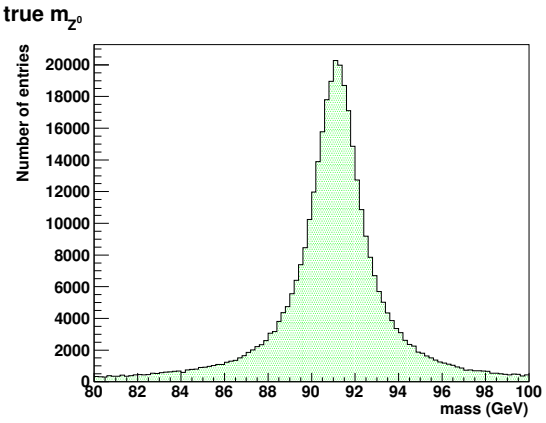

Figure 4.1: MC truth Z^0 mass

4.1 Mass reconstruction with MC truth taus.

4.1.1 The purpose of Z^0 reconstruction.

m_{Z^0} is a very important property, which is already well known. In the PDG [1] 2008 the value of the Z^0-mass is determined to the KeV-scale: 91.1876 ± 0.0021 MeV [5]. m_{Z^0} is already used to calibrate the detectors, so why study something that is already well known? The main answer is that the Higgs may decay following the process $H^0 \rightarrow \tau^+\tau^-$. And that the Higgs may have a mass near to the Z^0-mass. The nearer it is, the more difficult it is to separate the signal from Z^0. But the more we understand the process $Z^0 \rightarrow \tau^-\tau^+$, the easier it is to separate the two processes.

4.1.2 The mass reconstruction of a two body decay.

Two taus with known momentum and energy are collected and assumed to be the only decay product of a single Z^0. Since momentum and energy is conserved, the invariant mass of the Z^0 can be calculated. Z^0 is assumed to be at rest.

It is convenient to use four-momentum, defined like this:

$$p = (E, p_x, p_y, p_z) \tag{4.1}$$

or more compressed:

$$p = (E, \vec{p}). \tag{4.2}$$

The invariant product of two four-vectors is

$$p_1 \cdot p_2 = E_1 \cdot E_2 - \vec{p}_2 \cdot \vec{p}_2 \tag{4.3}$$

If particle 1 and 2 are equal, then

$$p^2 = E^2 - |\vec{p}|^2 \tag{4.4}$$

which again, using

$$E^2 = |\vec{p}|^2 + m^2 \tag{4.5}$$

shows that a four-momentum squared, is the invariant mass of the particle:

$$p^2 = m^2. \tag{4.6}$$

Since both the momentum and energy are conserved in the decay, the 4-momentum is conserved.

[1] Particle Data Group

$$p_Z = p_\tau^+ + p_\tau^- \tag{4.7}$$

The four-momentum is then squared

$$\begin{aligned}(p_Z)^2 &= (p_\tau^+ + p_\tau^-)^2 \\ &= (p_\tau^+)^2 + (p_\tau^-)^2 + 2p_\tau^+ p_\tau^-\end{aligned} \tag{4.8}$$

Recall that the 4-momentum squared is the invariant mass itself, and since $\tau^-$and τ^+have equal masses, they just add up. Following calculation rule in equation (4.3), the 4-momentum is

$$\begin{aligned}m_Z^2 &= 2(m_\tau)^2 + 2E_{\tau^+}E_{\tau^-} - 2\vec{p}_{\tau^+} \cdot \vec{p}_{\tau^-} \\ &= 2(m_\tau)^2 + 2\sqrt{(m_\tau^2 + \vec{p}_{\tau^+}^{\,2})(m_\tau^2 + \vec{p}_{\tau^-}^{\,2})} - 2\vec{p}_{\tau^+} \cdot \vec{p}_{\tau^-}\end{aligned} \tag{4.9}$$

$m_\tau \approx \frac{1}{50} m_{Z^0}$. Neglecting m_τ simplifies the calculation to

$$(p_Z)^2 = 2|\vec{p}_{\tau^+}||\vec{p}_{\tau^-}| - 2\vec{p}_{\tau^+} \cdot \vec{p}_{\tau^-}, \tag{4.10}$$

which gives the Z^0 reconstructed mass

$$m_Z = \sqrt{2|\vec{p}_{\tau^+}||\vec{p}_{\tau^-}|(1 - \cos(\alpha))}. \tag{4.11}$$

α is the spacial angle between the two taus. In figure 4.2, we check the validity of neglecting m_τ by comparing the mass distributions of Z^0 from two MC truth τ-particles encountering (right) and neglecting (left) m_τ in the calculation.

There is a 130 MeV difference, where the Z^0-mass with m_τ included lies closest up to the PGD value of of Z^0, which is about 91.19 GeV [5]. Thus, it is seen that neglecting m_τ makes a small change in the mass reconstruction.

4.2 With reconstructed taus

In the MC truth samples, the tau momentum, p_τ, is exactly known. In real collisions this is not the case. In each tau decay there are neutrinos escaping with some part of the momentum. The invariant mass calculated from the visible parts of the taus is therefore expected to be smaller than for the truth taus.

In figure 4.3, the visible taus are reconstructed and the invariant mass is calculated from all tau candidates, with the cuts defined in the previous chapter.

The decay is, as described in section 1.4, both leptonic and hadronic. Where hadronic means mostly pions. We should therefore be able to construct the Z^0-mass from visible decay products by using the collected momenta from pions, and get the same result as the reconstructed taus as shown in figure 4.4, which shows the mass reconstructed when the generated pion energies are used.

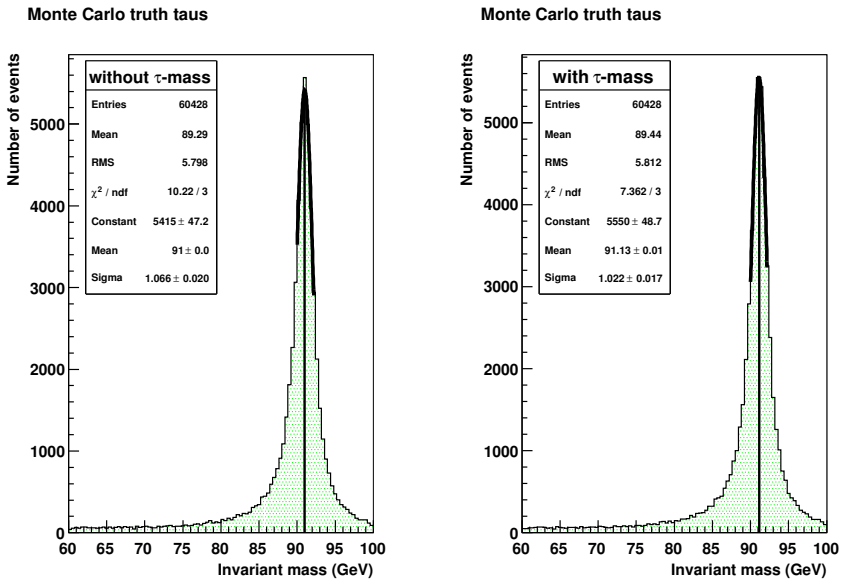

Figure 4.2: Z^0 mass reconstruction with m_τ neglected (left) and included (right).

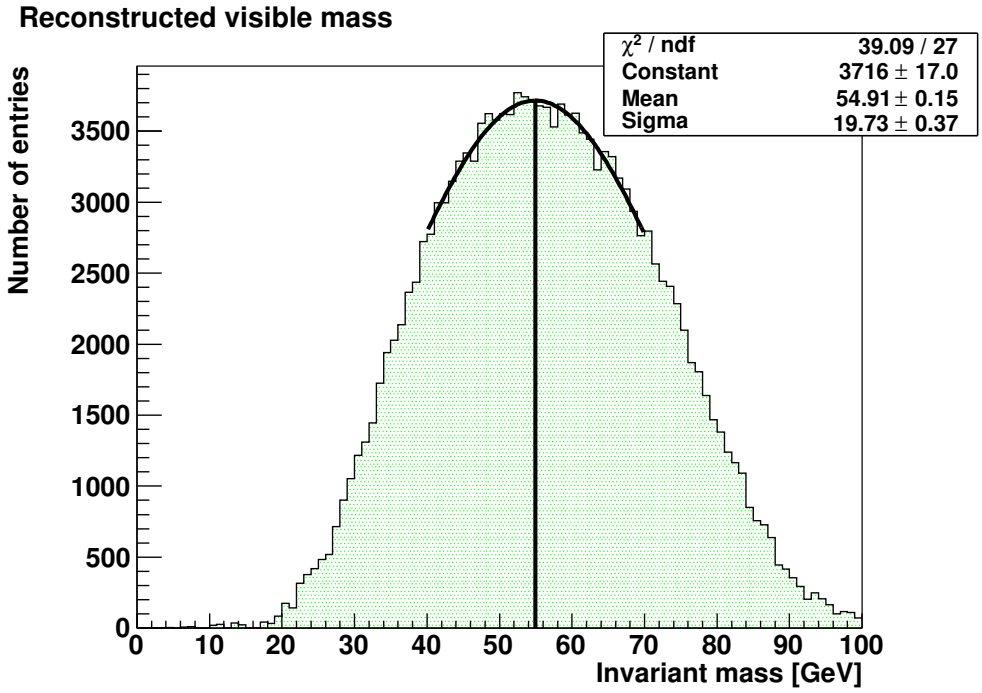

Figure 4.3: Mass reconstruction of visible tau decay products in $Z^0 \rightarrow \tau^-\tau^+$

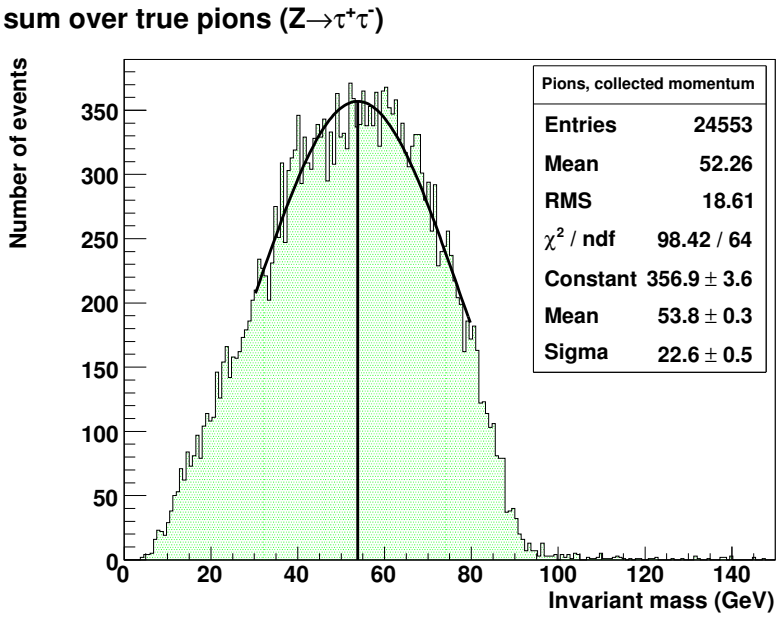

Figure 4.4: Z^0 mass reconstruction with sum over MC truth pions.

Chapter 5

Collinear Approximation

In the previous chapter, the mass reconstruction became as good as it can get using just the visible parts of the tau decays. This chapter will focus on the optimisation of the mass reconstruction with a method called Collinear Approximation (CA). The strengths and limits of the CA, cuts that are needed and the need of complementary methods will be discussed.

5.1 The concept of missing energy, E_T^{miss}

In order to understand the CA, the concept of missing energy has to be understood.

In LHC, the colliding protons is travelling along the z-axis (Recall figure 2.3). The momentum in the xy-plane hence is zero before the collision, and because of momentum conservation also after collision. Summing up the momentum of visible and invisible particles should give zero:

$$\vec{p}_T(visible) + \vec{p}_T(invisible) = 0 \tag{5.1}$$

By invisible particles hereby particles not detected in ATLAS are meant.

Since the neutrino have neglectable mass (<2 eV [5]), the momentum carries all its energy, $\vec{p}_\nu = E_\nu$. By saying that E_T^{miss} is only due to neutrinos, one obtains:

$$\vec{E}_T^{miss} = E_T(\nu) = \vec{p}_\nu = -\vec{p}_T(visible). \tag{5.2}$$

And this is the clue of calculating E_T^{miss} : the sum of all transverse momenta is detected and the vector missing in order to have zero momenta is constructed and called E_T^{miss} .

Figure 5.1 shows the energy and transverse angle distribution of the E_T^{miss} for events containing $Z^0 \rightarrow \tau^-\tau^+$. This angular distribution is expected to be uniform, and the reason for the non-uniform distribution is not known. The same

strange distribution occurs in the J3 and J4 samples as well as in real data (figure 8.2).

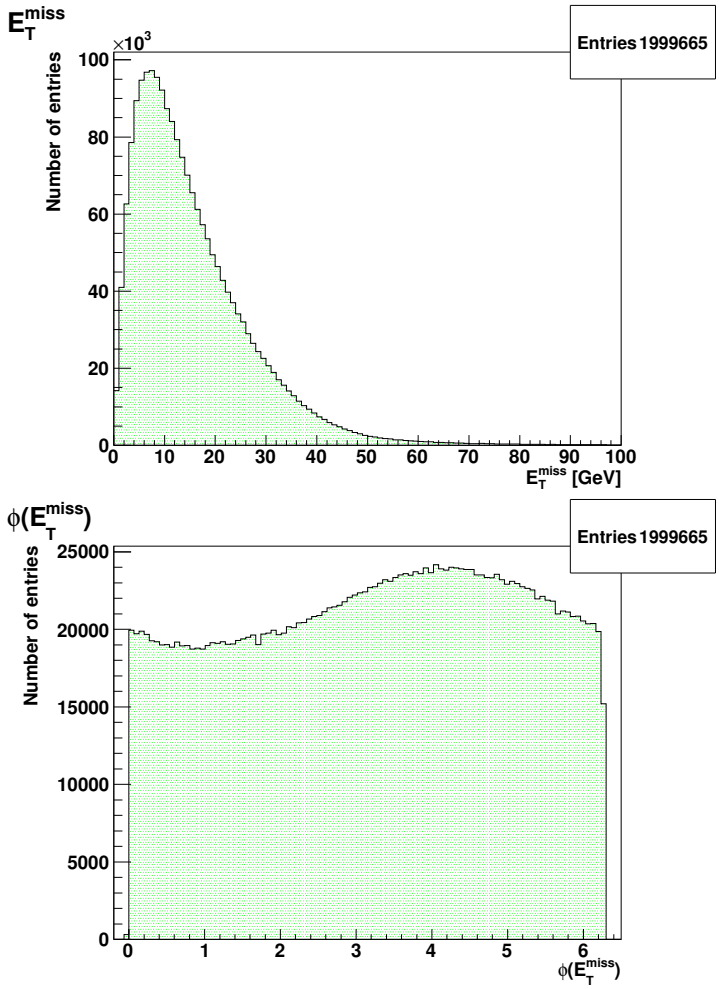

Figure 5.1: Reconstructed E_T^{miss} . $\sqrt{s} = 7$ TeV.

One could wish to calculate the missing energy in the z-direction as well, but this is not possible because

- Protons have an inner structure, and the partons, not the whole proton is colliding. Thus the momentum in the z-direction in general is not zero.
- ATLAS is designed to cover $|\eta| < 4.9$ [26], meaning that particles travelling with $|\eta| > 4.9$ escapes.

The latter is also a reason that some of the transverse momentum being lost as well. This is shown in figure 5.2.

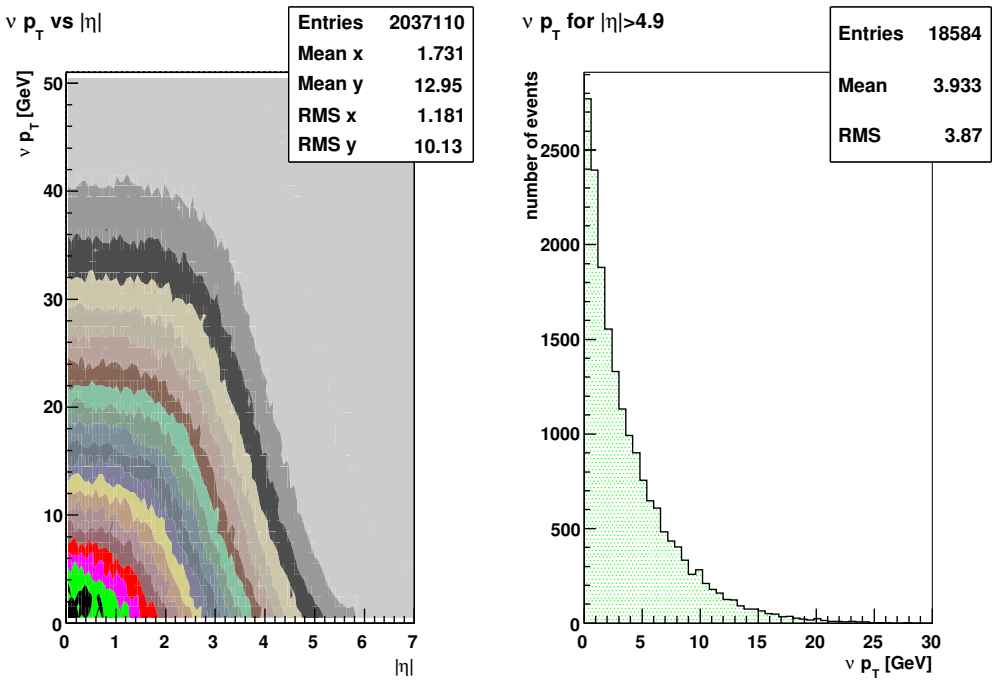

Figure 5.2: $|\eta|$ vs ν_τ p_T and ν_τ p_T for $\eta > 4.9$. $\sqrt{s} = 7$ TeV.

To the left $|\eta|$ of the neutrino is plotted versus the p_T of the neutrino. This shows both less entries and smaller p_T in $|\eta| > 4.9$. To the right is the p_T distribution of only neutrinos with $|\eta| > 4.9$. The fraction of neutrinos with $|\eta| > 4.9$ is 1.8%. The mean value is also much lower for $|\eta| > 4.9$: 3.9 GeV against 13.2 GeV for the whole η-range. A cut on a lower $|\eta|$, done in section 5.5, will remove events with this problem.

5.2 The concept of the CA

The CA builds upon two assumptions.

1. **The neutrinos are collinear (go in the same direction) as the visible decay products.**

   This holds, since $m_Z/m_\tau \gg 1$.

2. **All the missing energy is due to neutrinos from tau decays.**

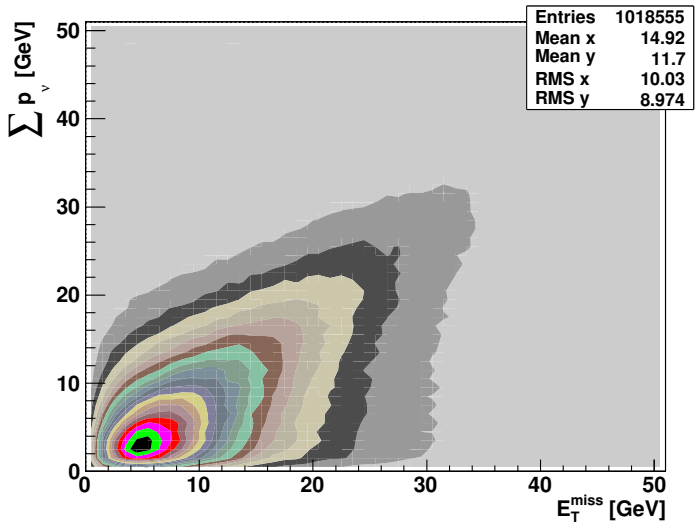

Figure 5.3: E_T^{miss} versus vector sum of the neutrino transverse energy. $\sqrt{s} = 7$ TeV.

This is verified in figure 5.3, where all true tau-neutrinos in each event are summed up, $\sum \vec{\nu_\tau}$, and plotted versus the reconstructed E_T^{miss} . Ideally a straight line with slope 1 should be seen; a better tau selection would improve this.

3. **Then the transverse angle of the vector sum of the neutrino momenta should coincide with the transverse angle of the missing energy**.

   When assumption 1 and 2 holds, number 3 follows. In figure 5.4, the transverse angle between E_T^{miss} and the sum of the neutrinos are plotted. The peak at zero verifies the coincidence between the E_T^{miss} transverse angle and the transverse angle of the missing energy.

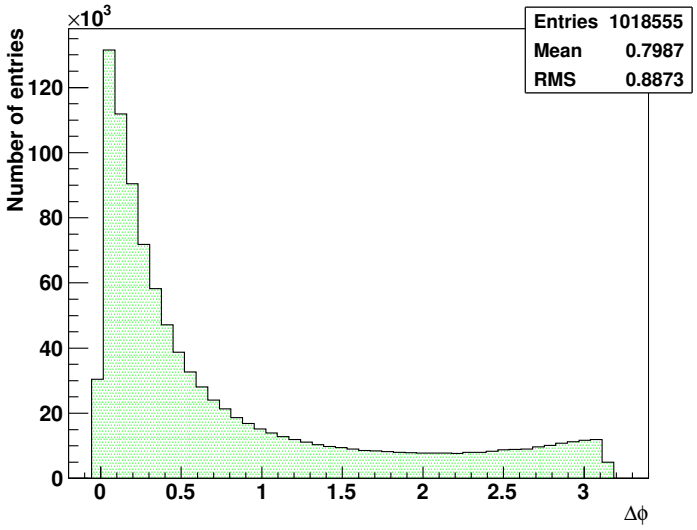

Figure 5.4: $\Delta\phi$ between reconstructed E_T^{miss} and the sum of MC truth neutrinos. $\sqrt{\text{s}} = 7$ TeV.

5.3 Z boost

For kinematic reasons, the assumption of collinearity is more likely to hold if the decay products from Z^0 are boosted. The method of CA is known from the work with $H^0 \rightarrow \tau^-\tau^+$, where it is a good method since $m_H/2m_\tau \gg 1$, and hence the taus are highly boosted [27]. The first task is to find out whether the taus from $Z^0 \rightarrow \tau^-\tau^+$ is boosted as well.

To that purpose, the spacial angle between two taus is introduced, α, and the angle in the xy-plane, $\Delta\phi$. They are calculated as follows:

$$\cos(\alpha) = \frac{(p_x^1 p_x^2 + p_y^1 p_y^2 + p_z^1 p_z^2)}{\sqrt{p_x^1 p_x^1 + p_y^1 p_y^1 + p_z^1 p_z^1}\sqrt{p_x^2 p_x^2 + p_y^2 p_y^2 + p_z^2 p_z^2}} \tag{5.3}$$

$$\cos(\Delta\phi) = \frac{(p_x^1 p_x^2 + p_y^1 p_y^2)}{\sqrt{p_x^1 p_x^1 + p_y^1 p_y^1}\sqrt{p_x^2 p_x^2 + p_y^2 p_y^2}} \tag{5.4}$$

In figure 5.5 (without cuts), the $\cos(\Delta\phi)$ to the left show a large tendency of the taus to be back-to-back in the transverse plane, while in 3D the taus have a tendency of being both back-to-back and having same direction. This — that the taus are boosted in the z-direction — is expected from figure 1.1, since the decay products have to be boosted in the same direction as their mother.

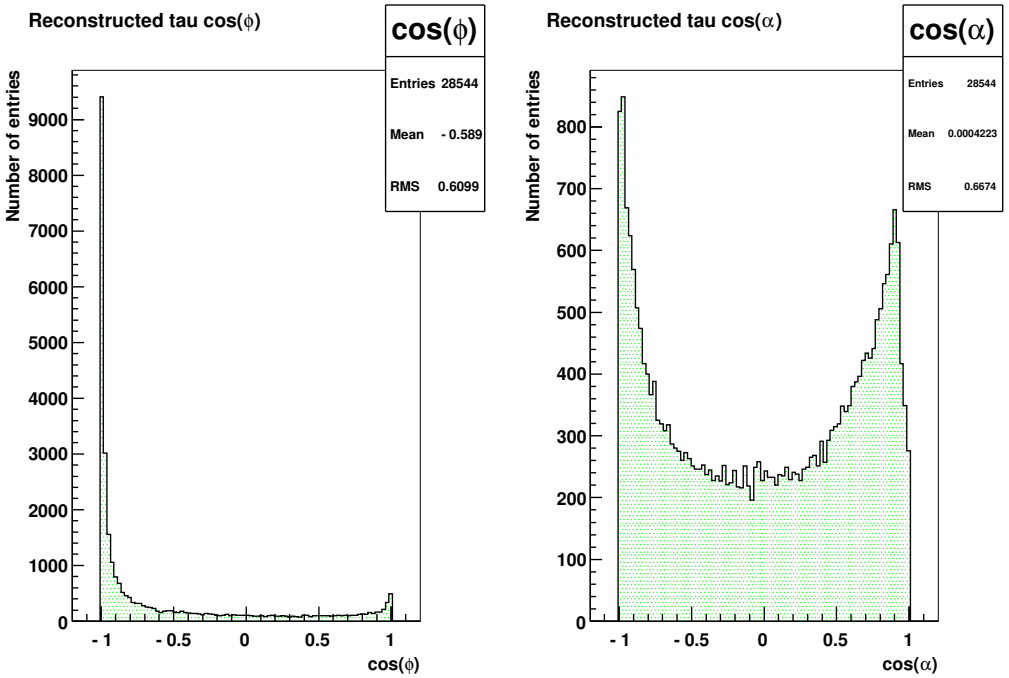

Figure 5.5: $\cos(\Delta\phi)$ and $\cos\alpha$ between the two leading taus. $\sqrt{s} = 7$ TeV.

5.4 Explanation of the method

The visible mass can be illustrated by subtracting the MC truth neutrinos from the MC truth taus, see figure 5.6 (left). To the right, the neutrinos are treated as E_T^{miss} and fed into the method as such. This verifies that the CA method works properly.

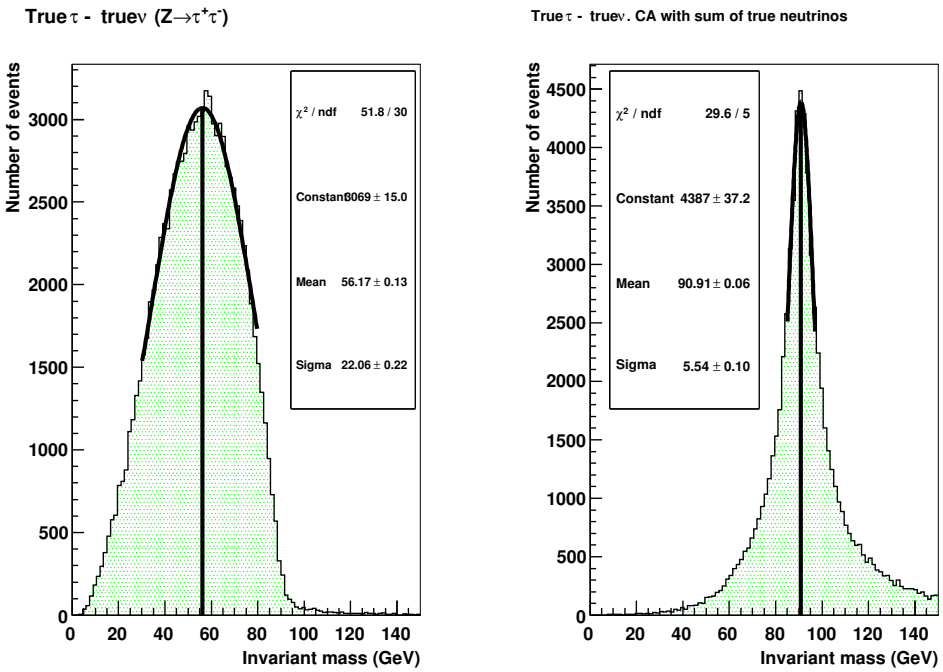

Figure 5.6: Mass reconstruction of MC true τ - $\sum$ true $\vec{\nu_\tau}$ (left), the CA with true $\sum \vec{\nu_\tau}$ (right). $\sqrt{s} = 7$ TeV.

Figure 5.7 shows the reconstruction of the invariant mass without any corrections to the left, and with the CA to the right, using reconstructed E_T^{miss} to correct for the neutrino energy. One can see that the CA shifts the mass peak to a higher mass, closer to the known m_Z, and makes the peak narrower as well.

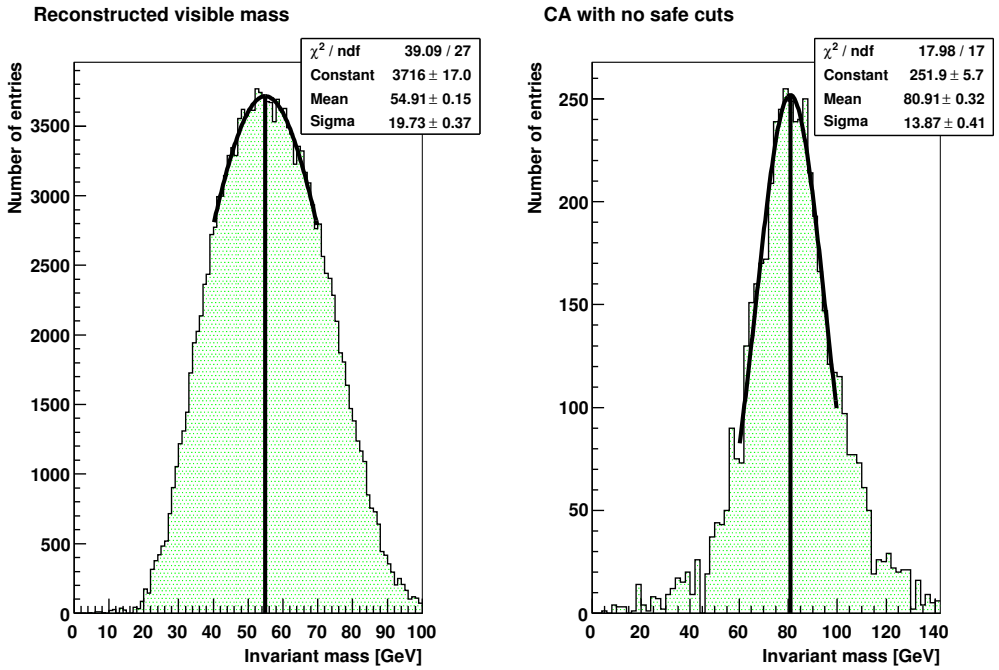

Figure 5.7: Reconstructed visible mass (left), m_{CA} with E_T^{miss} (right). $\sqrt{s} = 7$ TeV.

The details of the method is as follows:
Starting from assumption 2, all E_T^{miss} is due to neutrinos,

$$\vec{\nu_1} + \vec{\nu_2} = \vec{E}_T^{\text{miss}}, \tag{5.5}$$

the CA algorithm projects the E_T^{miss} unto the basis made by the two visible taus. In the following, τ_{1x} should be understood as p_x for the τ_1, etc. Collinearity requires the neutrino to be a fraction a of the tau vector, with the same direction:

$$a \cdot \vec{\tau_1} + b \cdot \vec{\tau_2} = \vec{E}_T^{\text{miss}} \tag{5.6}$$

With a decomposition in x and y, two equations are obtained, from which a and b

can be solved.

$$a \cdot \begin{pmatrix} \tau_{1x} \\ \tau_{1y} \end{pmatrix} + b \begin{pmatrix} \tau_{2x} \\ \tau_{2y} \end{pmatrix} = \begin{pmatrix} E_T^{\text{miss}} x \\ E_T^{\text{miss}} y \end{pmatrix} \tag{5.7}$$

$$a\tau_{1x} + b\tau_{2y} = E_T^{\text{miss}} x$$

$$a\tau_{2x} + b\tau_{2y} = E_T^{\text{miss}} y$$

$$I \quad a = \frac{E_T^{\text{miss}} x - b\tau_{2x}}{\tau_{1x}}$$

$$I \text{ in } II \quad \left(\frac{E_{Tx}^{\text{miss}} - b\tau_{2x}}{\tau_{1x}} \right) \tau_{1y} + b\tau_{2y} = E_{Ty}^{\text{miss}}$$

$$\frac{E_{Tx}^{\text{miss}} \tau_{1y}}{\tau_{1x}} - \frac{b\tau_{2x}\tau_{1y}}{\tau_{1x}} + b\tau_{2y} = E_{Ty}^{\text{miss}} \tag{5.8}$$

$$b = \frac{\tau_{1x} E_{Ty}^{\text{miss}} - E_{Tx}^{\text{miss}} \tau_{1y}}{\tau_{1x}\tau_{2y} - \tau_{2x}\tau_{1y}} \tag{5.9}$$

Summing up all directions, i.e. including the z-direction, the energy of the neutrinos is calculated as follows:

$$\nu_1 = \sqrt{(a\tau_{1x})^2 + (a\tau_{1y})^2 + (a\tau_{1z})^2} \tag{5.10}$$

and similarly for ν_2. Adding the reconstructed neutrino energies to the reconstructed taus, a better approximation of the taus is obtained.

$$\tau_1^{\text{CA}} = \tau_1^{\text{reco}} + \nu_1^{\text{reco}} \tag{5.11}$$

and similarly on τ_2.

These new τ^{CA} momenta are now ready to be filled into equation (4.11) on page 52. The tau-mass does not contribute to the CA method and will from this point on be neglected.

5.5 Requirements for a successful application of the CA

In this section the cuts on $\cos(\Delta\phi)$and E_T^{miss} are discussed.

The CA breaks down for $\cos(\Delta\phi)$=1, i.e. when the visible taus are back-to-back. The reason is that E_T^{miss} cannot be projected down to back-to-back events, since there is then only one independent axis (see fig. 5.8). The mathematical explanation is that one of the lines in the matrix equation (5.7) gets filled with zeros. By small deviations from a back-to-back scenario, it is mathematically

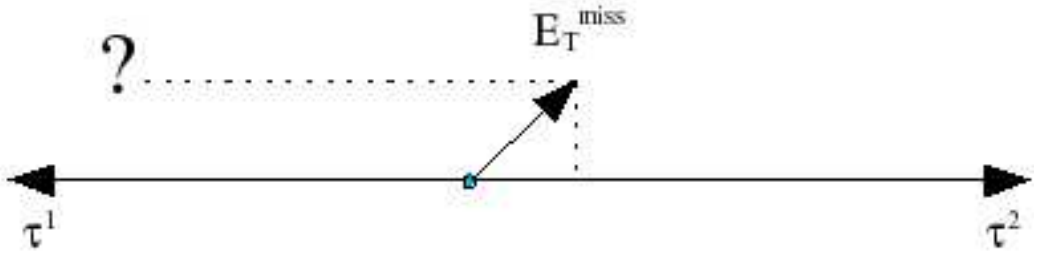

Figure 5.8: Trying to decompose a vector unto a basis of parallel vectors.

possible to reconstruct the neutrinos, but they become enormously energetic in order to correct for the E_T^{miss} in the direction perpendicular to one of the taus.

Low E_T^{miss} indicates that the two neutrinos are back-to-back, or close to such. The momenta cancel each other out, and therefore the reconstruction algorithms register only a small or no deviation from summing the visible momenta up to zero.

From figure 5.9 one can see that E_T^{miss} and $\cos(\Delta\phi)$are not completely independent of each other; a cut on $\cos(\Delta\phi)$will affect the results of E_T^{miss} and vice versa — one should keep that in mind. Short studies have indicated that the CA will depend much more on a $\cos(\Delta\phi)$-cut than on a cut on E_T^{miss} . In the following, a cut on $\cos(\Delta\phi)$will first be carefully examined, and then will come a smaller discussion on E_T^{miss} afterwards.

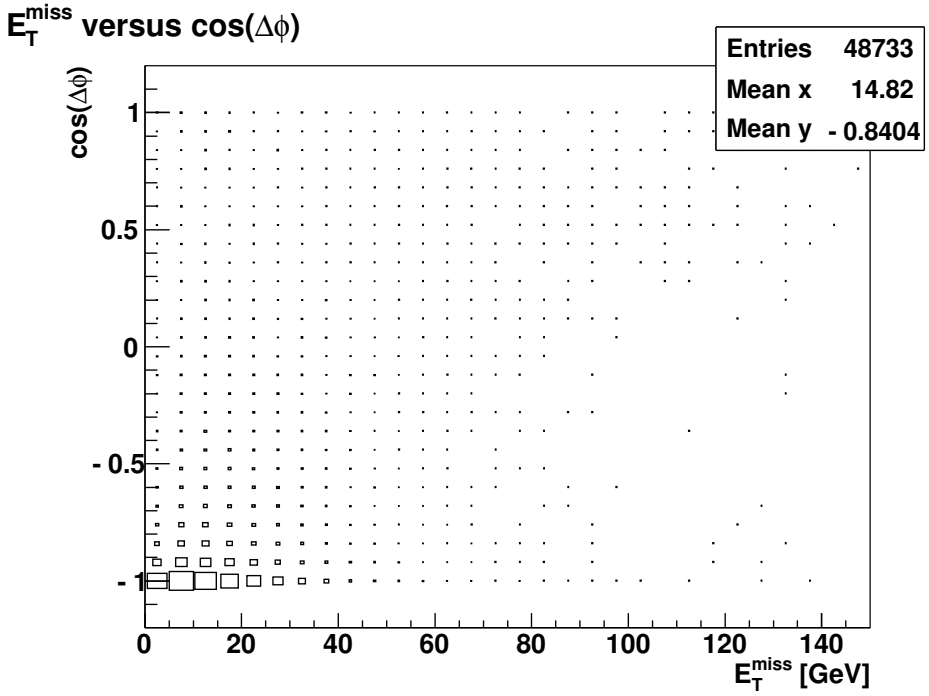

Figure 5.9: E_T^{miss} versus $\cos(\Delta\phi)$. They are not completely unrelated. $\sqrt{s} = 7$ TeV.

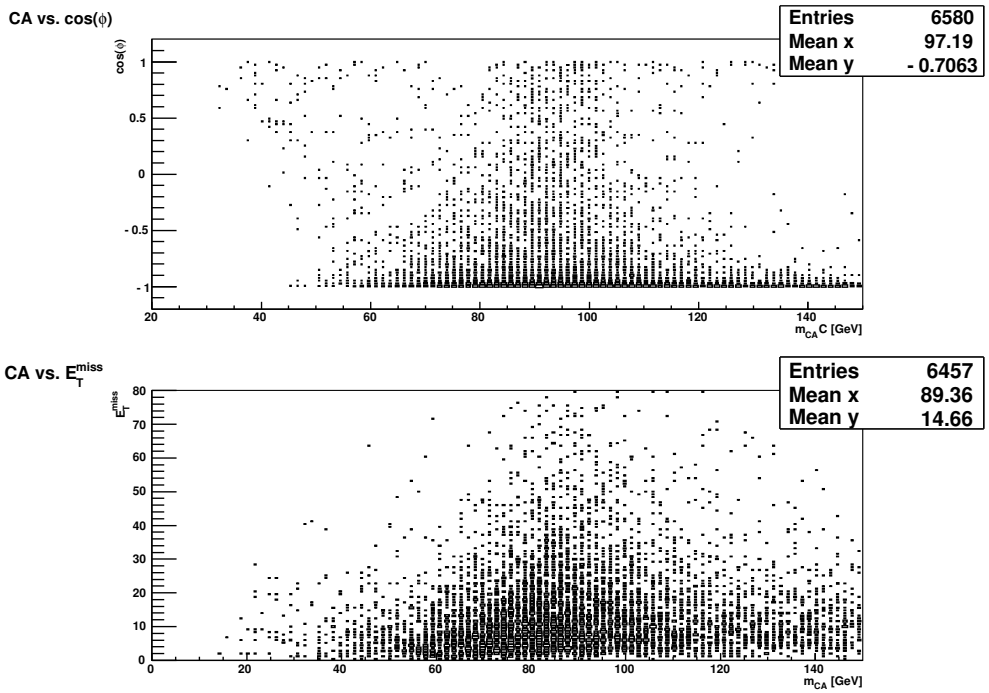

Figure 5.10: Invariant mass with CA versus $\cos(\Delta\phi)$, and E_T^{miss} . $\sqrt{s} = 7$ TeV.

Figure 5.10 shows mass reconstruction using the CA (m_{CA}) versus $\cos(\Delta\phi)$(top), and E_T^{miss} (bottom). Optimal cuts are not trivial to determine from these plots. A closer analysis is needed and made in the following.

5.5.1 Cut on cos($\Delta\phi$)

In the figure 5.11, m_{CA} versus $\cos(\Delta\phi)$(upper left) is divided into horizontal slices, each slice fitted with a Gaussian. The upper plot shows the mean value, the middle the sigma of the Gaussian, and the lower shows the number of entries in each slice. Values for $\cos(\Delta\phi)$>0.8 is not shown in figure 5.11; because of low statistics the uncertainties are extremely large. One can see the mean value increasing towards $\cos(\Delta\phi)$=-1; therefore, the range between -1 and -0.9 is further investigated.

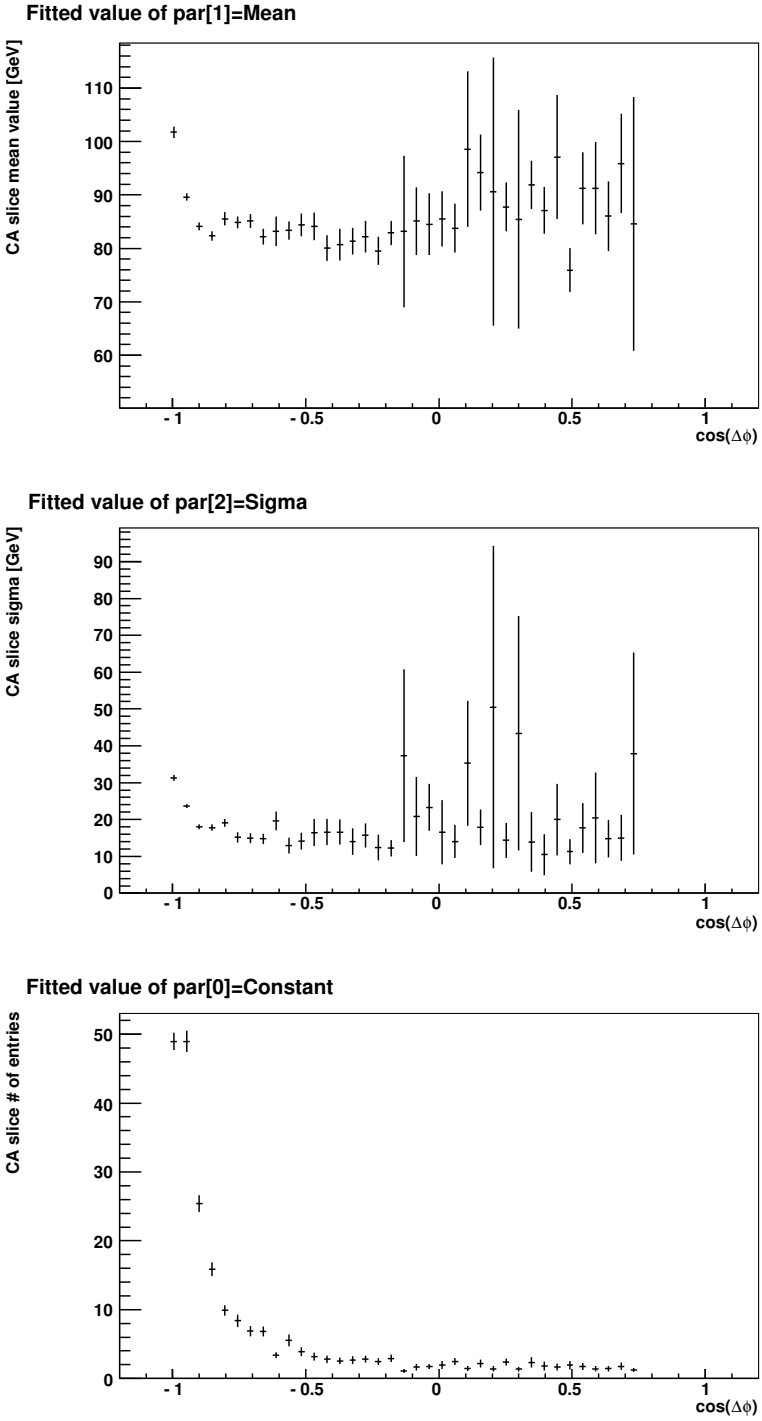

Figure 5.11: Analysis plots of the CA versus $\cos(\Delta\phi)$. $\sqrt{s} = 7$ TeV.

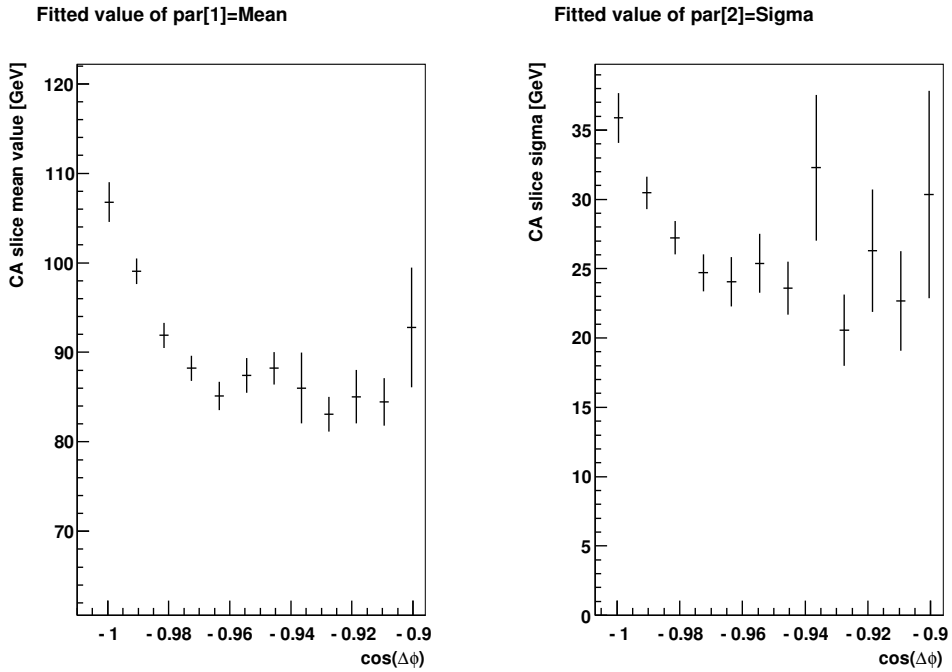

Figure 5.12: Analyse plots of the CA versus $\cos(\Delta\phi)$for $-1 < \cos(\Delta\phi) < -0.9$. $\sqrt{s} = 7$ TeV.

Figure 5.12 shows slice plots for -1 <$\cos(\Delta\phi)$< -0.9. Here, one can see that the m_{CA} holds good values up to about -0.99. One can gain much statistics by going from a requirement of $\cos(\Delta\phi)$>-0.9 to -0.99. Figure 5.13 shows m_{CA} for a cut at $\cos(\Delta\phi) > -0.9$ (upper left), m_{CA} when $-0.9 > \cos(\Delta\phi) > -0.99$ (upper right), m_{CA} for $-0.99 > \cos(\Delta\phi) > -0.999$ (lower left), and the remaining events where $\cos(\Delta\phi) < -0.999$ (lower right). Here one can also see that a cut on $\cos(\Delta\phi)> -0.99$ is harmless, but a cut on -0.999 would be less fruitful. A cut on -0.99 keeps 93.9% of the signal, against only 39.8% on -0.9. A requirement of $\cos(\Delta\phi) > -0.99$ is hence recommended, and also consistent with [28] and [29].

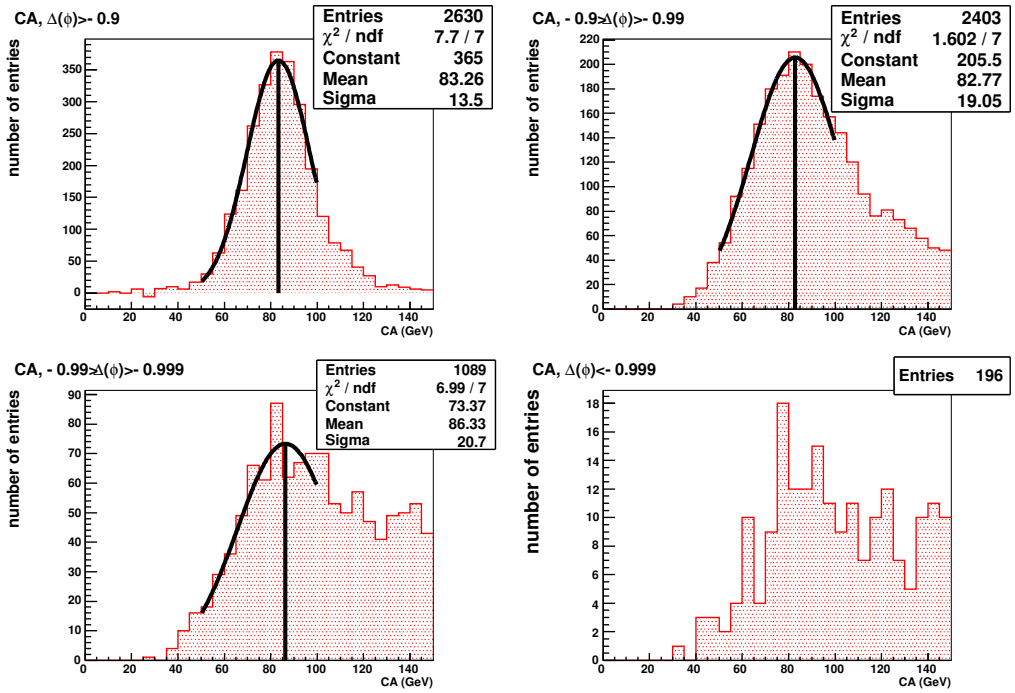

Figure 5.13: CA mass reconstruction with different $\cos(\Delta\phi)$cuts. $\sqrt{s} = 7$ TeV.

5.5.2 Cut on E_T^{miss}

One commonly cuts on E_T^{miss} >20 GeV. The argument for this requirement is that by low E_T^{miss} there probably are neutrinos escaping in opposite directions (back-to-back) cancelling each other's energy and the total E_T^{miss} hence is lower than it should be.

Figure 5.14 shows the CA versus E_T^{miss} with background (J3 and J4). One cannot set a reasonable cut on E_T^{miss} from these plots, and a deeper study is needed. Figure 5.14 is divided into horizontal slices each fitted with a Gaussian. This will give an idea of how well the CA performs in the different E_T^{miss} regions.

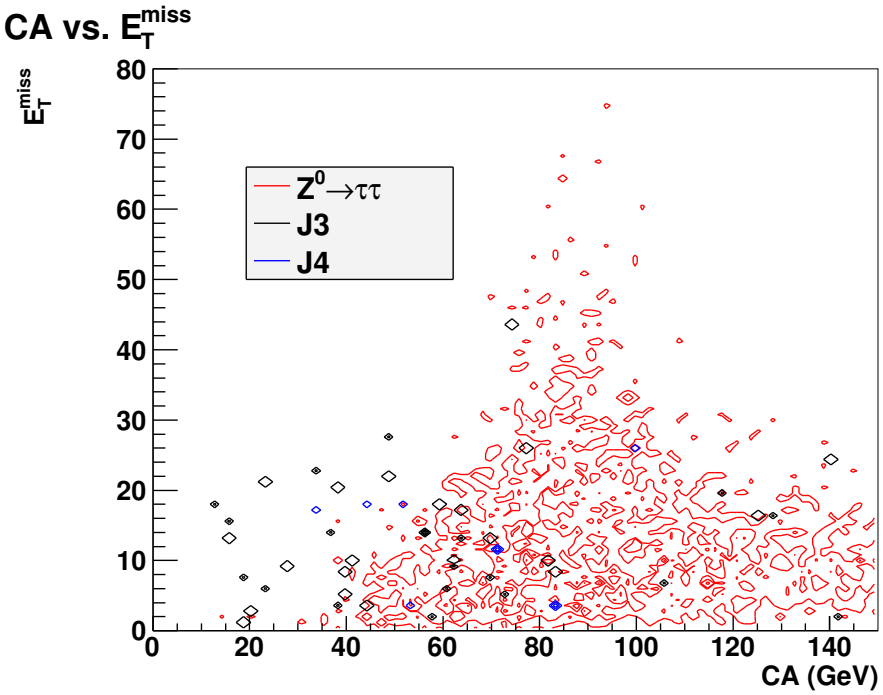

Figure 5.14: Profile plot of m_{CA} versus E_T^{miss} for $E_T^{miss} < 20$ GeV. $\sqrt{s} = 7$ TeV.

At the top in figure 5.15 one can see a stable m_{CA} even for small E_T^{miss} . The middle shows the sigma of the Gauss fit of each slice. The strange behaviour for large E_T^{miss} is due to low statistics, which one can see from the bottom plot. There is too low statistics in background to make such analysis plots.

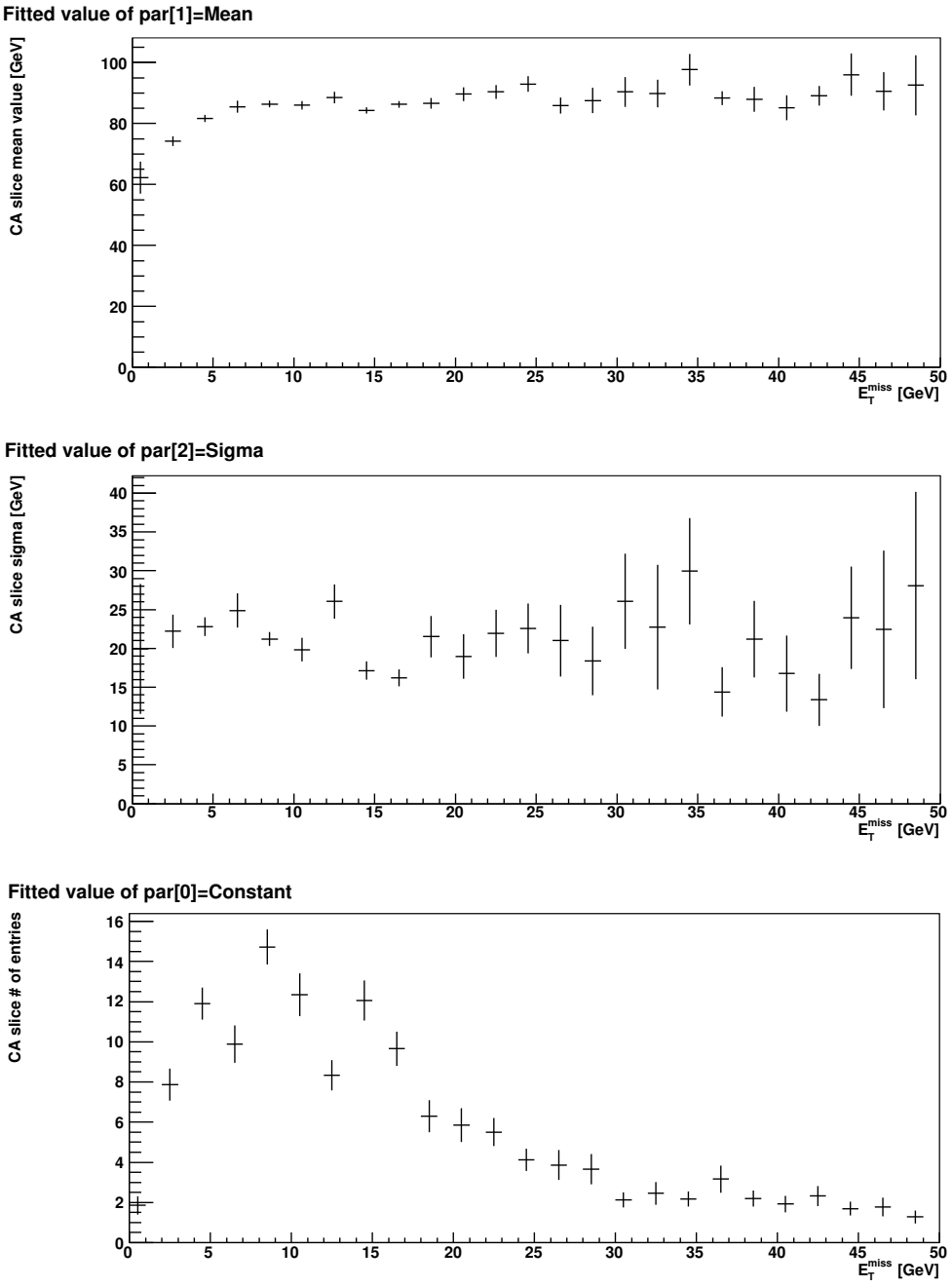

Figure 5.15: Profile plot of m_{CA} versus E_T^{miss} . $\sqrt{s} = 7$ TeV.

No cut on E_T^{miss} is recommended for the CA.

5.6 Absolute limitations in the CA

5.6.1 Unphysical neutrino energies

It is only possible to project the E_T^{miss} onto τ_1 and τ_2 directions if E_T^{miss} lies between the smallest angle between the two taus. Otherwise the fraction of τ_1, a, or τ_2, b, (or both) in equation 5.7 has to be negative in order to reconstruct the direction of E_T^{miss} . The reconstructed neutrinos will then have negative energy, which is unphysical. This happens in about 84% of the cases (after all other cuts). Table 5.1 shows for how much signal and background the CA can create physically allowed neutrinos. The uncertainities are calculated as:

$$\frac{1}{\sqrt{\text{number of cases}}} \tag{5.12}$$

Signal	$(15.6 \pm 0.4)\%$
J3	$(20 \pm 6)\%$
J4	$(26 \pm 16)\%$

Table 5.1: Signal surviving requirement of physically allowed neutrinos.

Probable reasons for this happening:

1. The neutrinos are not collinear with the tau directions
2. There is missing energy that originates from other sources than the tau decays
3. There are holes in the detector providing fake missing energy
4. Badly selected taus

Table 5.2 shows how much of each $\cos(\Delta\phi)$-region that passes the requirement of positive neutrino energy in $Z^0 \rightarrow \tau^-\tau^+$.

region	$E_\nu > 0$	amount of signal
$\cos(\Delta\phi) > -0.9$	$(20.1 \pm 0.8)\%$	27%
$-0.9 > \cos(\Delta\phi) > -0.99$	(14.8 ± 0.7) %	32%
$-0.99 > \cos(\Delta\phi) > -0.999$	(13.2 ± 0.8) %	25%
$\cos(\Delta\phi) < -0.999$	(13.3 ± 1.1) %	15%

Table 5.2: Signal surviving requirement of physically allowed neutrinos in different $\cos(\Delta\phi)$-regions.

5.7 Result

In figure 5.16, the mass distribution made with the CA on $Z^0 \rightarrow \tau^-\tau^+$ after all recommended cuts is shown. A Gaussian fit gives a mean value of 83.5 with $\sigma = 14.8$. The known Z^0 value of 91.2 GeV is within 1σ.

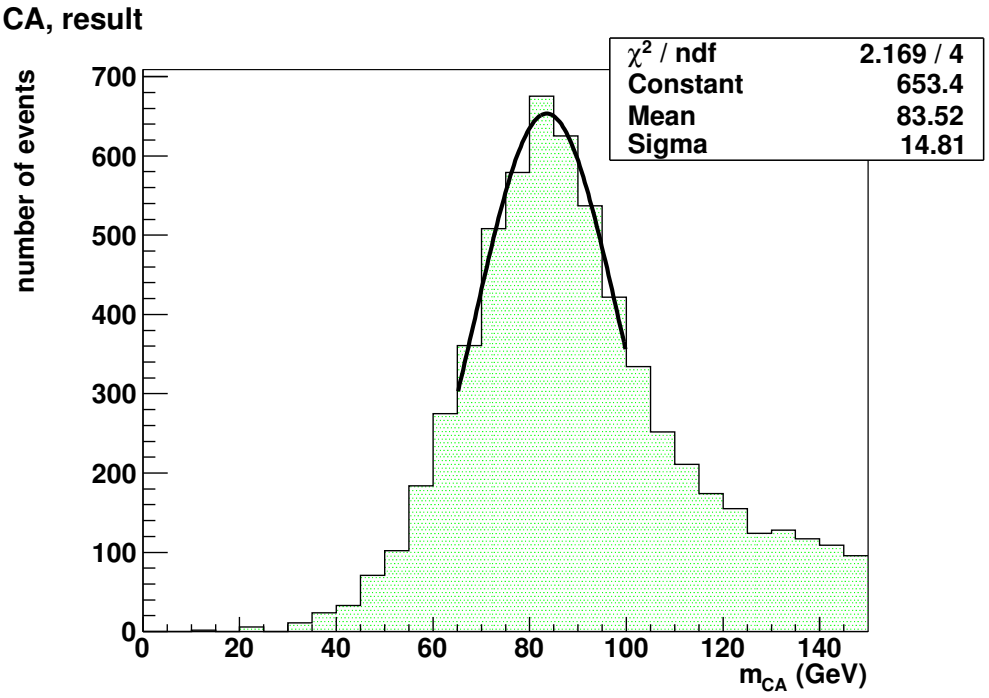

Figure 5.16: Reconstructed invariant mass using the CA with all recommended cuts. $\sqrt{s} = 7$ TeV.

5.8 Summary

- The CA is a good method with some limitations:
  - The CA reconstructs unphysical neutrinos in (81.5 $\pm$ 0.5)% of the events, which are rejected.
  - The CA breaks down when the reconstructed visible taus are back-to-back. A cut on $\cos(\Delta\phi) > -0.99$, which keeps 84.8 % of the signal, is recommended.
- No need of a E_T^{miss} -cut.
- Need of a new method that can gain more information from the taus.

- Reconstruction of invariant mass with CA in $Z^0 \rightarrow \tau^-\tau^+$ gives $m_Z^0 = 84 \pm 15$ GeV (figure 5.16).

Chapter 6

Boost method

In the previous chapter, the limitations of the CA by high transversal angle between the two visible taus became clear. A new method, developed by Bjarne Stugu [1] , and Thomas Burgess [1] has potential to be a better approximation in these cases.

The method builds upon ideas from Boost Mass technique [30] and a naïve approach saying that the leading tau must have least loss from the neutrino and hence be more similar to the mother tau.

The visible taus are boosted into the Z^0's centre-of-mass frame. This is done using the fact that the taus decay close to back-to-back in the this frame. The method guesses a boost iteratively until one reaches a reference system where the taus are back-to-back. As shown in section 5.3, taus are mainly boosted in the z-direction. Figure 6.1 shows β from MC truth Z^0 and calculated from boost method: $\beta = \frac{p_{||}}{\not{\mathrm{E}}}$. This verifies that the boost method finds β quite precisely. The chipped structure is due to a too large range of accepted β. This should be regulated in the improvement of the method. A further project could be to improve the method by implementing information from E_T^{miss} to boost in both z- and transverse directions.

[1]Department of Physics and Technology, University of Bergen

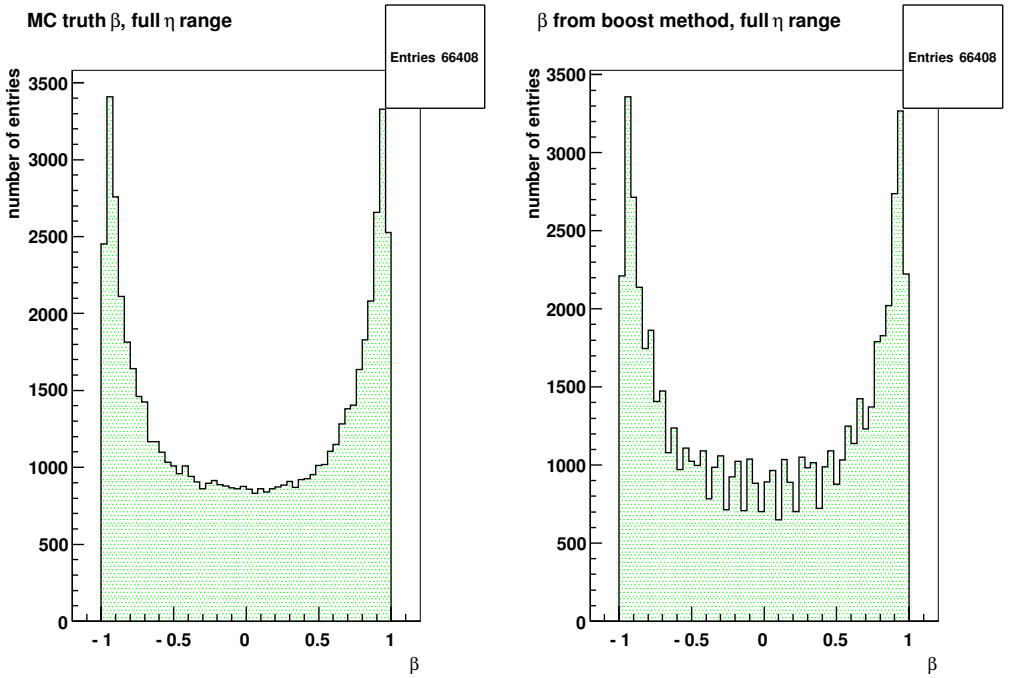

Figure 6.1: β for Z^0 in z-direction from MC truth (left) and from boosting method (right). $\sqrt{\mathrm{s}} = 7$ TeV.

The momenta of the visible taus in the Z^0 centre-of-mass frame cannot be larger then the half of the Z^0 mass. Or, if decaying from H^0, not larger than $\frac{m_{H^0}}{2}$. The plot of twice the momentum of the leading tau is hence expected to have a smeared triangular shape with the Z^0 mass at the end-point. Figure 6.2 shows the distribution of this quantity for fully simulated $Z^0 \rightarrow \tau^-\tau^+$.

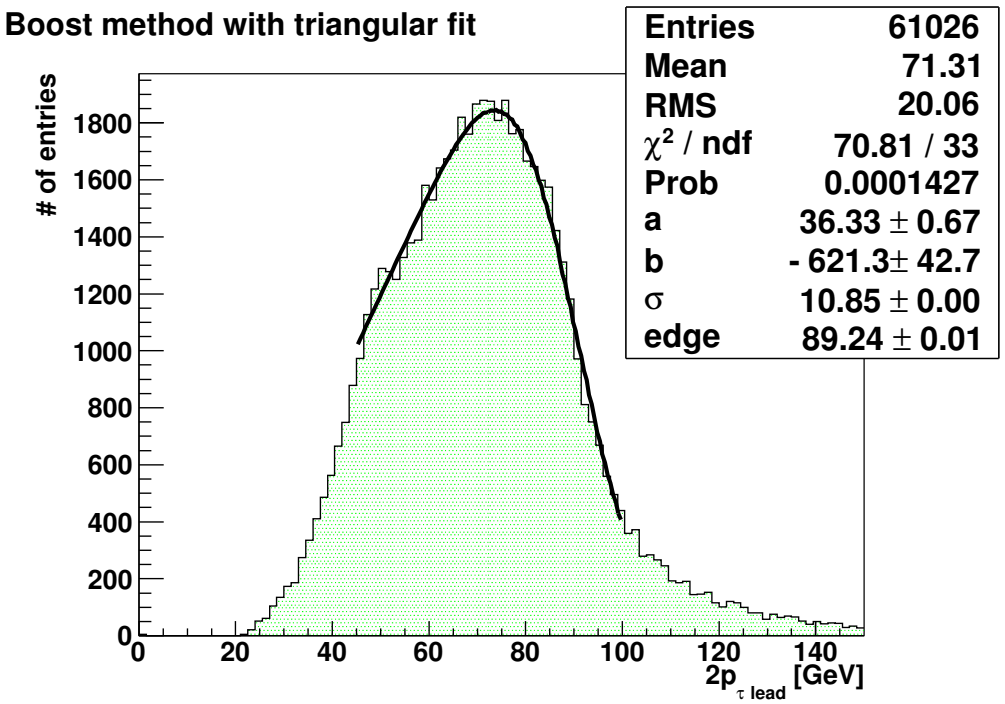

Figure 6.2: Boost method with triangular fit. $\sqrt{s} = 7$ TeV.

The plot is fitted with a Gaussian smeared triangle where the end point represent the reconstructed mass. The parameters are optimised to give the smallest χ^2/ndf[2]. Table 6.1 list the input (i.e. first guess) parameters used in this analysis.

Parameter	Size
Min	45 GeV
Max	100 GeV
Slope of triangle(p0)	28.9 GeV/number of entries
Crosses y-axis (p1)	-99 number of entries
Sigma of Gaussian (p2)	11 GeV
End point (p3)	89.2 GeV

Table 6.1: Parameters for triangle fit

The triangle fit is strongly dependent on the input parameters and has a tendency to give negative values of σ, which is unphysical. The problem is temporarily solved by setting limits on $\sigma \in \{0, 100\}$. An advantage of the fit method would

[2]number of degrees of freedom

be to use the quantities of the distribution itself to determine the input parameters like mean value, maximum, RMS etc. This will save much time spent on fitting the individual distributions, as done in this analysis. Note that the outcome endpoint parameter is 89.24 with a very small error, not reaching the known Z^0 mass of 91.2 GeV. The small errors are obviously wrong, and a better method of calculating the errors is done in section 6.5. Therefore, the errors listed in figure 6.2, 6.4, 6.6, 6.7, 6.8, 6.9, and 7.8 should be ignored.

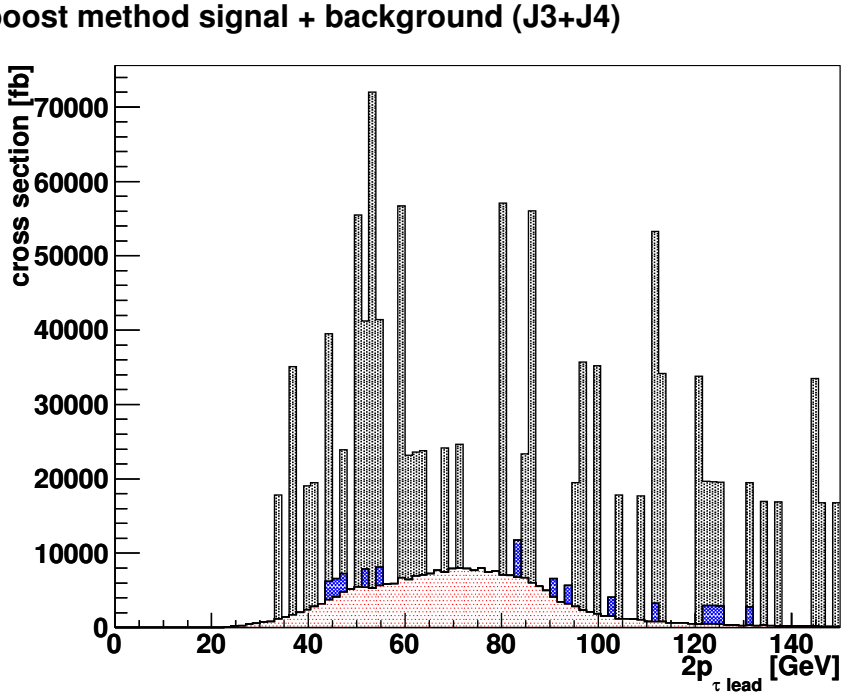

Figure 6.3: Boost method with $Z^0 \rightarrow \tau^-\tau^+$ (red), J3 (black) and J4 (blue). $\sqrt{s} = 7$ TeV.

6.1 Crack regions, a review

The cuts on tau η in chapter 3, was to avoid fake taus and fake E_T^{miss} . The boost method does not (yet) use information from E_T^{miss} and fake E_T^{miss} is not a problem. The plot to the left in figure 6.4 verifies this statement as the boost method seems to work in the region of $1.3 < \eta < 1.7$. The right plot in figure 6.4 shows the E_T^{miss} fake rate region, $\eta > 2.4$, which one can see is not affecting the boost methods. One actually expects the boost method to be especially good in this region because taus with high eta tends to have high boost in the z-direction. Due to this, no cut on η is recommended in the boost method.

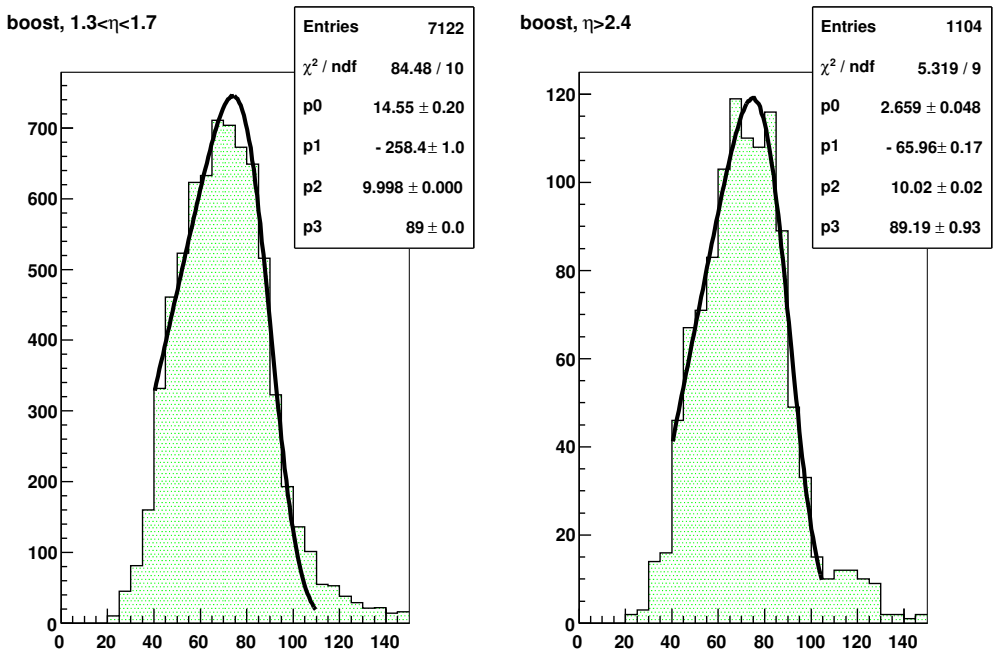

Figure 6.4: Boost method for different η cuts. $\sqrt{s} = 7$ TeV.

6.2 Cut on $\cos(\Delta\phi)$

For small $\cos(\Delta\phi)$ (more back-to-back), the taus have a smaller boost in the transverse plane. Since the boost method neglects possible transverse boosts, it performs better when there is no transverse boost. This makes the boost method a complementary method to the CA. Analysing the boost method versus $\cos(\Delta\phi)$ is done by the FitSlices method in root. Using the parameters of the triangle fit set in table 6.1, slices with different range of $\cos(\Delta\phi)$are fitted with the triangle method. As seen left in figure 6.5, the end point parameter stabilises with decreasing $\cos(\Delta\phi)$, as expected. The values lie mostly above the known $m_Z^0 = 91.2$ GeV. χ^2/ndf is around 1-2, slightly increasing for smaller $\cos(\Delta\phi)$ending up with an extremely large value of 100, close to $\cos(\Delta\phi)$= -1. This is due to the weakness by using the same input parameters for all slices, and the method being strongly dependent of them. It is therefore hard to recommend a cut on $\cos(\Delta\phi)$from this alone. For this purpose, m_{boost} is plotted for four different $\cos(\Delta\phi)$regions, see figure 6.6. The same regions as for CA in figure 5.13 are chosen afterwards to make it directly comparable with the CA performance.

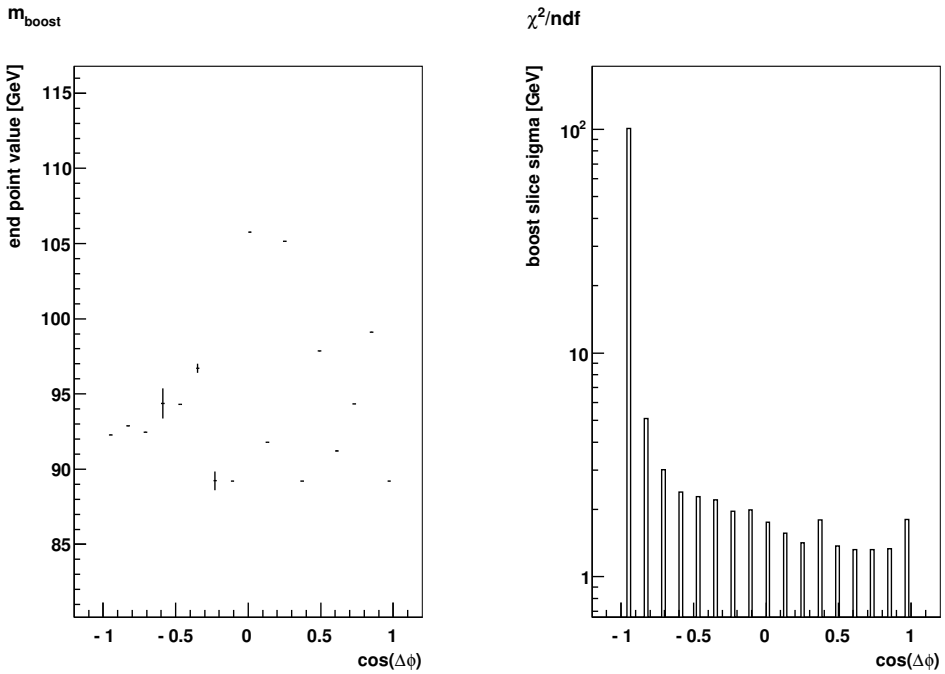

Figure 6.5: Boost method end point versus $\cos(\Delta\phi)$ $\sqrt{\mathrm{s}} = 7$ TeV.

They are all fitted with the triangle fit, but with different input parameters giving the individual lowest χ^2/ndf. Contrary to m_{CA} , m_{boost} has a tail of events with high energies for low $\cos(\Delta\phi)$, but a sharper edge for lower $\cos(\Delta\phi)$. For the three plots with $\cos(\Delta\phi)$<-0.9, a lower χ^2/ndf is achieved than by $\cos(\Delta\phi)$>-0.9. A requirement of $\cos(\Delta\phi)$<-0.9 keeps $81.6 \pm 0.4\%$ of the events and is recommended.

6.3 Cut on E_T^{miss}

Since the boost method neglects the E_T^{miss} , one could expect it too have a sharper edge for small E_T^{miss} . Figure 6.7 shows four different E_T^{miss} regions: > 20 GeV, $10 <$ GeV < 20, $5 <$ GeV < 10, GeV< 5. One cannot, from these plots, observe a change in the sharpness of the edge. Due to this, no requirements on the E_T^{miss} is recommended.

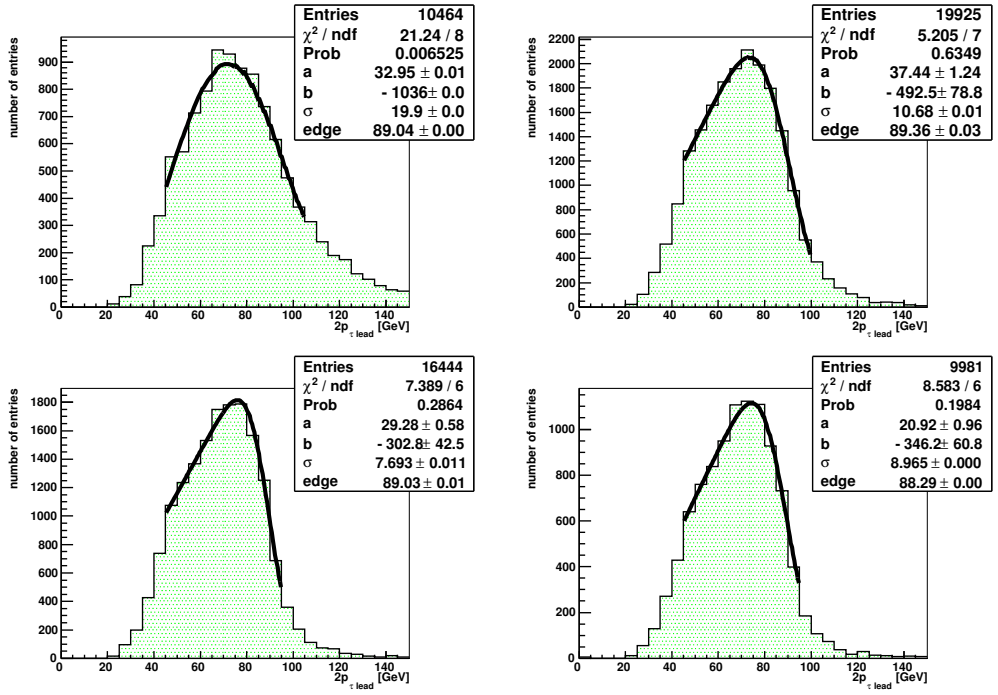

Figure 6.6: Boost method for different $\cos(\Delta\phi)$cuts. $\sqrt{s} = 7$ TeV.

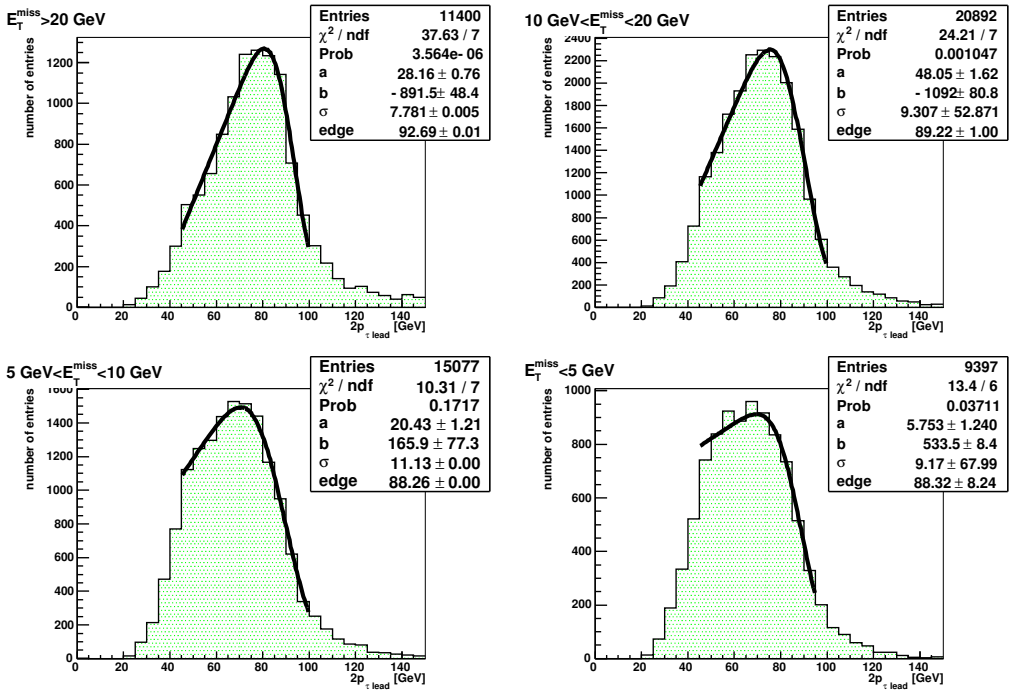

Figure 6.7: Boost method for different E_T^{miss} regions. $\sqrt{s} = 7$ TeV.

6.4 When CA does not work

About 84% of the signal is lost in CA because the method reconstructs neutrinos with negative energy. The boost method does not have any such constraints and it is interesting to see that the boost method performs well when CA doesn't. This, together with good performance for low $\cos(\Delta\phi)$, makes the boost method a good complementary method to the CA. In figure 6.8, one can see that the boost method works well, when it is applied on events where the CA reconstruct neutrinos with negative energy.

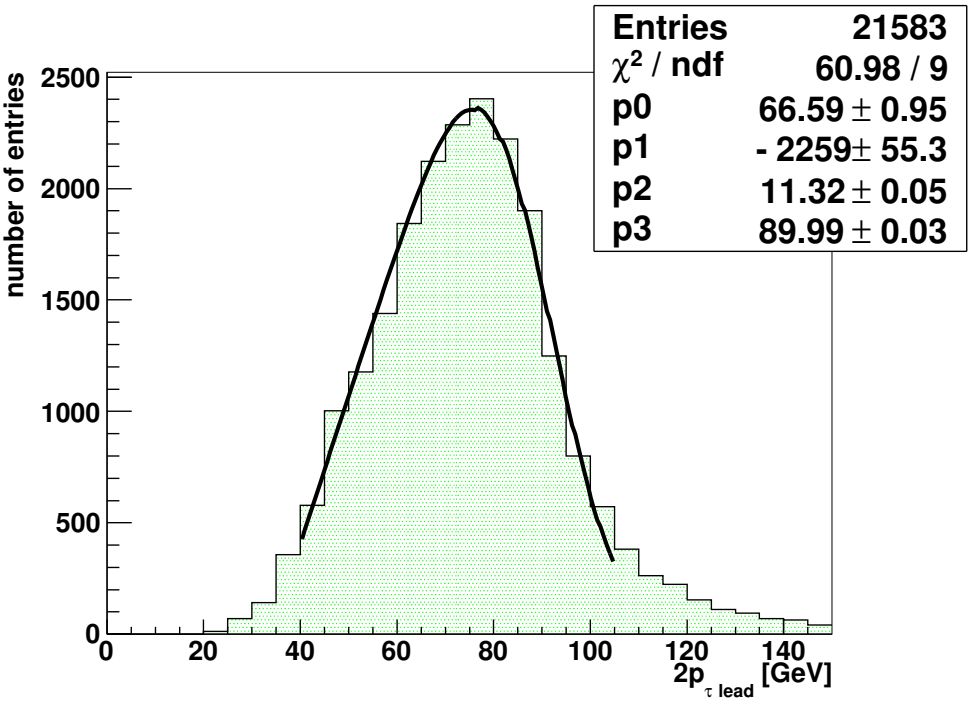

Figure 6.8: Boost method for events where the CA doesn't work because of neutrinos with negative energy. $\sqrt{s} = 7$ TeV.

6.5 Result

With all recommended cuts, one gets a $2{\cdot}_{\tau,\text{lead}}$-distribution shown in figure 6.9. The stability of the fitted edge value was tested by randomising the distribution. The error is gained through a randomisation of the distribution 1000 times (1000 pseudo-experiments). By fitting each pseudo experiment, one gets the edge distribution shown in figure 6.10. This gives $m_Z^0 = 88.7 \pm 0.2$ GeV. This error is obviously to small, which is due to fixed input parameters (edge input parameter

= 88.6 GeV). The same input parameters are used for all 1000 pseudo experiments, resulting in a too small variation in the edge, but large values of χ/ndf. The value is also consistently too small compared to the known m_Z^0-value. This could be a calibration issue; the calorimeters register less energy than the particles really have, and one gets generally lower energy values. It could also be that the smeared triangle fit is too simple, this first guess of a fit function should be further investigated and improved.

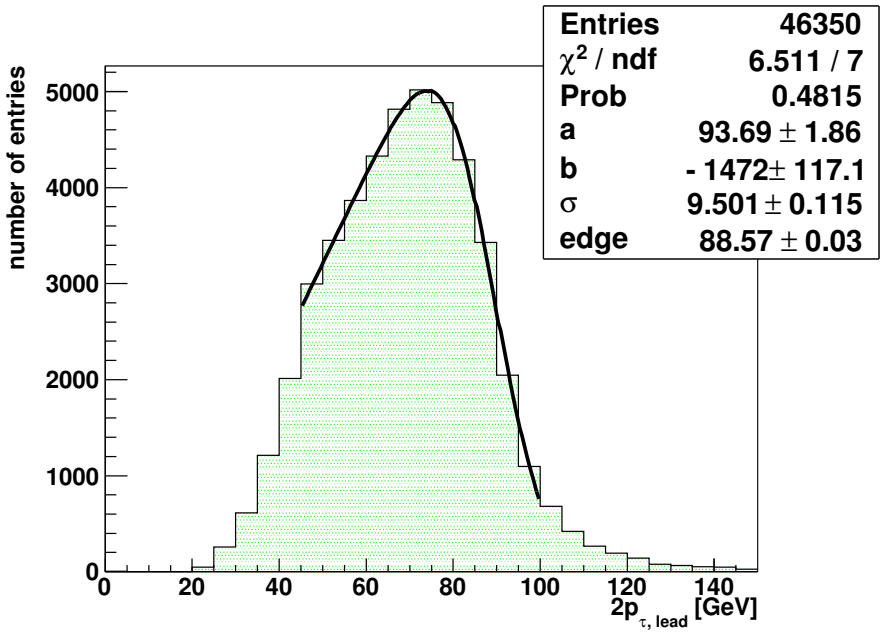

Figure 6.9: Boost method with all recommended cuts. $\sqrt{s} = 7$ TeV.

6.6 Summary

- In the boost method, the reconstructed taus are boosted along the z-axis until they are back-to-back. Two times the momentum of the leading tau should give a smeared triangle distribution with endpoint in the mass value of the mother particle.
- The boost method works better for transverse back-to-back taus and any E_T^{miss} direction and is therefore a good complementary method to the CA. A requirement of $\cos(\Delta\phi)$<-0.9 keeps $81.6 \pm 0.4\%$ of the events and is recommended.
- A possible upgrade of the method is to implement E_T^{miss} information.

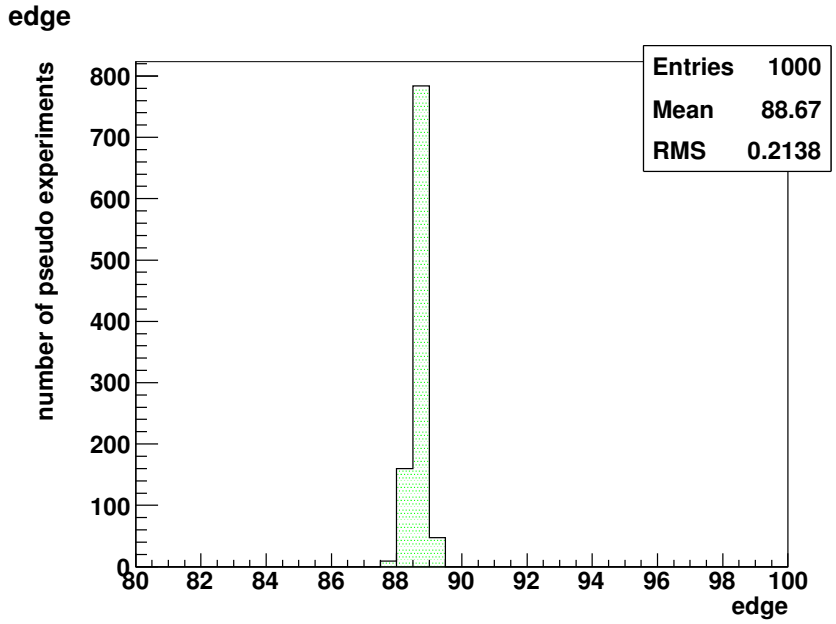

Figure 6.10: The edge of 1000 randomised $2p_{\tau,\text{lead}}$-distributions.

- The triangular fit is strongly dependent on the input parameters, and a better way of setting the parameters is required. It should also be considered to make a fit function that fits the distribution better.

Chapter 7

Comparing with $H^0 \rightarrow \tau^-\tau^+$

H^0 is so similar to the Z^0 that the methods discussed in chapter 5 and 6 should work properly with a sample of $H^0 \rightarrow \tau^-\tau^+$ as well.

From figure 7.1 one can see that a Higgs at this mass would decay to $b\vec{b}$ in about 70% of the cases, WW in 10-11%, and $\tau\tau$ and gg in 7% of the cases. $b\vec{b}$ and gg produce hadronic showers, which contribute to QCD background. W decays to one tau in ≈11% of the cases, and to hadrons in 68% og the cases. Therefore, the main background will be QCD jets and taus from $Z^0 \rightarrow \tau^-\tau^+$.

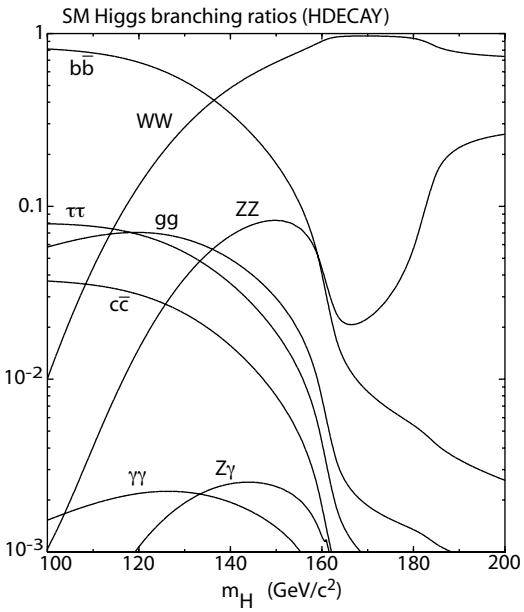

Figure 7.1: Branching fractions for Higgs decay versus m_H^0 [3]

Used in this analysis is a $H^0 \rightarrow \tau^-\tau^+$ sample, with $m_H^0 = 120$ GeV. Each of the 9998 events consist of one H^0 decaying to two taus, which again decays

hadronically. The cross section is $75.3 \cdot 10^{-6}$ nb. This causes a weighting factor of $5.75451 \cdot 10^{-9}$. With this cross section, one expects to find four orders of magnitude more Z^0s than Higgs. One can already see the main difficulty of finding the Higgs: separating it from the Z^0.

7.1 Energy and opening angle

Figure 7.2 shows the longitudinal (left) and transverse (right) momentum of the reconstructed taus in $H^0 \rightarrow \tau^-\tau^+$. The lack of entries in p_T for small energies comes from trigger requirements.

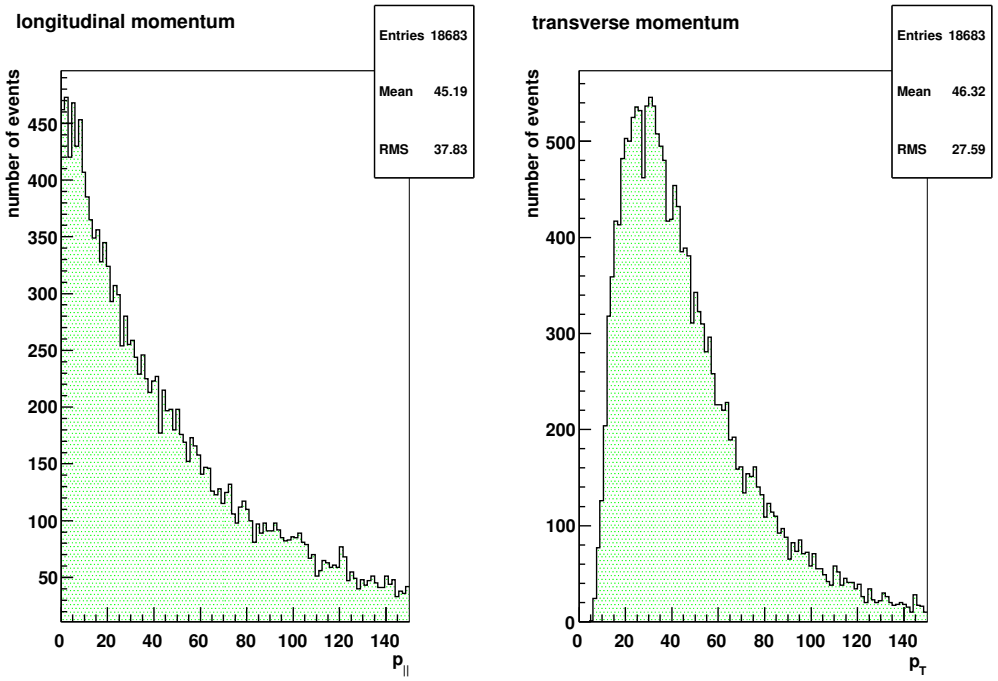

Figure 7.2: Longitudinal (left) and transverse (right) momentum of the reconstructed taus in $H^0 \rightarrow \tau^-\tau^+$. $\sqrt{s} = 7$ TeV.

Since the $m_H^0 > m_Z^0 \gg 2m_\tau$, it is expected that the decaying taus are boosted. This is validated in figure 7.3 where one can see a back-to-back tendency in the transverse plane, while in 3D, all angles are about equally represented. One expects both the CA and the boost method to work well.

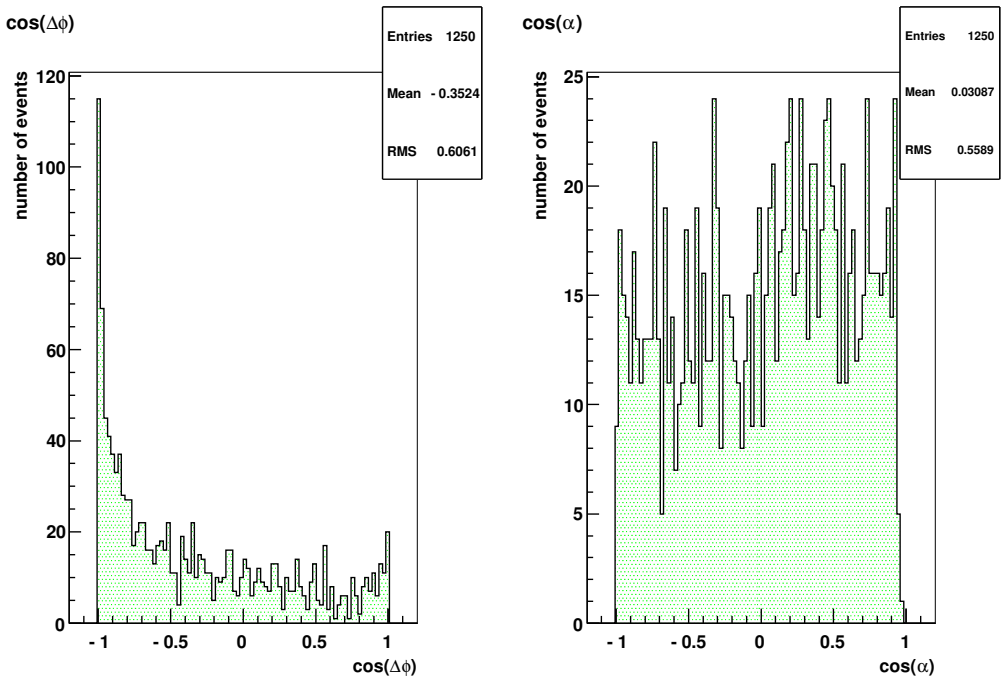

Figure 7.3: $\cos(\phi)$ and $\cos(\alpha)$ between the two leading reconstructed taus in $H^0 \rightarrow \tau^-\tau^+$. $\sqrt{s} = 7$ TeV.

The β in $H^0 \rightarrow \tau^-\tau^+$, calculated from the boost method is shown in figure 7.4. Due to low statistics, it is hard to compare directly to the β-plot in figure 6.1 calculated from $Z^0 \rightarrow \tau^-\tau^+$. In $H^0 \rightarrow \tau^-\tau^+$ no significant peaks are observed, while there in $Z^0 \rightarrow \tau^-\tau^+$ are significant peaks in $\beta = \pm 1$.

7.2 CA with $H^0 \rightarrow \tau^-\tau^+$

In figure 7.5 the CA performance is shown on $H^0 \rightarrow \tau^-\tau^+$ alone. A Gaussian fit gives a peak at (110.9±10.0) GeV, which is about the expected value; $m_H = 120$ GeV is within the errors. In figure 7.6 the background ($Z^0 \rightarrow \tau^-\tau^+$, J3 and J4) is taken into account. The Higgs bosons drown in the tail of Z^0s at high energies. A harder cut on $\cos(\Delta\phi)$ would remove much of the high energetic events. Requiring $\cos(\Delta\phi)$ >-0.9, instead of the recommended -0.99 (figure 7.7, gives the Higgs a better ratio to background, but it drowns still. The method of CA cannot discover a Higgs with $m_H = 120$ GeV alone.

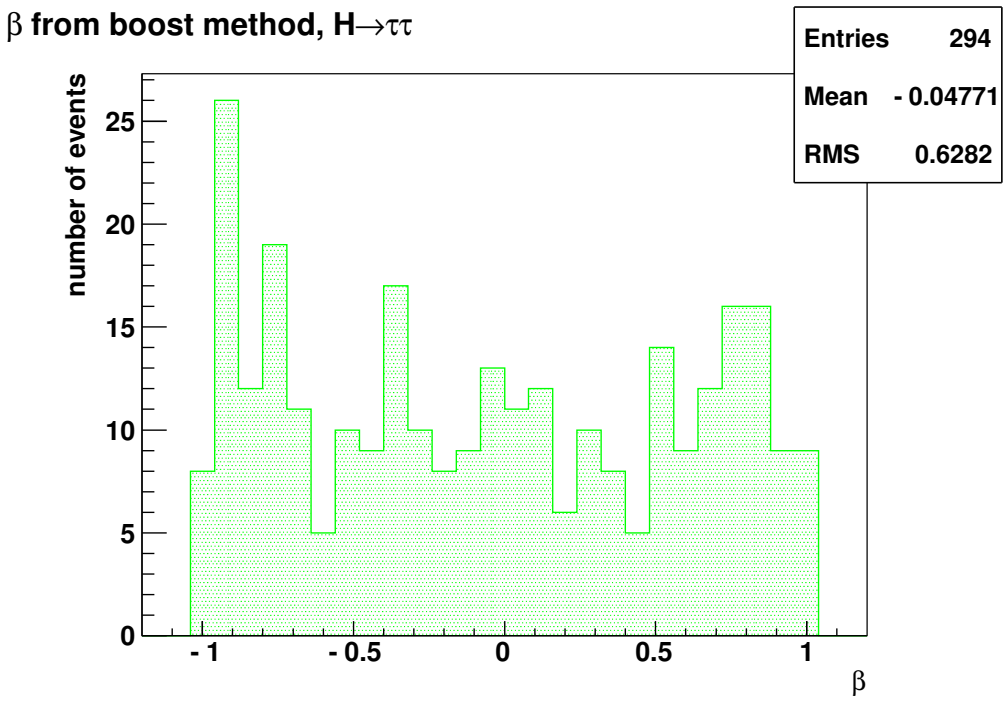

Figure 7.4: β calculated from the boost method with reconstructed taus from $H^0 \rightarrow \tau^-\tau^+$. $\sqrt{s} = 7$ TeV.

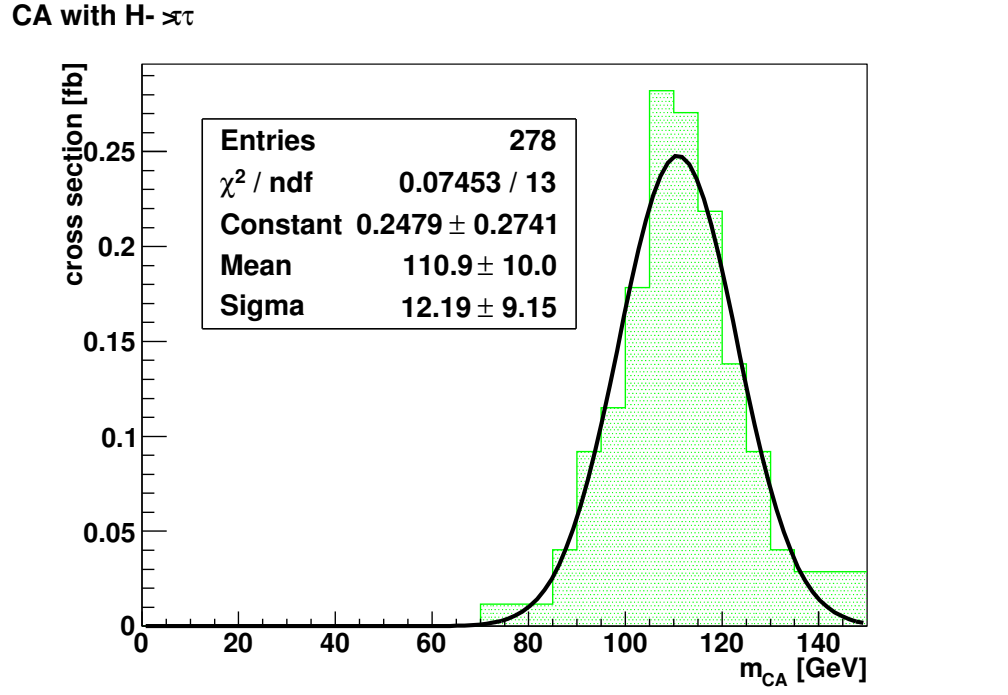

Figure 7.5: CA with $H^0 \rightarrow \tau^-\tau^+$. $\sqrt{s} = 7$ TeV.

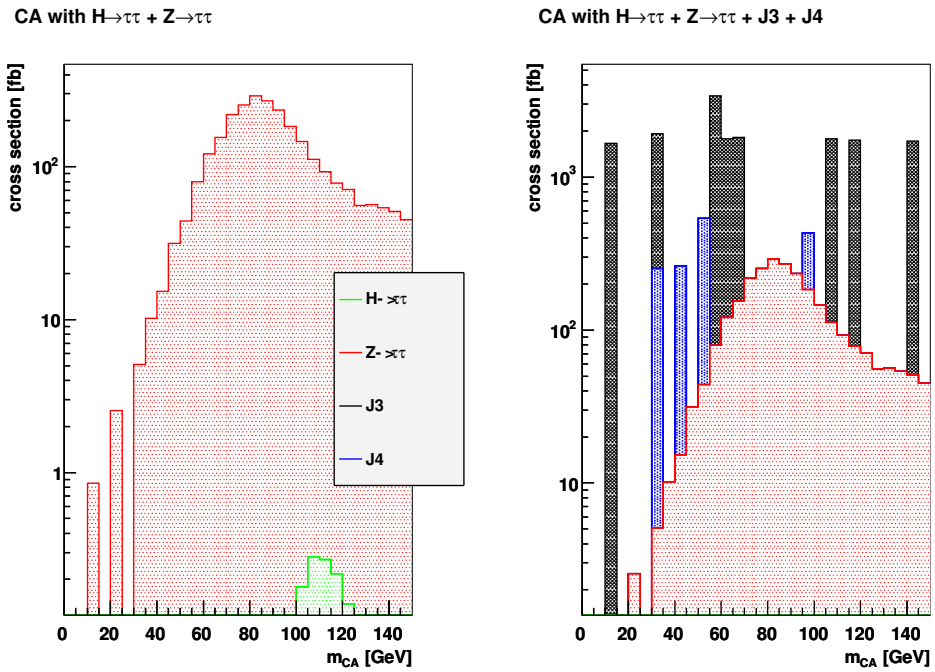

Figure 7.6: CA with $Z^0 \rightarrow \tau^-\tau^+$ + $H^0 \rightarrow \tau^-\tau^+$ *(left)* and additionally + J3 + J4 *(right)*. $\sqrt{s} = 7$ TeV.

7.3 Boost method with $H^0 \rightarrow \tau^-\tau^+$

In figure 7.8 is the boost method performance shown on $H^0 \rightarrow \tau^-\tau^+$ alone. The number of events passing the requirements is only 241. This low number is mainly due to the recommended cut on $\cos(\Delta\phi)$<-0.9, which in $H^0 \rightarrow \tau^-\tau^+$ cuts $78 \pm 3\%$. Using the triangle fit described in chapter 6, the lowest χ/ndf gives an end-point value of 119.2 GeV, but the error is hard to say anything about. The parameter errors listed in the figure are wrong. With a better way of determinating the input parameters, the method of rendomised pseudo-experiments, explained in section 6.5, could give a reasonable error. With a good separation from $Z^0 \rightarrow \tau^-\tau^+$ background, e.g. with spin studies, this method can be used to determine the m_H. Figure 7.9 takes the background ($Z^0 \rightarrow \tau^-\tau^+$, J3 and J4) into account. The Higgs signal drowns in the background, especially the $Z^0 \rightarrow \tau^-\tau^+$, and can not be separated by the boost method only.

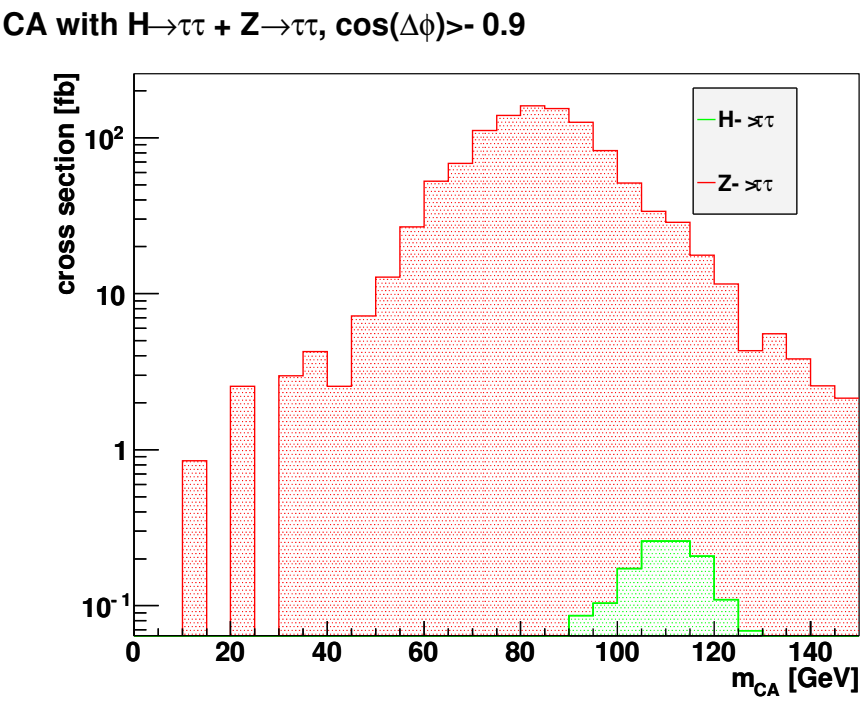

Figure 7.7: CA with $Z^0 \rightarrow \tau^-\tau^+$ + $H^0 \rightarrow \tau^-\tau^+$, $\cos(\Delta\phi)$ >-0.9. $\sqrt{s} = 7$ TeV.

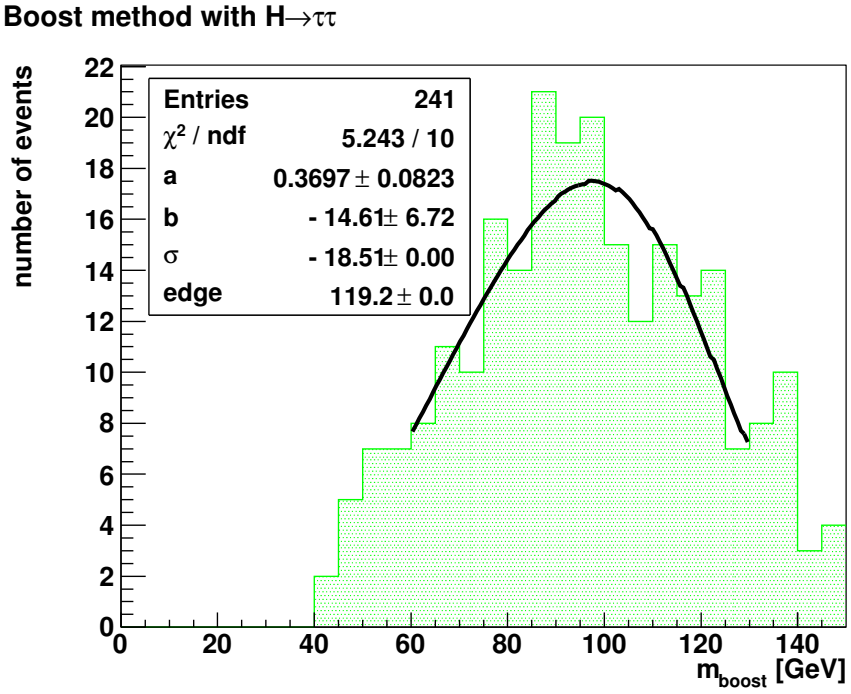

Figure 7.8: boost $H^0 \rightarrow \tau^-\tau^+$. $\sqrt{s} = 7$ TeV.

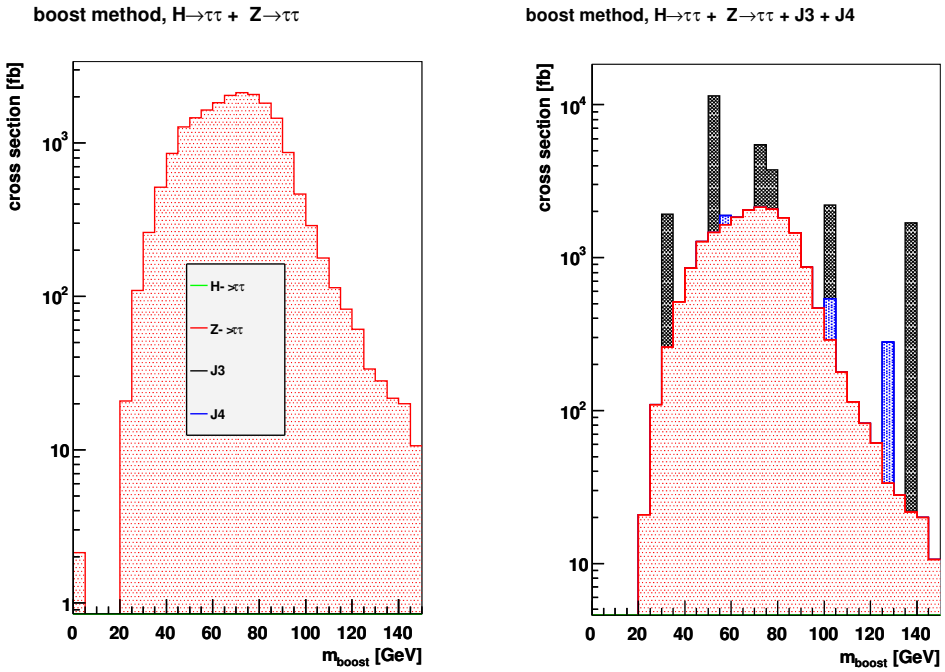

Figure 7.9: boost with $Z^0 \rightarrow \tau^-\tau^+$ + $H^0 \rightarrow \tau^-\tau^+$. $\sqrt{s} = 7$ TeV.

7.4 Discussion

The CA and the boost method are not good enough to separate $Z^0 \rightarrow \tau^-\tau^+$ events from $H^0 \rightarrow \tau^-\tau^+$ events with a H^0 mass at 120 GeV at 7 TeV. In CA, the H^0 signal seems to drown in the high energetic tail of Z^0s. A looser $\cos(\Delta\phi)$-cut; > 0.9 instead of the — in this analysis — recommended -0.99, removes much of the tail and gives a better ratio between H^0 and Z^0, but the difference is still too large to separate them. Also the boost method has no chance of separating the two signals. The $H^0 \rightarrow \tau^-\tau^+$ signal is simply too weak. A better separation goes in the direction of better tau selections, and even more with a method taking other differences into account between the Z^0 and the H^0 than the difference between their respective masses. A spin study is a good candidate for this. After finding a method to remove the $Z^0 \rightarrow \tau^-\tau^+$ background, one can use the CA and the boost method to determine the Higgs mass.

Chapter 8

Comparing with real data

The first period of data taking with the LHC is at 7 TeV. The plan is to run until 1 fb^{-1} of data is collected. This is estimated to take 18-24 months. The dataset used in this chapter is run number 152409, created April 5th 2010 with 5593559 events. This will be studied with the CA and the boost method as far as is reasonable.

In table 8.1 the number of tau pairs that pass the safe cut requirements are listed. When applying the OS-SS on these data, only (7.8$\pm$1.6)% of the tau pairs when applied on the CA and (3.2$\pm$0.8)% of the tau pairs when applied on the boost method, is left. The requirements — recommended in section 3.2.4 — would remove too much data, and hence, the only requirement on the tau candidate is charge = $\pm$1.

Safe cut	Number
taus	141291
loose taus	10279
medium taus	3675
tight taus	840
tau pairs	17518
tau pairs, 2 loose	320
tau pairs, 2 medium	55
tau pairs, 2 tight	2

Table 8.1: Number of taus and tau pairs that pass different safe cuts.

8.1 Observables

The transverse and longitudinal momentum, shown in figure 8.1, is from single taus. More high energetic entries in $p_{||}$ than in p_T show a boost in the z-direction, as expected.

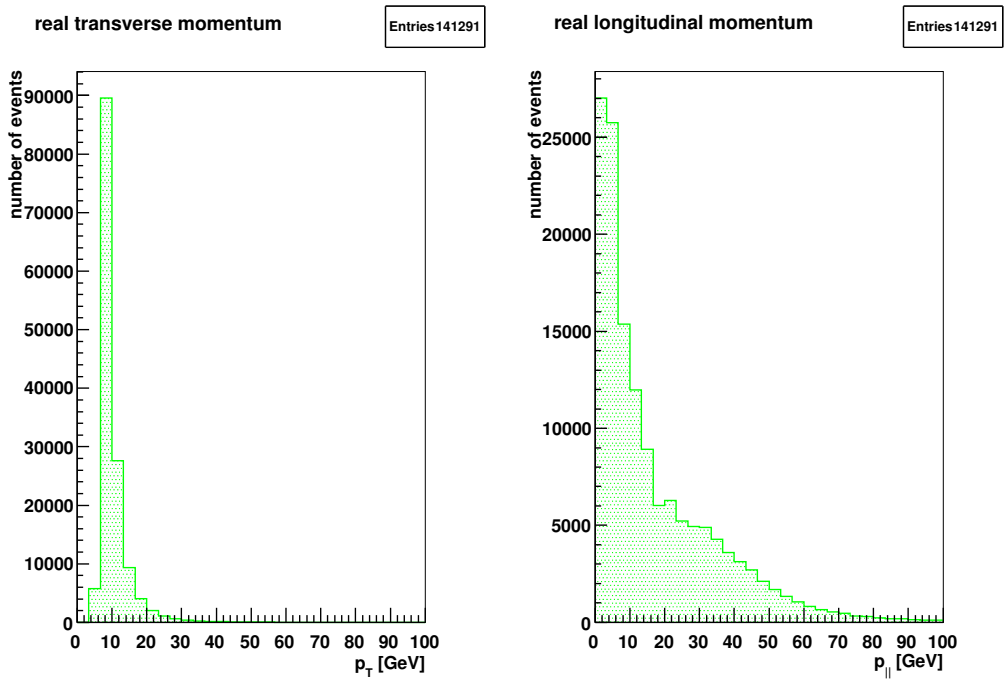

Figure 8.1: Transverse *(left)* and longitudinal *(right)* momentum for real tau candidates, $\sqrt{s} = 7$ TeV.

The E_T^{miss} have been an important quantity through this analysis, so let's take a look on what it looks like in the real data. In figure 8.2, the E_T^{miss} distribution shown left is similar to what we got from simulation (figure 5.1). The $\cos(\Delta\phi)$distribution to the right in figure 8.2 shows the same distribution as the simulation (figure 5.1).

As a pair, no further constrains are done except of finding two qualifying taus in the same event, and OS-SS.

8.2 The CA with real data

From 17518 tau pairs, 3805 of them pass the criteria of the CA reconstruction of positive neutrino energies. This amounts to $17.8 \pm 0.7\%$. The 146 tau pairs

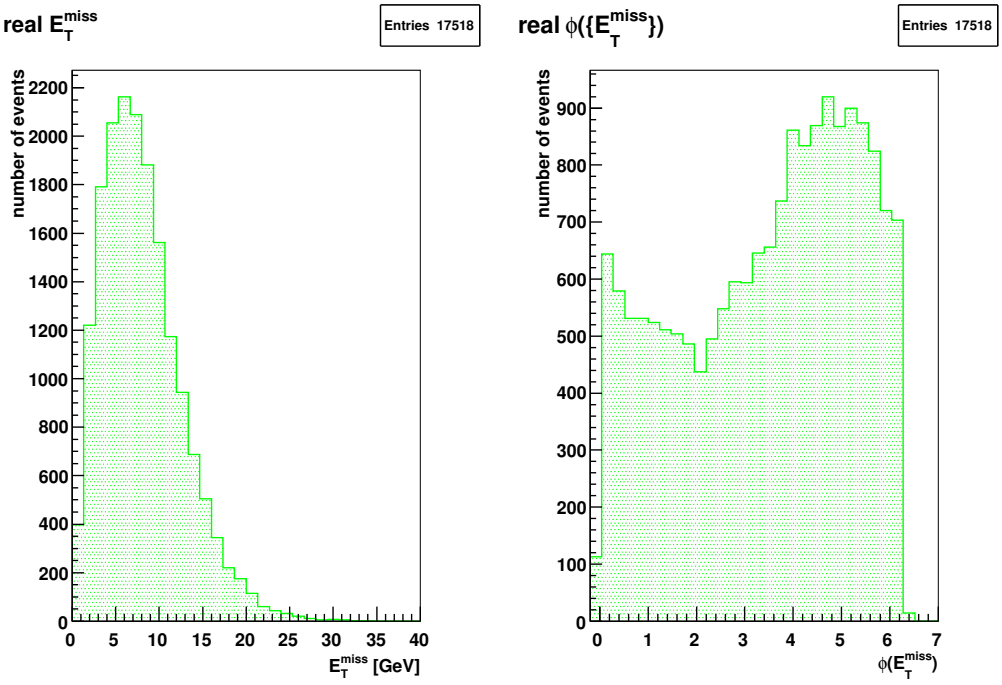

Figure 8.2: E_T^{miss} *(left)* and $\cos(\Delta\phi)(E_T^{\text{miss}})$ *(right)* on real data, $\sqrt{s} = 7$ TeV.

that are left after the OS-SS are shown in figure 8.3. Due to low statistics, the OS and SS background distributions are not equal, and do hence not cancel each other out. A little bump is observed around 80 GeV, but due to very low statistics and the fact that no $\cos(\Delta\phi)$-cuts, safe cuts, seed cuts nor η-cuts are applied, one cannot be certain this comes from Z^0 decaying taus, instead of from background fluctuations.

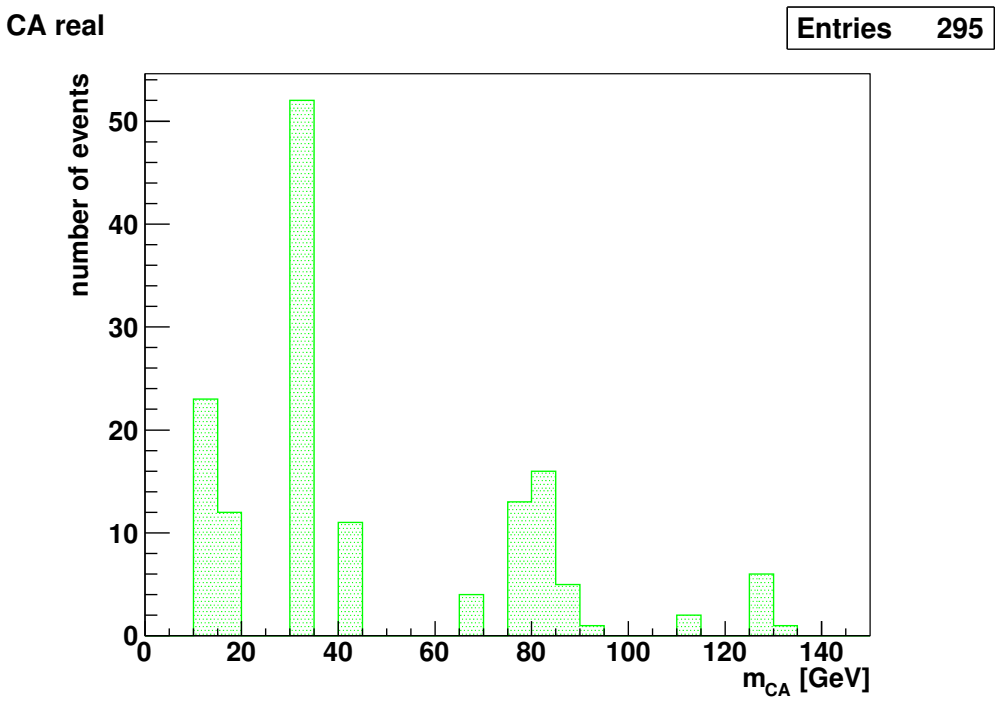

Figure 8.3: The CA applied on real data, $\sqrt{s} = 7$ TeV.

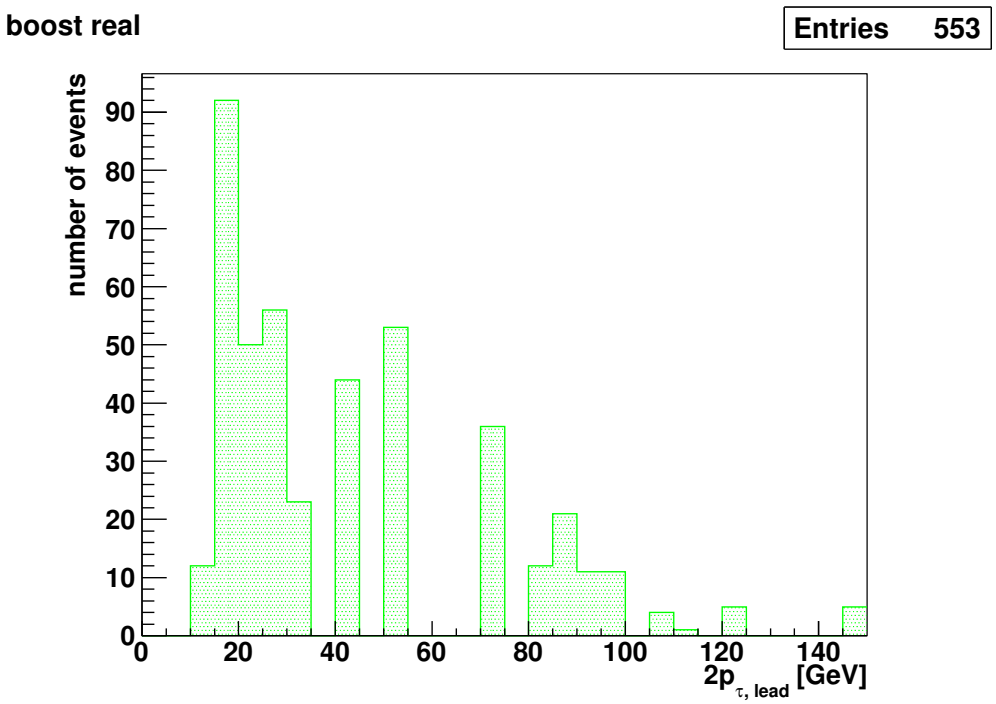

Figure 8.4: Boost method on real data, $\sqrt{s} = 7$ TeV.

8.3 Boost method with real data

The boost method works on all tau pairs, and 436 tau pairs are left after OS-SS. In figure 8.4, one can see the boost method applied on these 436 tau pairs. Due to unreduced background, the distribution looks different from the simulations, and a triangle fit on this is meaningless.

The β generated from the boost method is shown in figure 8.5.

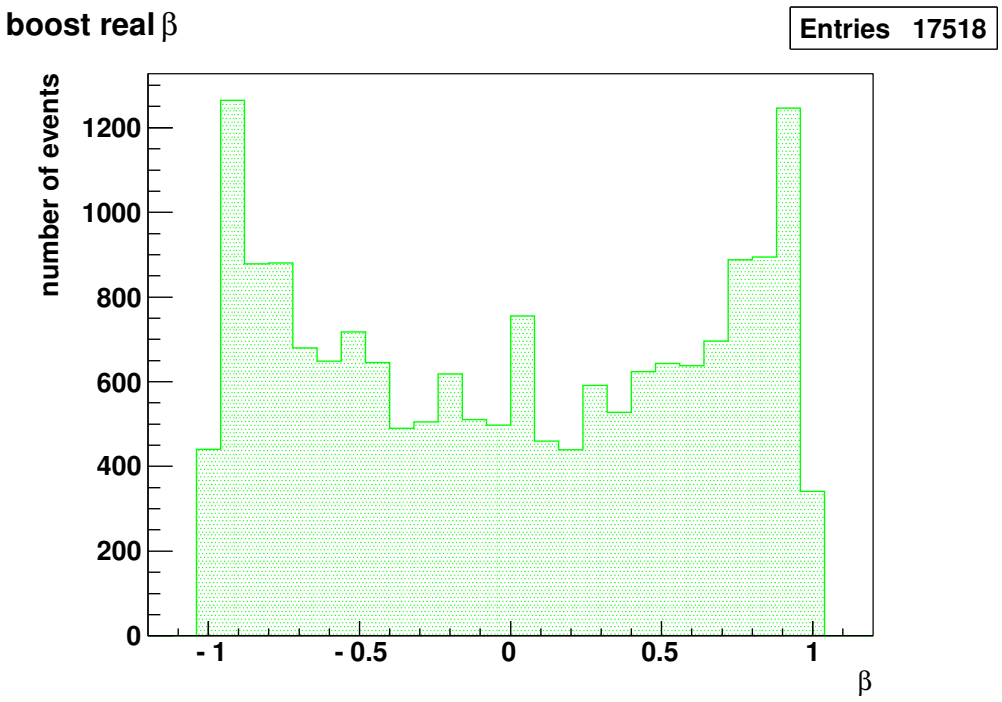

Figure 8.5: β from boost method on real data, $\sqrt{s} = 7$ TeV.

8.4 Conclusions

With 5593559 events, 141291 tau candidates and 17518 tau pairs have been handed in. Over 90% of the signal is removed by applying the OS-SS, and hence, no further cuts than the charge and OS-SS are applied. To get any result of mass reconstruction from such few tau pairs is near to meaningless, but one can see that the methods are working, ready to handle more data.

Chapter 9

Conclusion

The escaping neutrinos is the main problem in the mass reconstruction in simulated $Z^0 \rightarrow \tau^-\tau^+$ events. In this analysis two different methods of dealing with the neutrinos have been studied: the Collinear Approximation (CA), and the boost method. The CA uses the E_T^{miss} information to correct for the missing energy coming from neutrinos, by assuming that the visible and invisible decay products are collinear, and that the neutrinos are the only source of E_T^{miss} .

In the boost method the visible decay products are boosted in the z-direction until they are as back-to-back as possible. As the taus should have the same momentum in this frame, the neutrino contribution is assumed to be less dominant for the leading tau. Doubling this momentum gives a smeared triangular shape with its end-point at m_{Z^0}.

The CA calculates neutrinos with negative energy in 84% of the cases. These events cannot be used by the CA as it functions today. The boost method does not have any such constrains, and has the advantage of working for all events, which increases the statistics.

The CA breaks down for transverse back-to-back taus, and a requirement of $\cos(\Delta\phi) > -0.99$ is recommended from the results of this analysis. Transverse back-to-back taus have less transverse boost, and the boost method works better for these. A requirement of $\cos(\Delta\phi) < -0.9$ is recommended. This makes the two methods overlapping in $\cos(\Delta\phi)$and good complementary methods of each other.

A requirement on E_T^{miss} is not found necessary for the CA, nor for the boost method.

With both methods, the reconstructed mass tends to be lower than the known value. This might be a calibration problem.

The triangle fit function describes the $2 \cdot p_{\tau,\text{lead}}$-distribution quite well as a first guess, but can be improved in order to fit the distribution better. It needs also an improvement by making it independent of the input parameters.

Both methods work well on $H^0 \rightarrow \tau^-\tau^+$ isolated, but are not able to separate the Higgs signal from the background of $Z^0 \rightarrow \tau^-\tau^+$; the cross section of the Higgs signal is too small.

From 5593559 events of real data, 17518 tau pairs, with the requirement of |charge|=1, were found. 3805 of them pass the criteria for positive neutrino energy in the CA. A little bump around 80 GeV were observed, but this could be due to fluctuations; there were only 30 events in this bump. The boost method uses all 17518 pairs, but no triangular shape was observed, as expected when no signal is present. This will probably change with more data and the possibility to remove more background.

Further work

The CA is an established method and will be used without further improvements, yet a requirement of 1-prong decays may give a better approximation, since 3-prongs and more necessarily becomes more acollinear.

The boost method is a new method, developed this year. It is a promising method with room for improvements. The boost method does not make use of the E_T^{miss} information, which is the only empirical information we have about the neutrinos. One could improve the boost method by implementing the E_T^{miss} information into it.

Finally, a spin study could be a good approach to separate taus originating from $Z^0 \rightarrow \tau^-\tau^+$ from taus coming from $H^0 \rightarrow \tau^-\tau^+$. After a good separation, the CA and the boost method will greatly benefit future studies of mass reconstruction in $H^0 \rightarrow \tau^-\tau^+$, $Z^0 \rightarrow \tau^-\tau^+$ and other tau-related studies.

Appendix A

Glossary and list of acronyms

benchmark point
: In a model i.e. MSSM (Minimal Supersymmetric Standard Model), the constants may not be fixed. In many cases it is customary to choose a set of parameters. Such a set with parameters in a model is called a benchmark point.

combinatorics
: In an event there may be really many tracks. In order to combine the right e.g. two, we combine each track with all the other. The false combined tracks will then be like a background. Some times possible to reduce by smarter programming, sometimes not possible to reduce.

jet
: A narrow shower of tracks

leading (tau)
: The most energetic (tau).

pileup
: When a new collition is happening before the previous is gone all trough the detector, the reconstruction algorithms have to cope with pileup. With high luminosity the n̈ewp̈articles may even react with the öldönes.

punch-trough
: A particle not fully absorbed by the calorimeter. This can give us fake E_T^{miss} .

prong
: charged track. E.g. is $\tau^+ \rightarrow \pi^+\pi^-\pi^+\pi^0\nu_\tau$ a 3-prong decay.

QCD

Quantum Cromo Dynamics: major background in high energy collisions between partrons.

seed

The first guess of a particle candidat from data.

SM

Standard Model

Appendix B

Source codes

B.1 CA

Here is the CA piece of code following the argument at page 56

```
double CA(double METx, double METy,
  double recoTau1x, double recoTau1y, double recoTau1z,
  double recoTau2x, double recoTau2y, double recoTau2z,
  double recoTau1_phi, double recoTau2_phi){
  double mass = -100.;

  //a = eNu1/tau1          //b = eNu2/tau2
  double b = (recoTau1x*METy - METx*recoTau1y)/
    (recoTau1x*recoTau2y - recoTau1y*recoTau2x);
  double a = (METx - b*recoTau2x)/recoTau1x;
  long double recoTau1 =
           TMath::Sqrt(recoTau1x*recoTau1x +
   recoTau1y*recoTau1y +
   recoTau1z*recoTau1z);
  long double recoTau2 =
           TMath::Sqrt(recoTau2x*recoTau2x +
   recoTau2y*recoTau2y +
   recoTau2z*recoTau2z);
  long double eNu1 =
           TMath::Sqrt( TMath::Power(a*recoTau1x,2)+
   TMath::Power(a*recoTau1y,2)+
   TMath::Power(a*recoTau1z,2));
  long double eNu2 =
```

```
          TMath::Sqrt( TMath::Power(b*recoTau2x,2)+
   TMath::Power(b*recoTau2y,2)+
   TMath::Power(b*recoTau2z,2));
  long double eTau1 = eNu1 + recoTau1;
  long double eTau2 = eNu2 + recoTau2;
  long double cos_alpha =
    cos_alpha(recoTau1x, recoTau1y, recoTau1z,
              recoTau2x, recoTau2y, recoTau2z);

    /////Cut On Negative Neutrino Energies/////
TVector2 MET_Final(METx, METy);
double MET_phi = MET_Final.Phi(); //0,2pi
  double dphi_tau1MET = dPhi(recoTau1_phi, MET_phi);
  double dphi_tau2MET = dPhi(recoTau2_phi, MET_phi);
  double dphi_tauMET = dPhi(recoTau1_phi, recoTau2_phi);
  double epsilon = 10E-6;
  if((dphi_tau1MET + dphi_tau2MET)<=(dphi_tauMET +epsilon)){
    mass = 2. * eTau1 * eTau2 * (1. - cos_alpha);
    mass = TMath::Sqrt(mass);
  }
  return mass;
}
```

where

```
double cos_alpha(double px1, double py1, double pz1,
                 double px2, double py2, double pz2){
  double P1=sqrt(px1*px1+py1*py1+pz1*pz1);
  double P2=sqrt(px2*px2+py2*py2+pz2*pz2);
  if((P1==0)||(P2==0)) return 0;
  double cos_alpha=(px1*px2+py1*py2+pz1*pz2)/(P1*P2);
  return cos_alpha; }
```

and

```
double dPhi(double phi1, double phi2){
  double dphi=TMath::Abs(phi1-phi2);
  if ( dphi>TMath::Pi())
     dphi=TMath::Abs(dphi-2*TMath::Pi());
  return dphi; }
```

B.2 Boost method

Here is the piece of code for the boost method — written by Bjarne Stugu [1] , and Thomas Burgess [1] .

```
double m_boost = 0.;
TLorentzVector tau1;
TLorentzVector tau2;
tau1.SetPtEtaPhiM((*tau_Et)[leading_tau_id],
                  (*tau_eta)[leading_tau_id],
                  (*tau_phi)[leading_tau_id],
                  (*tau_m)[leading_tau_id]);
tau2.SetPtEtaPhiM((*tau_Et)[next_to_leading_tau_id],
                  (*tau_eta)[next_to_leading_tau_id],
                  (*tau_phi)[next_to_leading_tau_id],
                  (*tau_m)[next_to_leading_tau_id]);
double pi1cm_e=0.;
double pi2cm_e=0.;
double beta=0.;
void boost_method(double tau1_px, double tau1_py,
                  double tau1_pz, double tau1_E,
  double tau2_px, double tau2_py,
                  double tau2_pz, double tau2_E,
  //Variables that will be changed
  //(all should be initially 0.):
  double& pi1cm_e,
  double& pi2cm_e,
  double& beta)
{
    // Acol is pi-alpha
    // TLorentzVector pi1,pi2,pi1cm,pi2cm
    // needs to be defined

    double alpha = TMath::ACos(cos_alpha(
                          tau1_px, tau1_py, tau1_pz,
                          tau2_px, tau2_py, tau2_pz));
    double acol = TMath::Pi() - alpha;

    // try to reconstruct the beta that we put in.
    int iter=0;
```

[1] Department of Physics and Technology, University of Bergen

```
    beta=0.0;
    double dbeta=0.05;
    double acolnew=acol, dacol=acol,step = 1.;


    TLorentzVector pi1;
    pi1.SetPxPyPzE(tau1_px, tau1_py, tau1_pz,tau1_E);
    TLorentzVector pi2;
    pi2.SetPxPyPzE(tau2_px, tau2_py, tau2_pz,tau2_E);

    TLorentzVector pi1cm;
    TLorentzVector pi2cm;
    while(acolnew>0.01 && dacol>0.001 && iter<100){
      iter++;
      double acolprev=acolnew;
      beta = beta+step*dbeta;
      // copy lab vectors to cm and try new boost.
      pi1cm.SetPxPyPzE(pi1.Px(),pi1.Py(),pi1.Pz(),pi1.E());
      pi2cm.SetPxPyPzE(pi2.Px(),pi2.Py(),pi2.Pz(),pi2.E());
      pi1cm.Boost(0.,0.,-beta);
      pi2cm.Boost(0.,0.,-beta);
      acolnew = TMath::Pi()-pi1cm.Angle(pi2cm.Vect());

      //Fix step length near +-1
      double db_z=1.-TMath::Abs(beta);
      double sign=step/TMath::Abs(step);
      step=(step*sign<db_z)?step:sign*db_z/2.;
      // change direction
      if (iter==1 && acolnew>acolprev) step = -step;
      // new direction and step
      if (iter > 1 && acolnew>acolprev)  step = -step/2.;
      dacol = fabs(acolnew-acolprev);
    }

    pi1cm_e = pi1cm.E();
    pi2cm_e = pi2cm.E();
}
m_boost =  2*TMath::Max(pi1cm_e, pi2cm_e);
```

Bibliography

[1] cern.ch.

[2] https://twiki.cern.ch/twiki/bin/view/Atlas/WorkBookFullChain.

[3] J.Kalinowski A.Djouadi and M.Spira. Comp. phys. commun., 1998. 108 C (1998) 56, hep-ph/9704448.

[4] Ernest M Henley Alejandro Garcì a. *Subatomic Physics*. World Scientific, third edition, 2007.

[5] C. Amsler et al. (Particle Data Group). The review of particle physics. http://pdg.lbl.gov/2008/listings/s035.pdf, 2008. Physics Letters B667, 1 (2008).

[6] Povh, Rith, Scholz, and Zetsche. *Teichen und Kerne*. Springer, seventh edition, 2006.

[7] The Nobel Foundation. Nobelprize.org. http://nobelprize.org/nobel_prizes/physics/laureates/1984/.

[8] T. Guillemin for the ATLAS collaboration. Production of w and z in atlas. http://cdsweb.cern.ch/record/1126046/files/ATL-PHYS-PROC-2008-025.pdf, 2008.

[9] Atlas metadata interface. http://ami.in2p3.fr/opencms/opencms/AMI/www/.

[10] Martin L. Perl. Reflections on the discovery of the tau lepton. http://nobelprize.org/nobel_prizes/physics/laureates/1995/perl-lecture.html, 1995.

[11] Peter Rosendahl. Study of pairs of tau leptons in atlas data. Ph.D to be published in 2013.

[12] http://map.gsfc.nasa.gov/.

[13] CERN. History highlights. http://public.web.cern.ch/public/en/About/History-en.html, 2008.

[14] CERN. press release. http://press.web.cern.ch/press/PressReleases/ Releases2009/PR18.09E.html, 2009.

[15] ATLAS. - enews. http://atlas-service-enews.web.cern.ch/atlas-service-enews/2010/news_10/news_2010outlook.php.

[16] CERN Communiaction Gruop. Cern faq - lhc guide. http://cdsweb.cern.ch/record/1165534/files/CERN-Brochure-2009-003-Eng.pdf, 2009.

[17] CERN. Lhc design report volume i. https://ab-div.web.cern.ch/ab-div/Publications/LHC-DesignReport.html, 2009.

[18] http://public.web.cern.ch/public/en/lhc/LHCExperiments en.html.

[19] Ola Kristoffer Øye. *Preparing the ATLAS experiment - SemiConductor Tracker commissioning and simulation studies of SUSY models*. PhD thesis, University of Bergen, 2007.

[20] ATLAS collaboration. Atlas annual report 2003. Technical report, ATLAS, 2003.

[21] ATLAS collaboration. Expected performance of the atlas experiment. Technical report, ATLAS, December 2008. CERN-OPEN-2008-020.

[22] http://physics.gac.edu/ huber/envision/instruct/montecar.htm.

[23] J.Cranshaw et.al. A data skimming service for locally resident analysis data. *Journal of Physics: Conference Series 119*, 2008.

[24] Ø rjan Svandal. Studier av algoritmer for tau-identifikasjon. Master's thesis, University of Bergen, 2010.

[25] Caterina PIZIO. $z \rightarrow \tau\tau$ analysis results. http://iktp.tu-dresden.de/ATLAS-Tau-Workshop/ talk[6] slidepage 4, 2008.

[26] ATLAS collaboration. Atlas detector and physics performance technical design report. Technical Report Volume 1, ATLAS, May 1999. ATLAS TDR 14, CERN/LHCC99-14.

[27] ATLAS Collaboration with A. Ahmad et.al. Search for the standard model higgs boson via vector boson fusion production process in the di-tau channels. In *ATLAS NOTE*, page 36. april 2009.

[28] Z. Czyczula on behalf of the ATLAS collaboration. Tau physics with first data in atlas. *Science direct*, 2009.

[29] Stan Lai on behalf of the ATLAS collaboration, editor. *Tau Physics at the LHC with ATLAS*, 2009. arXiv:0910.4727v1.

[30] Qi Tao (Tony) Shao. Mass boost technique. University of Melbourne.